Regenerative biomaterials for maxillofacial applications

Salzlechner, Christoph

Awarding institution:
King's College London

Regenerative biomaterials for maxillofacial applications

Christoph Salzlechner

Thesis submitted for the degree of Doctor of Philosophy at King's College London

2020

King's College London

Centre for Craniofacial & Regenerative Biology

SE1 9RT, London, United Kingdom

Declaration

I hereby certify that this report is my own work unless stated otherwise and all sources of information used in this report have been fully acknowledged.

"*Science advances slowly, with halting steps. But does not therein lie her eternal fascination? And would we not soon tire of her if she were to reveal her ultimate truths too easily?*"

» Karl von Frisch (Nobel Prize in Physiology and Medicine 1973)

Acknowledgement

Science is a truly mesmerising profession, giving one the opportunity to explore your own curiosity to the fullest. However, pursuing a PhD has proven to be a fairly challenging voyage after all. Not for the sake of failed experiments or negative results, but because life is not on hold during such a mentally and physically straining period. Especially because of that, I am thankful beyond words for being surrounded by people who supported me professionally as well as personally throughout my PhD project, helping to overcome all obstacles and making this an entirely wonderful experience.

I would like to express my deep appreciation to all my colleagues at King's College London and the Centre for Craniofacial & Regenerative Biology, and specifically to: Andrew Atkinson, Brian Burke, Ana Caetano, Dhivya Chandrasekaran, Cecile Dreiss, Silvia Ferreira, Angela Gates, Agi Grigoriadis, Chris Healy, Helena Lewis-Greene, Susmitha Rao and Lucia Zaugg.

Of course, this extends to all the amazing people that have worked directly on this project. Their scientific input and, even more importantly, their friendship have made this project a unique experience. I consider myself lucky to have worked with every single one of them: Tabasom Haghighi, Isabella Hübscher, Sophie Maier-Schell and Anders Runge Walther.

Immense gratefulness goes to the Diana Trebble Fund to financially enable this project. I feel incredible honoured having received this generous PhD scholarship.

I especially want to highlight both of my supervisors, Eileen Gentleman and Kathy Fan. Starting this journey together and seeing it come to this successful milestone is a truly incredible feeling. In my home country Austria, doctoral supervisors are often considered being 'father/mother to your PhD'. In that spirit, I would like to emphasise my overwhelming gratitude to my doctoral mums.

Without a doubt, my family has been most supportive on every level throughout this journey. Eternal thanks to my parents Roswitha and Andreas, my sisters Verena and Claudia, my brother-in-law Stefan, my nephew Thomas and my best friend Marlen. I love you!

Abstract

Arthroscopic surgical procedures aiming to regenerate maxillofacial tissues are troubled by its complex structures and challenging surgical access. Indeed, while minimal invasive procedures that deliver regenerative materials and/or cells are common in articulating joints such as the knee, there are currently no standardised treatments that place cells, regenerative factors or materials into maxillofacial tissues to foster bone, cartilage or muscle repair. This project aimed to develop hyaluronic acid (HA)-based hydrogels, which are suitable for use in minimally invasive procedures, that can adhere to the surrounding tissue, and deliver cells and drugs. Consequently, cells produce cartilage-specific extracellular matrix (ECM) components to replace the hydrogel with, resulting in neo-tissue. This effect might be further increased by introduction of Dimethyloxalylglycine (DMOG).

Modifying HA with both methacrylate (MA) and 3,4-dihydroxyphenylalanine (Dopa) groups using a completely aqueous synthesis route, MA-HA-Dopa hydrogels can be applied under aqueous conditions, gel quickly using a standard surgical light, and adhere to tissue. Moreover, upon oxidation of the Dopa, human marrow stromal cells (hMSC) attach to hydrogels and survive when encapsulated within them. In order to assess the formation of extracellular matrix components, non-canonical amino-acid tagging (FUNCAT) with Raman spectral imaging have been utilised. Combining those, 3D spectral and fluorescence maps of cells and their secreted ECM allow qualitative and quantitative analysis. FUNCAT and Raman are unbiased, inexpensive and rapid techniques. Results show peptides/proteins being secreted, with them accumulating in the immediate space around the plasma membrane. Depending on the hydrogel formulation, DMOG did increase quantity as well as distance of newly synthesised peptides/proteins being detected away from the cell membrane. The overall findings suggest that MA-HA-Dopa hydrogels may find use in minimally invasive procedures to foster maxillofacial tissue repair.

Table of content

List of figures

List of tables

Abbreviations

^{1}H-NMR	Proton nuclear magnetic resonance
2D	Two-dimension
3D	Three-dimension
ABAM	Anti-biotic/anti-mycotic solution
BMP	Bone morphogenic protein
CSD	Critical size defect
DMOG	Dimethyloxalylglycine
DOM	Degree of modification
Dopa	3,4- dihydroxyphenyl-L-alanine
DTT	Dithiothreitol
ECM	Extracellular matrix
FBS	Foetal bovine serum
FGF	Fibroblast growth factor
GAG	Glycosaminoglycan
HA	Hyaluronic acid (or: hyaluronan)
HAse	Hyaluronidase
hBM-MSC (also: hMSC)	Human bone-marrow derived mesenchymal stem cell
HCl	Hydrochloric acid
I2959	Irgacure 2959
MA	Methacrylate
MACI	Matrix-assisted chondrocyte implantation
Mfp	Mussel foot protein
MSCs	Mesenchymal stem cells
MTT	3-(4,5-dimethylthiazol-2-yl)-2,5-diphenyltetrazolium bromide
MWCO	Molecular weight cut-off
NaOH	Sodium Hydroxide
NSAID	Non-steroidal anti-inflammatory drug
Pa	Pascal
PBS	Phosphate buffered saline
PCR	Polymerase chain reaction
PEG	Linear dithiol-Poly(ethylene glycol)1000 (or HS-PEG1000-SH)
RGD	Arginylglycylaspartic acid
RT	Room temperature
TE	Tissue engineering
TGF	Tumour growth factor
TMD	Temporomandibular joint disease/disorder
TMJ	Temporomandibular joint

1 Introduction to Thesis

Osteochondral defects are classified as diseases/damage to the bone (Greek ‘osteo’) and cartilage (Greek ‘chondro’) components of all bodily joints. First, general osteochondral defects, treatment and research on joints are described (see 1.1), followed by focus on the temporomandibular joint exclusively (see 1.2, page 23).

1.1 General osteochondral defects

Osteochondral lesions and defects can appear in any bodily joint, with highest rate of occurrence in knee and ankle. The management of articular cartilage defects represents a common clinical problem for orthopaedic surgeons. This appears especially problematic as articular cartilage has limited healing capacity, resulting in rapid deterioration following trauma or degenerative pathology. Such damages are ultimately leading to joint pain, functional impairment and degenerative arthritis.[1, 2]

1.1.1 Current clinical approaches

The gold-standard for terminal osteochondral lesions is common total joint replacement.[2] However, the use of inorganic artificial joint materials like metals or ceramics are limited by their insufficient mechanical and bioactive properties. Such artificial joints require extensive surgery and need replacement after several years.[3, 4] Restoring living structural tissue in early-stage osteochondral defects is merely based on autograft or allograft transplantation. This comes with drawbacks like host-graft rejection, donor pain as well as insufficient donor availability.[5] Further clinical treatments for osteochondral defects are common methods since late 1970’s and include debridement, bone marrow stimulation techniques like microfracturing, autologous chondrocyte implantation (ACI) and osteochondral

transplants like mosaicplasty (see Figure 1).[2, 6] However, these techniques not always reach a fully curative solution.

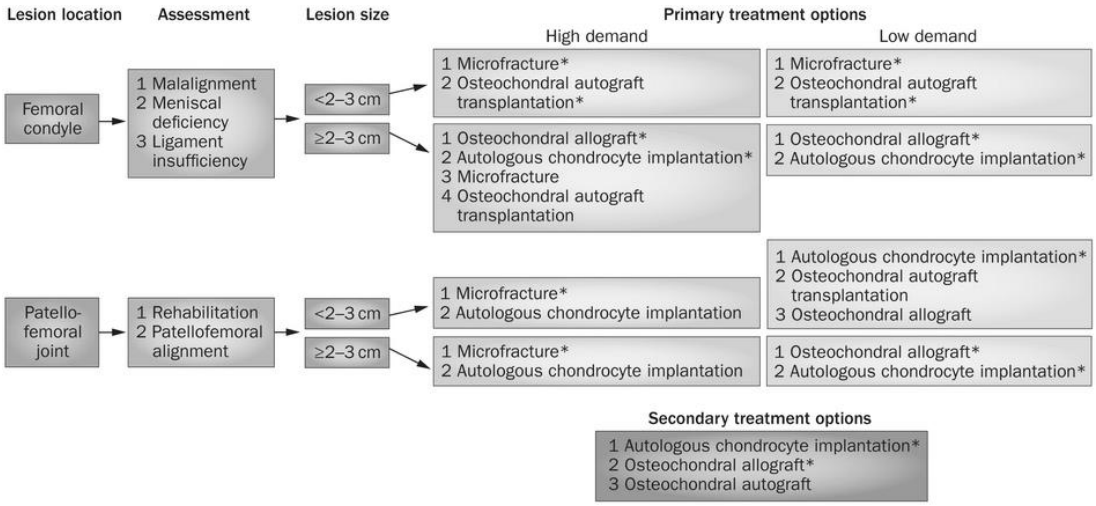

Figure 1: Treatment algorithm for defects of articular cartilage. [2]
Depending on the location of the lesion, surgeons assess symptoms and lesion size. Considering the lifestyle of the patient and previous therapy will identify possible surgical treatments.

1.1.2 Tissue engineering for osteochondral defects

Over the last decades, tissue engineering (TE) has emerged as promising approach for a wide range of medical areas. This is especially true for osteochondral defects, as cartilage is known to have no natural healing response.[7] Still, TE seems to have great potential to fully functionally and structurally regenerate tissue. TE-based techniques currently used in clinical applications include Matrix-induced autologous chondrocyte implantation (MACI)[8] and scaffolds inspired by natural tissue components (i.e. Hyaluronic-acid-based scaffolds).[2] MACI is the most common technique. Similar to autologous chondrocyte implantation, it requires two separate surgical procedures, one to isolate the cells and one to implant the processed cells with the scaffold into the patient. Although several publications reported good clinical outcome [9, 10], there is only limited proof for superiority of this technique over existing treatments.

In order to address the lack of efficient care, research has focused on cell-only strategies, as well as TE-based approaches including material-only strategies and combined cell-material strategies.[11]

Cell-only approaches rely on a range of different cell types. These can be delivered directly via procedures like microfracturing (mesenchymal stem cells) as well as harvested autologous or allogenic and delivered to the injury site (i.e. chondrogenic cells). Providing mature chondrocytes has shown better extracellular matrix (ECM) production over using progenitor cells [12], although delivering chondrocytes has several disadvantages over mesenchymal progenitors. Chondrocytes require a separate surgical procedure harvesting them, with biopsies resulting in low cell yields. Furthermore, isolating and cultivating mature chondrocytes can trigger dedifferentiation which drives them to lose their cartilage-like phenotype.[13] Hence, mesenchymal stem cells have gained more focus as they are abundant, regenerate and potentially allow single-procedure approaches via microfracturing techniques. Another key characteristic is their differentiation potential, allowing them to assume different cell types. Well-established methods relying on soluble factors are in place to drive stem cell fate in 2D. For chondrogenic differentiation, these factors include hypoxia as well as bone morphogenic proteins 2 and 4 (BMP-2, BMP-4) [14-16], fibroblast growth factor 2 (FGF-2) [17] and transforming growth factor β1 (TGF-β1) [18]. Interestingly, some of these chondrogenic factors are also able to induce osteogenesis, f.e. BMP-2 [18, 19] or TGF-β1 [18]. Various groups, including Taheem and colleagues, have investigated the importance of physiological oxygen content for chondrogenesis, by lowering oxygen levels to the natural hypoxic concentration of 0.5 – 10 % in mature cartilage.[20] This was achieved pharmacologically by addition of hypoxia inducible factor-1α hydroxylase inhibitor Dimethyloxalylglycine (DMOG) to human bone-marrow derived mesenchymal stem cells.[21-23] DMOG acts as pan-hydroxylase inhibitor, which leads to an upregulation

of hypoxia-inducible factor (HIF).[21, 24] However, delivering these agents and stabilising cells within the defect has proven challenging. Anchoring cells in place was tested with fibrin [25] and cell aggregates [26], but still, this reached low stability, rendering regeneration of larger defect areas troublesome. Overall, cell-only approaches are difficult to shape to the volume needed and are at risk of being separated from the defect site before tissue regeneration has happened, as there is little to no material holding cells in place.

Material-only strategies are based on the concept of cell recruitment of cells present in the immediate surrounding of the material. Most approaches rely on the migration of progenitor cells, i.e. bone-marrow derived mesenchymal stem cells, which can infiltrate the site via microfractures. To fully regenerate the tissue, materials are often designed to be fully biodegradable, leaving only the ECM produced by the cells. It is hypothesised, that materials providing cell adhesion points may drive proliferation and differentiation via mechanical cues like stiffness or topography. Such materials can be either synthetic or derived from natural materials. Natural biomaterials including chitosan, various collagens, alginate, bacterial polymers or hyaluronic acid (HA) have proven promising for TE purposes.[27] Although, mechanically weaker than their synthetic counterparts, natural polymers can facilitate cellular responses like cell attachment via integrins (i.e. collagens) or cell survival via CD44 (i.e. HA). As such, these materials can be exploited in different forms ranging from sponges, sheets to hydrogels. Utilising a collagen scaffold, Wang and colleagues delivered an anti-inflammatory compound into osteochondral defects in rabbits.[28] Their material managed to recruit cells and lower the overall inflammatory response, leading to production of neo-cartilage. Sofu and colleagues have investigated the regenerative potential of HA-based scaffolds via microfracturing.[29] This comparative study has reported repair tissue by magnetic resonance observation, however, long term performance of this neo-tissue *in vivo* is yet to be confirmed. As osteochondral defects

in the knee often involve both cartilage and bone, multi-layered techniques have been investigated. MaioRegen® by JRI Orthopaedics is composed of three layers – a collagen layer for cartilage, a collagen layer enriched with hydroxyapatite for calcified cartilage and a layer of hydroxyapatite for subchondral bone.[30] Although, new lineage specific tissues have formed, the quality and integration of the graft into the surrounding tissue lacked conclusive evidence, as shown by Brix et.al.[30] Other products like TruFit™ by Smith+Nephew Endoscopy, are based on poly-lactide glycolide, which mimics the macro-structure of bone. However, results were not convincing of better clinical outcome over mosaicplasty.[31] Considering all those results, material-only techniques seem to suffer from issues related to defect size, as cell migration is often limited and therefore cells might not be able to repopulate the whole implant.

Combined cell-material strategies have benefits over cell-only and material-only approaches. Encouraging here are materials that are applied to the defect side as solids or such that are delivered as solutions and are solidified after application. Solid materials can be shaped upfront and moulded specifically for the injury site. 3D-printing techniques have emerged as promising for such purposes.[32-35] Modern printers are able to encapsulate cells as well as bioactive components. Injectable compositions, like hydrogels, are also capable of delivering cells and biological active components and can be shaped on site. As described for the material-only TE approaches, a wide range of synthetic and natural polymers have been utilised. Alginate has been used widely as basic hydrogel material for osteogenic regeneration. It is cheap and easy to produce, and due to its electrical charge, it can cross-link quickly with cations (i.e. Ca^{2+}). Alginate hydrogels were used to encapsulate mature chondrocytes in spheres, which resulted in an increase in cell number as well as upregulation of chondrogenic genes.[36] Fonseca and colleagues have encapsulated human MSCs in MMP-degradable Alginate hydrogels.[37]

Subcutaneous implantation in severe combined immunodeficiency(SCID)-mice has shown cartilage-like tissue after 4 weeks. Further materials like Chitosan, have been used for hydrogel production. Chitosan hydrogel as carrier, was mixed with cartilage ECM components type-II collagen and chondroitin sulphate.[38] Encapsulating either mature chondrocytes or progenitor MSCs, lead to increase cell condensation as well as cartilage like ECM secretion, for both cell types. As one of the most abundant ECM components, collagen is a prominent candidate amongst hydrogels. Muhonen and colleagues synthesised a recombinant human type-II collagen based hydrogel, allowing a xeno-free and donor-free production.[39] They concluded, that when encapsulating high density pellets of human bone marrow derived mesenchymal stem cells, cartilage-like ECM is secreted after 84 days in chondrogenic induction media. Another common natural material for hydrogel formation is hyaluronic acid. Modifying HA with the catechol group tyramine, allowed cross-linking between HA macromers upon introduction of oxidising agents, here hydrogen peroxide and horseradish peroxidase.[40] Encapsulating mesenchymal stem cells showed reduced quantity of cells over time. Cell condensation of the remaining cells seems to play a significant role for chondrogenesis. Other groups have further increased the complexity of hydrogels used, by using two or more materials, incorporate multiple cell types or provide a wide range of soluble bioactive components.[41-44]

Inflammatory responses to Temporomandibular Joint disorders (TMDs) may accelerate TMJ cartilage erosion and disease progression (see 1.2.2, page 25).[45] Considering this, immunomodulatory effects of type-I collagen upon mature chondrocytes has been investigated.[46] Similarly to the material-only approach by Wang and colleagues [28], Yuan and team have encapsulated neonatal rabbit chondrocytes in collagen hydrogels and incubated for up to 28 days *in vitro*. Introduced lymphocytes mimicked a natural immune response, potentially leading to a dedifferentiation of the chondrocytes and therefore a reduced production of

cartilage-like ECM. However, type-I collagen hydrogels appeared to exert regulatory effects on immune cells and increased the synthesis of ECM proteins.

Though promising progress has been made creating neo-cartilage *in vitro* as well as *in vivo*, the integration of cartilage into the surrounding tissue is a common problem in osteochondral reconstruction.[47-49] In prospect of overcoming this issue, adhesive strategies have been utilised. Elisseeff and colleagues have achieved a stable bonding of biomaterials to native tissue by 'painting on' a aldehyde and methacrylate functionalised chondroitin sulphate layer.[50] Aldehyde will react with amines in the tissue via spontaneous Schiff-Base reaction. The methacrylate groups then allowed covalent links between tissue and biomaterial upon UV light exposure. Others, like Zhu and colleagues, have utilised naturally inspired catechols to achieve tissue adhesion, including cartilage.[51] Catechols, like 3,4- dihydroxyphenyl-L-alanine (Dopa), are abundant in the mussel-foot proteins, allowing a range of different interactions.[52, 53] Dopa can be used to form cross-linking connections (Dopa-Dopa) and therefore solidify a material, or react with inorganic and organic materials alike, which could enable cell or tissue interaction. Kim et.al. have used gelatine as a backbone construct and further modified it with methacrylate and Dopa moieties.[54] Hydrogels were prepared by mixing the macromer with iron-dichloride ($FeCl_2$) as well as hydrogen peroxide (H_2O_2). The following Fenton reaction covalently cross-linked the methacrylate moieties and formed ionic interactions between Fe^{3+} ions and the reduced Dopa. They conclude that the material might have sufficient properties to be used as an injectable wound-dressing or other adhesive materials. Han and colleagues grafted a clay-polyacrylamide layer onto skin, with poly-dopamine as an adhesive layer.[55] The material shows rapid interaction with the host tissue, without resulting in an inflammatory response at the application site, confirming Dopa to be well tolerated by human tissues. Lee and team have modified poly-ethyleneglycols (PEGs) with Dopa.[56] They achieved cross-linking within several hours, by addition

of sodium periodate and horseradish peroxidase, or by mushroom tyrosinase. Others have utilised the Dopamine precursor tyrosine for adhesive purposes.[57, 58] Moreira Teixeira and colleagues have modified dextran and heparin with tyramine and filled cartilage defects with the resulting hydrogel.[57] Rapid enzymatic cross-linking occurred within 1 - 2 minutes after mixing the hydrogel with horseradish peroxidase and H_2O_2. In this manner, tyramine of the hydrogel reacted with itself and thereby solidified, as well as bound covalently to the tyrosine residues in the surrounding host cartilage, enabling stable adhesion. Similarly, Cui and colleagues have modified silk with tyrosine, however, their system is cross-linked by visible light (400 - 450 nm) via ruthenium (Ru)/sodium persulfate (SPS) reaction.[58] Further incorporating gelatine into their system, the systems shows higher flexibility in its use as the time for application was more compliant.

1.1.3 Hydrogels for tissue engineering

Utilising hydrogel-based system for tissue engineering is a rather new approach in clinical applications and seem to have attracted researchers interest quickly.[59] Hydrogels are composed of chains of hydrophilic macromolecules which are able to retain vast quantities of water, reaching up to several thousand-fold weight increase.[60] This is lowered by factors like modification or polymeric immobilisation. Stable gels are formed from a precursor solution by cross-linking single molecules via kinetic chains. Physical properties can be easily influenced by changing molecular weight or amount of macromer, as well as varying molecular weight and density of the cross-linker. Depending on the reactive moieties present on the macromer, cross-linking can be achieved in several ways. Most common are ionic, thermal, enzymatic, chemical and light cross-linking.[61] Chemical modification of such macromers is mostly easily achievable and once produced enables effortless and modular hydrogel fabrication, allowing versatile application. Those systems all have a strong focus on

biocompatibility. Here, cellular interactions are playing a key role. According to their surroundings, cells are highly capable of moulding and rearranging its pericellular space in order to maintain and thrive within their respective niche. Therefore, degradability is a major factor to consider when designing a hydrogel system, resulting in by-products that can be easily removed via bodily functions.[62] Once successful population has been completed, cells actively remodel their surrounding and secret their own ECM.[63] This results in the hydrogel carrier being fully replaced over time with newly synthesised ECM, recapitulating structural and functional neo-tissue. Formation of such extracellular components is mostly determined *in vitro* by immunohistochemistry, whereby quantity and composition of newly formed matrix elements allows comparison to natural tissue. This enables selection of ideal compositions for further testing. Although such immunohistochemistry techniques allow high spatial resolution and precise identification of individual matrix components, they also remain expensive and time-consuming methods, which request initial knowledge about the potential substances to be tested for. More recently developed techniques like non-canonical amino-acid tagging or Raman spectral imaging could be inexpensive and accessible tools to substitute immunohistochemistry for tissue engineering research.

1.2 Temporomandibular Joint Disorders

1.2.1 Anatomy of the Temporomandibular Joint

The temporomandibular joints (TMJs) connect the lower jaw on both lateral ends to the rest of the skull (Figure 2). They are composed of an articular head and a mandibular eminence, which are bone tissues. Both are separated by the articular disc, a cartilage-like tissue. The articular surface of the condylar head itself is covered with a thin layer of fibro-cartilage. Overall, the joint is held together via fibrous capsules and several muscles. Processes like chewing, speaking or yawning require

motion of the TMJ. The condylar head moves in an anterior direction when opening the mouth, by gliding on the articular disc along the mandibular eminence. Moving back in the posterior direction will close the mouth.

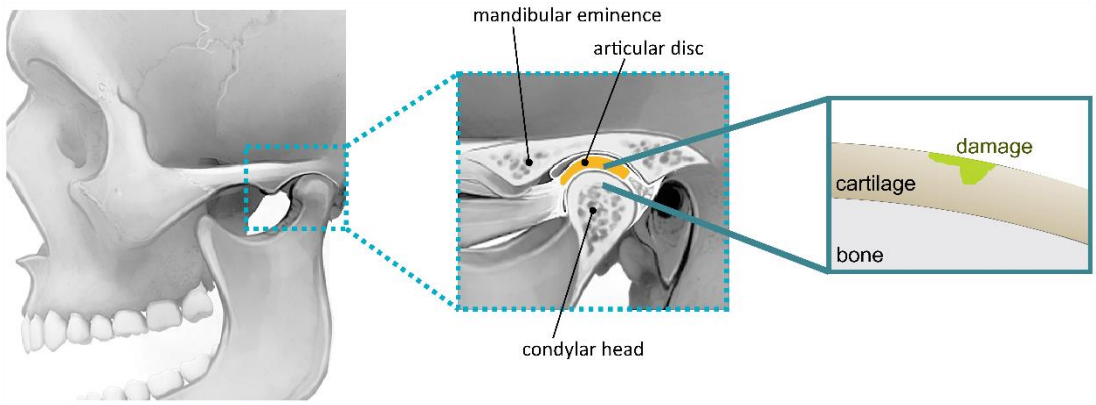

Figure 2:Temporomandibular Joint. [64, modified]
Two temporomandibular joints are connecting the lower jaw to the rest of the skull. They are fundamentally composed of a condylar head and a mandibular eminence, which are separated by an articular disc. Furthermore, the condylar head is covered in a fibrous-cartilage layer.

Although several components can factor in, this project has focused on damages to the fibrous cartilage of the condylar head exclusively (as illustrated in Figure 2, right image). Fundamentally, the cartilage layer of the TMJ differs from other articular cartilage tissues. With approximately 0.5 mm in thickness, TMJ cartilage is amongst the thinnest chondrogenic layers in the human body.[65] This articular cartilage layer in the TMJ it is mainly comprised of fibrous cartilage. Structural composition is divided into 4 histologically distinct layers (Figure 3); the fibrous layer on top contains mainly type I collagen, with low quantities of type II collagen, hosting morphologically flat fibroblast-like cells.[66] The proliferative layer underneath is made purely of type I collagen and contains undifferentiated mesenchymal progenitor cells, which function as a cell reservoir. Those progenitors have the potential to transition into type II collagen-synthesizing pre-hypertrophic chondrocytes.[67] Both of these layers have

parallel anterior-posterior alignment of ECM fibres, with chondroitin sulphate as the non-collagen matrix component. The thickest layer is made of actual fibrocartilage. This layer has a mature and a hypertrophic sheet, composed of type II collagen, as well as type I and X collagens, housing mature chondrocytes.[68] Here, collagens are aligned randomly, with aggrecan as an abundant matrix component.[69] Origin of the cellular content in the cartilage layer of TMJ remains unclear, however, reports suggest that initial formation of the TMJ osteochondral components is facilitated by neural crest cells and mandibular bone periosteum cells.[70] Recent studies have indicated that Wnt signalling and hypoxic oxygen conditions play crucial roles in terminally differentiating and maintaining homeostasis in TMJ chondrocytes.[71-74]

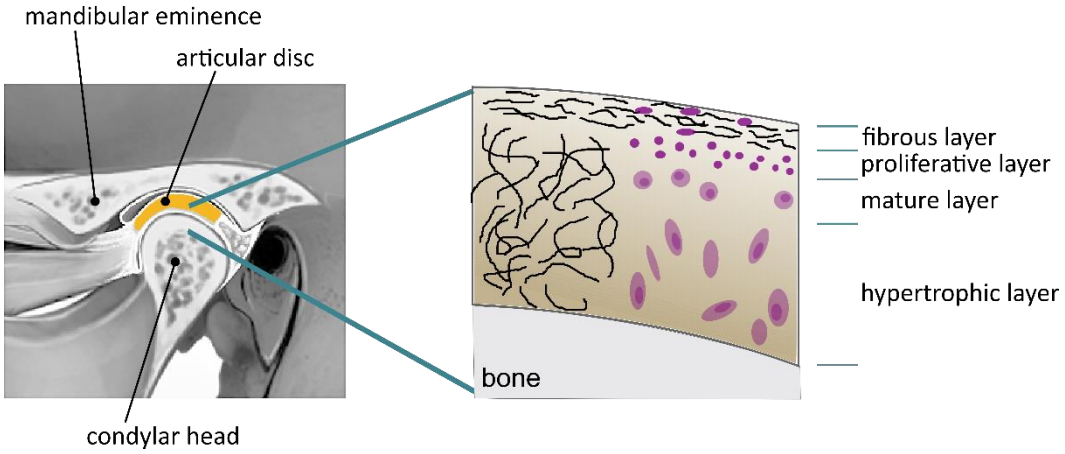

Figure 3: Structural composition of TMJ articular cartilage.
Black lines represent alignment of collagen fibres, with different cell types in purple.

1.2.2 Clinical appearance of Temporomandibular Joint Disorders

Damages to this joint are classified as Temporomandibular Joint Disorders (TMDs). Pathologically, TMDs are characterised as local deterioration of articular tissue, resulting in loss of function and high pain levels. Comparing to other osteochondral defects in the human body [2, 6, 9, 10, 75], TMDs appear in highly complex aetiology and are of multicausal origin.[76] There are three groups of factors influencing TMDs: predisposing factors (increasing the likelihood to develop a symptom of TMD),

initiating factors (causing the onset of TMD) and perpetuating factors (increasing the severity and progression of TMD as well as reducing the chances of successful treatment).[77, 78] Treating TMDs effectively relies on identifying all of the factors influencing the TMD in a particular patient. Factors triggering TMDs include occlusal abnormalities, bruxism, orthodontic treatment and orthopaedic instability, trauma (macro/micro traumata), joint laxity, hormonal imbalance (exogenous oestrogen), cancer, other degenerative diseases, malnutrition, stress, mental tension as well as anxiety and depression.[77, 78] Although not causative, inflammatory responses (i.e. osteoarthritis) seem to be a major driving aspect of TMDs.[45]

Clinically, TMD progression is classified in 5 stages, which are characterised via assessment of joint mobility and imaging techniques.[79] Stage 1 most often presents clicking sound of the joint, with no to low pain levels during jaw motion. In stage 2, sporadic pain occurs together with recurrent jaw locking and headache. Stage 3 shows advanced symptoms from stage 2, together with painful chewing and restricted range of joint motion. Imaging often reveals disc displacement.[80, 81] Following, stage 4 presents chronic mild to severe pain to joint and general headache with severely restricted jaw motion. When imaged, the disc often appears thickened, with abnormal contours of condylar head as well as mandibular eminence. Patients in stage 5 experience constant pain, with strong structural and functional deterioration of disk as well as mandibular and condylar surface.

Approximately 30% of Europeans will suffer from TMD at one point during their life [78], with the greatest risk of onset between 18 and 44 years of age.[82] It is estimated for every 100 million working adults in the United States, TMD contributes to 17.8 million lost working days.[83] More than 80% of these patients will recover with non-surgical conservative management. Such conservative treatments include immobilisation and rest, non-steroidal anti-inflammatory drugs (NSAIDs), behavioural therapy, pain management and bite splints.[78, 84] Unlike in the field of orthopaedics,

where a wide range of techniques are available to treat bone or cartilage disorders [2], maxillofacial surgeons are limited with their options. Often it is more a palliative approach rather than a curative treatment. Patients with refractory TMD and persistent pain as well as limitation of function along with structural pathology of the TMJ, are considered for surgical intervention. Surgical procedures range from intra-articular injections, to minimally invasive arthrocentesis and arthroscopy [85] through to open joint procedures.[78] Open TMJ surgeries includes disc surgeries, like discectomy and plication, as well as surgery on the bony elements of the TMJ, such as an eminectomy, high condylar shave or condyloplasty.[86] In the most severe cases, an alloplastic joint replacement is recommended. The process of open joint surgery can be destructive, has high risk of causing damage to the facial nerve, leaves scares in the facial area and requires long healing periods.[87]

1.2.3 Tissue engineering for TMDs

Compared to other regenerative approaches for osteochondral tissues (see 1.1), very few groups are focused on exploiting tissue engineering for TMJ repair. This is likely for a number of reasons such as the small size of the condyle and complex surgical access to it as well as a small group of patients suffering from TMDs. These reasons are also limiting the applicability of TE-techniques developed for other joints to be used in TMJ reconstruction. Furthermore, there is a lack of appropriate *in vivo* models available due to vast differences in structural and functional performance of the TMJ in various species. Comparing numerous species, minipigs are considered to be gold standard for a large animal TMJ model, established on similarities to the human anatomy, size as well as mechanical load and function.[88, 89] The use of other models could limit the clinical significance for human subjects. Adding to this, TMJ surgery perhaps inflicts significant reduction in jaw movement or complete immobility,

which might not allow the animal to feed and therefore cannot be considered ethically compliant. Altogether, this is restricting the ability to produce conclusive data.[90]

Accordingly, the existing published information is limited. For example, Zhu and colleagues [91] overexpressed NELL-1 (NEL-like molecule-1) in goat autologous bone marrow-derived mesenchymal stem cells (BM-MSCs) and incorporated them in a poly lactic-co-glycolic acid (PLGA) scaffold. They placed the solid scaffolds in critical size defects (CSD) of goat mandibular condyle. After 6 weeks, histological analysis showed bone and cartilage formation, which they concluded as successful recovery. However, PLGA degradation forms acidic side products which may contribute to bone decalcification. In summary, they showed short term structural recovery but do not analyse the functional recovery of the specimen. Further research has been done on cell-free tissue engineered approaches embedding soluble growth factors like fibroblast growth factor-2 [17] and bone morphogenetic protein-2 [16]. Although they have proven the stimulation of ECM secretion by present chondrocytes, this requires further testing for human applications. Wang and colleagues have further investigated cell types to promote optimal TMJ cartilage regeneration.[92] They have found that chondrocytes harvested from porcine hyaline cartilage produced significantly more ECM *in vitro* then those sourced from porcine TMJ cartilage. Besides low volume of TMJ cartilage, and therefore small quantities of cells available, chondrocytes harvested from other non-loadbearing cartilage might be a superior approach in TMJ fibro-cartilage regeneration. Considering that this approach would require another surgical intervention, extended time to process the cell material and chondrocytes harvested could lose their phenotype, mesenchymal stem cells delivered via microfracturing might overcome those concerns.

1.3 Project design and scope

Considering the literature available (see 1.1 page 15 following, and 1.2 page 23 following), this project has been targeted specifically for towards arthroscopic TMJ surgery. Subsequently, justification and critical analysis of the overall project design is stated, with specific aims summarised in 1.3.5 (page 41).

In order to comply with the complex structure and accessibility of TMJs, hydrogels have been utilised for this project. They bare the capacity to be applied in liquid/viscous form on site and therefore have the potential to be used in minimal invasive techniques. Such arthroscopic approaches would be favourable for TMJ surgeries, considering that solid materials would require destructive open-joint techniques (see 1.3.1, page 29). The hydrogels should further be able to support cell attachment and tissue adhesion.

1.3.1 Minimally invasive approaches

Arthroscopic surgeries in the TMJ have been performed for over 40 years.[93] The double puncture technique has allowed access to the TMJ to enable the use of laser [94], motorized shaver [95] and disc repositioning. Nevertheless, there is currently no option available to introduce a material which enables regeneration of the damaged tissue in a minimal invasive fashion. Some clinicians argue that arthroscopic techniques require more time during which the patient is sedated and involve special equipment and training. Although, the stress and discomfort patients experience from an open surgery as well as the long recovery period and possibility of pathological scar formation, suggest that minimally invasive procedures should be favoured. This is supported by evidence that pain and psychological factors play a key role in successful treatment courses.[96] These have the potential to be reduced with minimally invasive treatments. Furthermore, damages to the facial nerve can be reduced drastically with minimally invasive approaches. As such, arthroscopic

surgery is the superior technique with the reduction in complications, however, restoring damaged TMJ articular surfaces by delivering factors that stimulate endogenous repair remain unidentified.

Restoring the fibro-cartilage of the condylar head requires several specifications towards such a procedure. The proposed arthroscopic technique is summarised in Figure 4. Here, the damaged TMJ cartilage would be removed, an injectable hydrogel material (with/without cells and biologically active factors) would be applied and solidify upon dental blue light exposure.

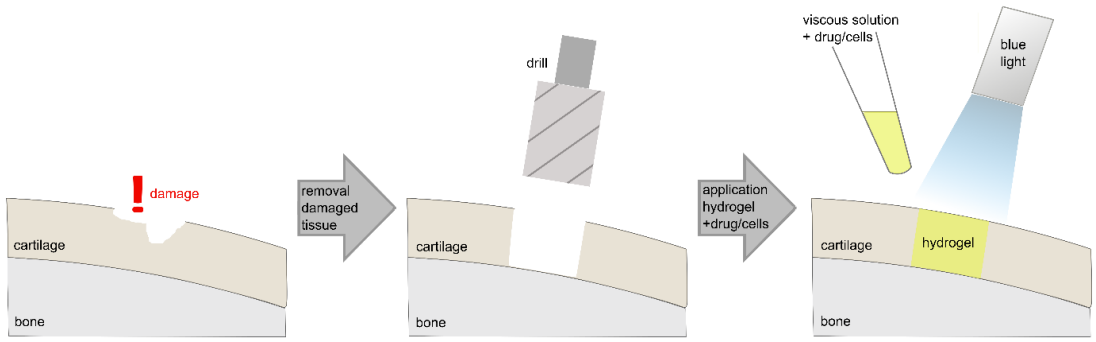

Figure 4: Proposed arthroscopic approach to repair fibrocartilage of condylar head in TMJ.
Damaged fibrous-cartilage is removed via drill or laser and debris is flushed out. Afterwards the defect side can be filled with the hydrogel solution, carrying cells and/or drugs. The solution can be moulded and solidified upon blue light stimulus.

Several key-factors have to be considered for the further design of a hydrogel to be used in such arthroscopic TMJ surgery. Firstly, the joint space is inflated with liquid. This has several benefits for the surgeon like cooling during abrasive processes, removal of floating debris to improve vision as well as increasing space for handling. Therefore, materials need to be applicable under aqueous conditions and solidify quickly upon exposure to a triggering stimulus (i.e. visible dental light). This allows the surgeons to apply, mould or simply remove and reapply the material if necessary, without a limited reaction window to do so. Secondly, the material needs to be

injectable via a syringe system. The application of a material can be troublesome, as the space is confined, so it should be easy to mould or remove, in case it needs to be re-applied. Viscosity is a crucial property here, as it should not dissolve in the liquid surrounding but should also be applicable via a syringe. Thirdly, possibility for preparing materials within an operating theatre is limited and ideally should be done before the surgery is starting. This makes shelf-life an important factor to be considered.

1.3.2 Advantages of methacrylated HA-hydrogel system

Choosing a backbone for the design of a hydrogel leaves one with a vast range of different materials available. However, hyaluronic acid (HA) is a material used on daily basis in clinics, showing high tolerance in patients across different physiological background, with less than 2 % of patients experiencing adverse effects like rash, nausea or muscle cramps.[97, 98] HA is a hydrophilic linear polysaccharide composed of repeating disaccharide units of N-acetylglucosamine and D-glucuronic acid. It is an integral part of most human tissues, including cartilage.[99] Moreover, the utilisation of hyaluronic acid in the TMJ is well documented and there is some evidence that it may positively influence inflammatory mediators in the osteoarthritic process.[100, 101] Unmodified HA could also be applied to increase the overall viscosity of a hydrogel-precursor solution, without drastically influencing the resulting cross-linking behaviour of the modified HA. In addition, the physical properties of HA-hydrogel scaffolds, such as stiffness, degradability and swelling play important roles in directing the differentiation of the encapsulated cells.[102, 103] Soluble factors as well as physical attributes of the extracellular scene are known to direct lineage specification.[104] Stem cells encapsulated in hydrogels have the ability to probe their surrounding stiffness and influence their fate by degrading that same hydrogel.[105, 106] More recently, Ferreira and colleagues have shown that

stem cells have the ability to swiftly remodel their surroundings to their needs by degrading and replacing HA-based hydrogels with their own matrix.[63] Here, stiffness can be influenced by the amount of modified HA macromere or degree of macromere modification. They directly correlate with other physical properties as an increase in those components would lead to reduced swelling and degradation behaviour. Consequently, hydrogels are supposed to be structurally stable but still remain degradable for cells. In addition, swelling is occurring due to the hydrophilic nature of HA, providing a microenvironment that facilitates delivery of nutrients, oxygen and the necessary growth factors to the encapsulated cells.[60, 107] This effect should occur rapidly within a few hours, to ensure cells are sufficiently supplied with necessary metabolites.

In order to cross-link HA into a solid polymeric network, members of the acrylate family are one of the most utilised modifications.[108-113] There are two common ways of triggering a polymerisation reaction with an acrylate, one is a redox reaction via thiols (Michael-addition reaction)[114], another one is light induced reaction. Michael-addition reactions occur spontaneously, which can be troublesome for clinical application as this is limiting to the application window. Light-induced reactions on the other hand, can be triggered in a controlled fashion. This reaction can be achieved by a radical source, i.e. Irgacure 2595, which emits a radical upon UV light exposure. This radical can attack the alkene group on an acrylate, which itself can lead to a covalent bonding with another nearby acrylate. Although frequently used for research purposes, UV light has raised doubts about its clinical safety, as it can lead to oxidative stress or DNA strand breaks in vital cells, resulting in uncontrolled mutations in those cells affected.[115] Here, clinical manifestation of UV mutagenic effects have been extensively investigated for melanoma skin cancer, where the UV portion of the sun light has been shown to have the potential of trigging several mutagenic changes. Relating to photochemical light exposure used for TE, Ruskowitz

and colleagues have shown that near-UV exposure at 365 nm wavelength has no effect on hMSC proliferation, compared to middle-UV light at 254 nm wavelength, where hMSCs were statistically significantly reduced in proliferation.[116] This indicates, that higher wavelengths (i.e. visible blue light at >400 nm) might be better tolerated by cells. A shift towards higher wavelengths as activator has been done in dental components. Dental composites, fillers and glues are often acrylate based with camphorquinone as photo-initiator, and can be solidified quickly upon exposure to blue light (dental light, 400 - 500 nm wavelength).[117-119]

In order to translate that into an acrylated hydrogel system, novel photo-initiator molecules with good water solubility are required. As promising candidate, Eosin-Y is classified as a visible-light-sensitive photo-initiator, that following excitation with blue light (low frequency band of visibility) can undergo a transition to a triplet state. In this triplet state, one electron is excited to a higher energy level in which it is reactive towards reducing components such as thiolated molecules, transitioning Eosin-Y from red to yellow (Figure 5, top).[120, 121] The created thyil radical then initiates a step-growth photo-polymerisation reaction with the carbon-carbon alkene of the acrylate group, leading to a solidified hydrogel (Figure 5, box). Using low molecular-weight (=short) dithiolated molecules like DTT might limit the cross-linking efficacy. Whereby high molecular-weight molecules (=long) like dithiolated PEG have the potential to interact with moieties in further proximity during the second polymerisation step.

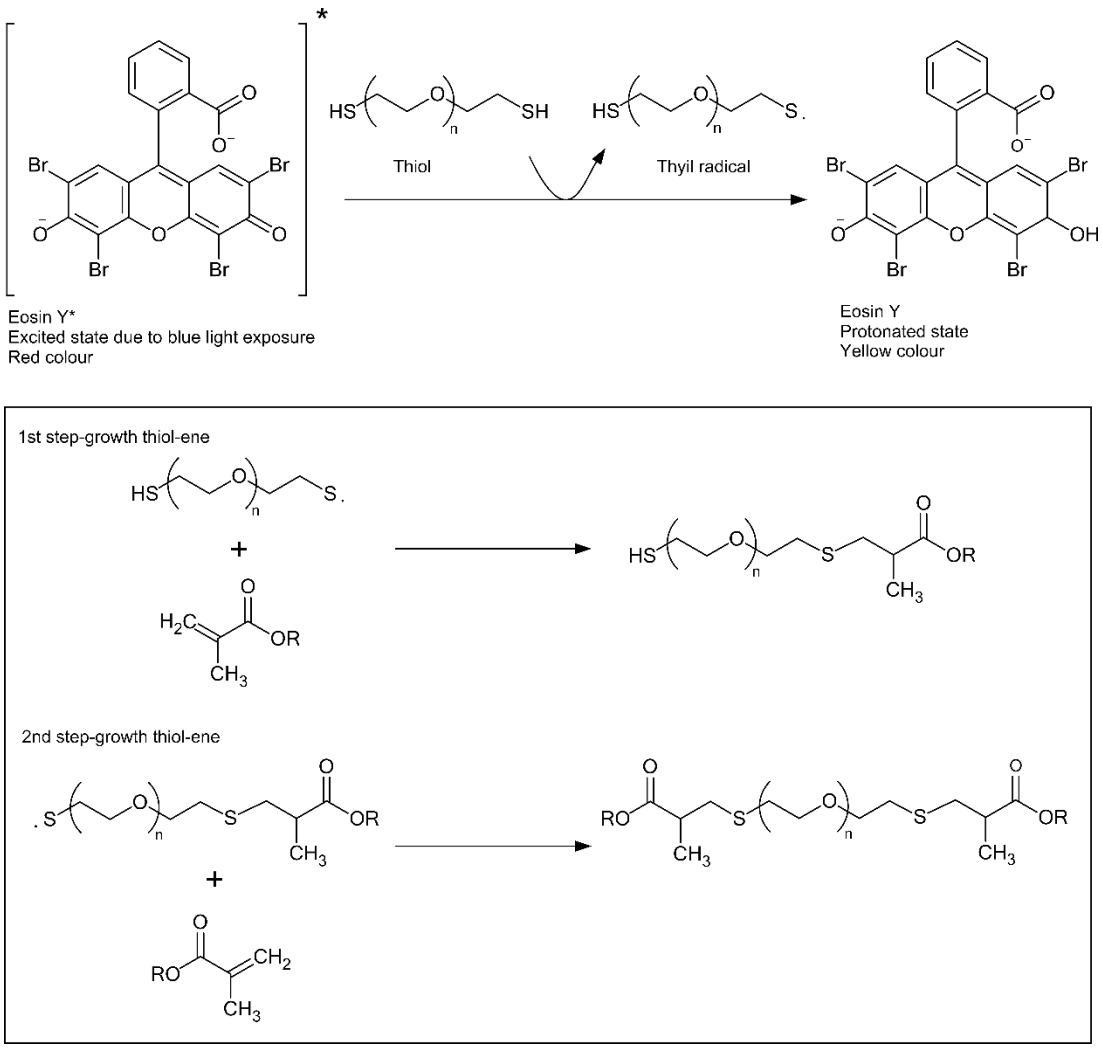

Figure 5: Eosin-Y photo-polymerisation system and thiol-ene cross-link formation. (Top) Schematic representation of radical generation reactions of HS-PEG-SH initiated by photo-induced activation of Eosin-Y. Eosin-Y can be excited upon visible light exposure to a higher energy level in which it is reactive towards reducing components such as thiolated molecules. (box) Polymerisation mechanism for visible-light-mediated thiol-ene photo-polymerisation. The created thyil radical initiates a dual step-growth polymerisation reaction with the carbon-carbon alkene. Other thiolated molecules (i.e. DTT) follow the same mechanism.

Synthesising acrylated macromers usually involves chlorinated solvents.[108, 122-124] Although traces of it might be considered safe for use in other parts of the body, the sensitivity of maxillofacial tissues to toxins leached from biomaterials has been described by Renard and colleagues.[125] This is critical as the facial nerve and

central nervous system are in close proximity to the TMJ. Such cases have made clinicians highly cautious when it comes to using biomaterials in maxillofacial therapies. Chlorinated solvents, particularly trichloroethylene (TCE), perchloroethylene (PERC) and dichloromethane (DCM), have been associated with general neurological toxicity.[126] Indeed, exposure to dichloromethane has been directly linked to facial nerve palsy, which is an important concern, particularly in TMJ application, which is in immediate surrounding of the facial nerve.[127] Even though modern processing techniques might be able to remove these solvents to a clinical grade, avoiding the use of such would eliminate any risk of toxicity and exclude suspicions of clinical end users. Consequently, the synthesis process for this project was designed completely solvent free, creating methacrylated hyaluronic acid (MA-HA) (see 2.2.1).

1.3.3 Importance of dopamination in MA-HA-hydrogel system

Hyaluronic acid as part of the ECM promotes cellular interactions via several transmembrane receptors like CD44 and RHAMM, which have been linked to cell survival and maintaining vital chondrocytes.[128, 129] However, HA is missing integrin binding-sites, which are required for migration and accumulation of cells. Furthermore, HA is lacking capability to adhere to the surrounding tissue.

Classical adhesive agents to foster tissue interaction are mainly based on synthetic (i.e. poly-cyanoacrylate [130], carbodiimide- or genipin-cross-linked gelatine [131]) or natural polymers (i.e. gelatine–N-hydroxysuccinimideactivated poly-L-glutamic acid [132], azide–lactose-modified chitosan [133], fibrin glue [134, 135]). However, those have none to limited application in arthroscopic procedures in the TMJ, as they either release cytotoxic components when degraded, require human-sourced products or would be unpractical for the type of surgery employed here. A more promising technique described by Elisseeff and colleagues[50] is based on research initially

done by Ono and colleagues[133]. Although improved, it is lacking applicability in arthroscopic approaches in the TMJ, as the ‘painted on’ chondroitin sulphate would be washed away in an aqueous inflated joint space before adhesion could take place.

As further described in 1.1.2, catechol modified hydrogels have shown promising results to overcome this limitation. Such catechols are naturally inspired by mussels, which have the ability to adhere strongly to organic as well as inorganic materials in marine saltwater environment. From the six identified mussel-foot proteins (Mfps) known so far, adhesion is caused by Mfp3 and Mfp5, which are abundant in the terminal ends of byssal threads.[53, 136] The adhesion effect is given by 3,4-dihydroxyphenyl-L-alanine (Dopa), an amino acid that represents up to 30 mol% of Mfp-5.[136]

This unique feature is caused by a catechol side group within the Dopa, which is capable of a dual chemistry to form reversible covalent or irreversible non-covalent interactions (see Figure 6).[52] In tissue engineering, catechol chemistry has been sourced for several of its properties. The dihydroxy functionality of catechol is capable of forming strong non-covalent hydrogen bonds with hydroxyapatite (Figure 6A), while the benzene ring of the catechol enables it to interact with aromatic rings and positively charged ions, found in the components of ECM, through $\pi - \pi$ and cation-π interactions (Figure 6B-C), respectively. This allows the material to interact with bone, glass and metals (Figure 6E). Some groups also utilise Dopa to cross-link hydrogel systems. This can be done via iron-ion-particles [137, 138] (Figure 6D) or by actively oxidising Dopa moieties [56, 139, 140] (Figure 6H-I). Oxidising Dopa forms semi-quinone or quinone states, in which Dopa is either reactive towards each other or interacts with nucleophilic moieties like amides ($–NH_2$) and thiols (–SH), which are found in proteins (Figure 6J). Thereby, Dopa performs interaction to either soluble proteins, which would allow integrin-mediated cell attachment, or tissue bound proteins, which would allow tissue interaction.

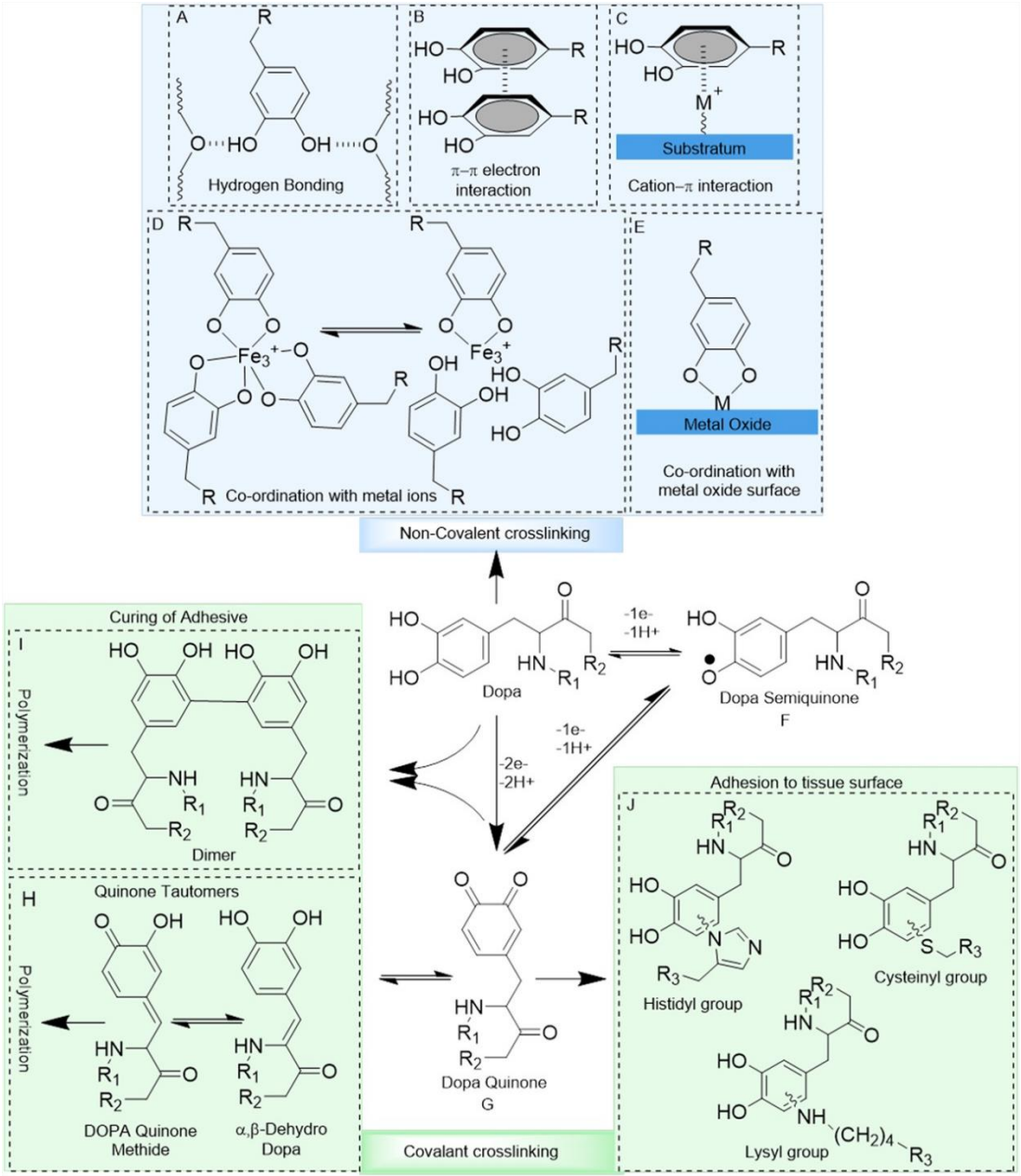

Figure 6: Non-covalent (blue) and covalent (green) interactions of Dopa catechol. ([52], modified)

In its reduced form catechols can interact non-covalently via: hydrogen bonds with its OH groups (A), π–π electron interactions with benzene rings (B), cation–π interactions with positively charged ions (C), chelates metal ions (D) and forms co-ordination bonds with metal oxide surfaces (E). In its oxidised state, Dopa creates semiquinone and quinone forms, which facilitate covalent interactions (F and G). Quinones can polymerise with each either by tautomersiation via quinonemethide and α,β-dehydrodopa formation (H) or by directly forming dimers with another catechol moiety (I). Quinones also react with various nucleophiles (i.e., –NH_2, –SH) found in proteins, which can lead to tissue adhesion (J).

In neutral pH range, catechols are usually fluctuating between (semi-)oxidised and reduced state. Consequently, acidic pH would tilt this balance towards a more reduced equilibrium (non-covalent interactions), basic pH towards an oxidised equilibrium (covalent interactions). pH therefore plays a crucial role during synthesis and storage. When applied bound to a hydrogel-network in an *in vivo* system, Dopa might be locked in the oxidised state, when it reacts with proteins and peptides alike. As this reaction is covalent, the Dopa may not be able to fall back into its reduced state. This effect is referred to here as auto-oxidation. A similar effect can be reached by using oxidising agents like sodium periodate.[54-56] However, such agents might be hard to apply within the liquid surrounding of an arthroscopic TMJ surgery and would limit the time window to apply the construct. Considering this, auto-oxidation of Dopa might be favourable for such a clinical approach.

1.3.4 Evaluating cellular matrix secretion within 3D hydrogels

Tissue-forming ability of regenerative materials is often assessed by the amount of matrix produced and secreted by cells present. Recent studies have shown that human mesenchymal stromal cells 3D-encapsulated within hydrogels have the ability to swiftly modify their local surroundings. They do so by degrading the hydrogel and replacing it with secreted proteins within their immediate pericellular space.[141-143] Consequently, techniques to characterise and visualise secreted pericellular matrix within hydrogels are essential to compare cellular behaviour, exposed to different chemical and physical conditions. Ultimately, this is crucial to evaluate potential regenerative therapies.

As gold-standard, immunostaining methods allow to visualise the location of specific proteins within tissues and hydrogels.[144] Still, in order to choose appropriate antibodies, such techniques require prior knowledge of the proteins targeted. In addition, these methods are time-consuming and expensive. Therefore, initial knowledge of potential composition of this secreted matrix might allow a limitation of the vast range of antibodies to choose from, which ultimately could reduce overall effort needed for immunostaining methods. Other approaches like mass spectrometry are utilised for various proteomics techniques, which are capable of identifying proteins within a sample.[145] Although a powerful tool, proteomics often lacks positional information. More advanced techniques combine desorption electrospray ionisation (DESI) with mass spectrometry[146] and emerging single cell proteomics techniques[147]. Such applications would overcome the limitation of missing special information, however, these approaches require highly specialised equipment and remain too expensive for high-throughput purposes. Hence, novel systems or a combination of already existing techniques, that are inexpensive, accessible and can provide information about the distribution and composition of the secreted matrix are desirable.

Fluorescent non-canonical amino acid tagging (FUNCAT), is based on the principle of replacing a canonical amino acid in cell culture medium with an analogue containing a bio-orthogonal functional group to which a fluorophore can be “clicked”[148]. FUNCAT is available as highly reliable and cost-effective kits. FUNCAT allows for 3D visualisation of proteins that have been translated whilst cultured with the amino acid analogue, allowing spatial imaging of the secreted matrix with minimal further manipulation. FUNCAT is used by several groups to investigate pericellular matrix formation.[63, 141, 143]

Raman spectroscopy is based on the inelastic scattering of monochromatic light that has been used to identify the biochemical composition of single cells[149], as well as tissues[150, 151] and matrix formed by cells *in vitro*[152-155]. Raman spectroscopy does not require additional staining methods and has the power to distinguish between biologics like proteins, lipids, and nucleic acids. Furthermore, it is inexpensive and accessible to many research facilities.

Combining FUNCAT with Raman spectral imaging, would allow to create 3D spectral and fluorescence maps of hMSC and their secreted matrix when encapsulated within hydrogels. Both techniques are simple, unbiased, inexpensive methods that require little manipulation and permit imaging without the need for sample sectioning. As such, the combination of both approaches should provide enough information to assess the effect of different hydrogel compositions and DMOG upon hMSCs ability to secret matrix. Quantitative and qualitative analysis can be done by signal intensity as well as distance of signal from the cell membrane.

1.3.5 Aims of thesis

Considering different TE tactics available, a combined cell-material strategy has been approached for this project. Subsequently, double-modifying HA with methacrylate as well as Dopa may present several beneficial effects for minimal invasive application in TMJ surgery. The macromer is synthesised avoiding potentially harmful reagents. It can be applied via syringe and withstands an aqueous environment similar to that during arthroscopic TMJ procedures. Furthermore, application and solidification does not require special training or equipment. As it is photo-polymerised, the material remains viscous and can be manipulated until light is applied. Eosin-Y also functions as an indicator, as it changes colour during the polymerisation process. Dopa as biological functional group, will oxidise without addition of reagents, decorating itself with soluble proteins and interact with neighbouring proteins within tissues.

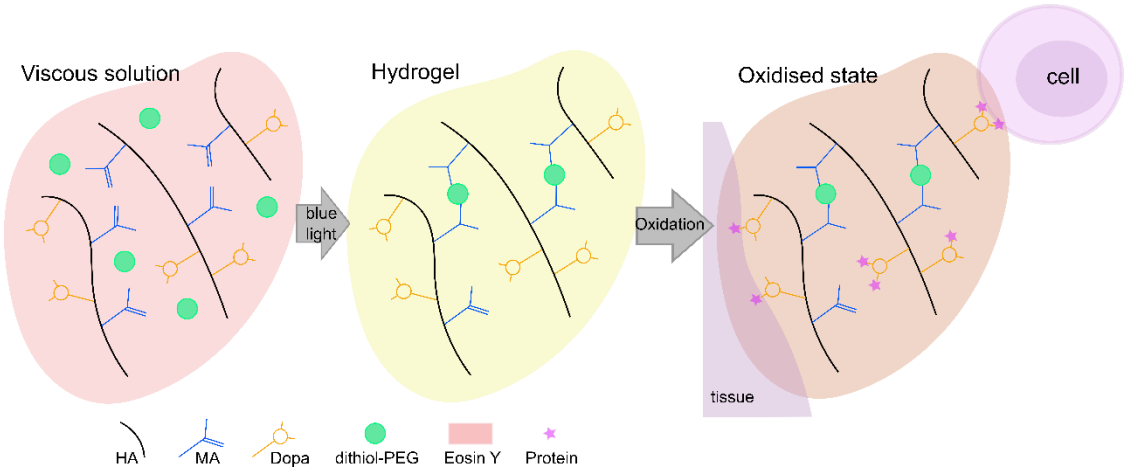

Figure 7: Schematic showing application, formation and oxidation of MA-HA-Dopa hydrogel.
Upon blue light exposure, Eosin-Y deprotonates di-thiol PEG, allowing it to react with methacrylate moieties on HA leading to a formation of kinetic chains. This process reduces Eosin-Y to a colourless state. Following Dopa oxidation impacts protein, cell and tissue interactions with hydrogels. This coincides with a characteristic brownish change of colour of the catechol groups.

Concluding therefrom, specific aims for this project cover the following:

A) Development and characterisation of MA-HA-Dopa hydrogels.

Aa) Synthesise double-modified HA-macromers with MA and Dopa moieties.

Synthesis is going to be established for double-modified MA-HA-Dopa macromers using a fully aqueous reaction protocol. Furthermore, the modification reaction will be optimised to achieve reproducible degrees of modification (DOMs) by investigating several buffers as well as manual pH adaption during the methacrylation process. Ensuring the dopamine is maintained in its reduced form is central because under basic conditions, the catechol functional group can form a semi-quinone or quinone.[156] Quinone is highly reactive and can form dimers with other catechols, potentially cross-linking MA-HA-Dopa macromeres prematurely during the synthesis process.[157] Varying the conditions for those reactions, a range of HA-macromers with total DOMs from 0 to 50 % will be produced. Confirmation of successful modification and determination of DOM is going to be performed with ^{1}NMR.

Ab) Characterise hydrogels for mechanical and physical properties.

A range of mechanical, physical and chemical properties can be limiting for the use in arthroscopic approaches in the TMJ.

- Viscosity has to be tailored to a certain range for optimal use in arthroscopic approaches. Addition of unmodified 1 MDa HA is expected to increase viscosity of MA-HA and MA-HA-Dopa precursor solutions significantly. Viscosities reached are supposed to be in a range of 10 to 20 Pa·s, which is similar to commercially available dental materials.[158] Gelation kinetics and bulk stiffness are going to be assessed via time-sweep rheology. Clinically relevant materials are required to solidify rapidly within <4 minutes exposure to standard clinical blue light. Shelf-life

is an important factor here as well. Precursor solutions are expected to reach similar bulk stiffnesses after being stored for longer than 24 hours. Here, RT as well as 4 ˚C (fridge) storage temperatures are investigated, reflecting potentially necessary conditions for when cyto-active components are incorporated into the precursor solution.

- Mass swelling and degradation are critical factors for evaluating hydrogels. Swelling and degradation are reflecting a behaviour of the bulk gel by liquid influx and the following degradation of the matrix due to cellular (i.e. enzymes) and mechanical influence (i.e. shear forces). Swelling is going to be assessed gravimetrically by determining the increase in wet-weight of the bulk hydrogels over time. Following, enzymatic degradation via hyaluronidase is going to be quantified by carbazole assay. Here, HA degradation products are detected in the gel-surrounding fluid by colorimetric changes using photometry.
- Oxidising Dopa moieties should facilitate cell and tissue interaction. In order to allow a certain time-frame for application, Dopa should self-oxidise after several hours. Oxidation is going to be determined qualitatively by characteristic colour change to brown. This will further be proven quantitatively over time by creating photometric absorption profiles of MA-HA-Dopa macromers. Oxidised catechols are supposed to have increased light absorption in a range between 250 to 450 nm wavelength. Comparing normoxic and hypoxic conditions is investigating catechol behaviour under cartilage-specific oxygen levels.

Ac) Optimisation for clinical use

Feedback on the surgical approach and material properties are given by maxillofacial surgeons, dentists and ENT specialists. This includes constant input during the material development. Combined with literature accessible on conventionally available materials, this should maximise the potential for

clinical translation. The effort is focused mainly on the synthesis (potential hazardous components, current use of materials in clinics; see (Aa), page 42) as well as the mechanical and physical characteristics (viscosity, gelation behaviour, preparation and storage, as well as material handling; see (Ab), page 42).

B) Cell and tissue interaction

Ba) Cytotoxicity and 3D cell survival

Firstly, all components of the hydrogel are required to be fully tolerated by human cells, showing no cytotoxic effect. Cytotoxicity is a key characteristic to be considered and is regulated by ISO 10993-1.[159] A range of concentrations of those components shall be tested via MTT assay to confirm absence of any toxicity. Secondly, the encapsulation of primary human cells is supposed to support cell survival, which considers mechanical forces (shear forces during mixing with hydrogel solution and application through needle) as well as physical forces (irradiation with blue light and potential local increase in temperature). Cell survival is going to be determined by L/D staining.

Bb) 2D cell attachment

Cell attachment could allow cell infiltration, which might sustain techniques like micro-fracturing. Stable cellular interaction (i.e. via integrins) with MA-HA-Dopa hydrogel will be proven via 2D attachment experiments. During a short incubation time, Dopa can bind soluble proteins, which further allow cell interaction with the hydrogel. Hydrogel formulations lacking Dopa moieties cannot support such stable interactions resulting in cells being washed off the MA-HA hydrogel surface.

Bc) Tissue adhesion

Interaction with surrounding host tissue might permit the hydrogel to withstand external forces and could facilitate adhesion of the neo-tissue formed. Similarly as for the cell attachment experiments, oxidised Dopa will interact with proteins in the tissue available. This effect shall be shown qualitatively by application of force to a tissue-hydrogel interface. Catechol-mediated adhesion is supposed to allow a transition of the displacement to the hydrogel, without rupture of the interface. Quantitative assessment is going to be performed via push-out tests. Hydrogels will be applied within a tissue biopsy. The weight necessary to push them out is going to be recorded and translated into force. Dopamination is supposed to statistically significantly increase the force necessary to drive the hydrogel out of the native tissue.

C) Intra- and extracellular matrix formation

In order to structurally and functionally restore tissue, cells have to produce and secret matrix components. This goes hand in hand with the degradation of the hydrogel matrix. Primary human mesenchymal stem cells from bone-marrow aspirates are going to mimic cellular behaviour (i.e. sourced via microfracturing). Therefore, these cells will be encapsulated in different MA-HA-Dopa hydrogels and their ECM production shall be analysed via the following techniques:

Ca) Non-canonical amino-acid tagging will report distance of newly synthesised proteins from the cell membrane.[160] This technique will allow to draw conclusions about cellular behaviour (production of proteinaceous content intracellular and extracellular) as well as about hydrogel behaviour in an *in vitro* setting (pore size and potentially degradability). Protein production and distance of secretion from cellular membrane is going to be compared between different hydrogel compositions.

Cb) Raman spectroscopy is going to be utilised to analyse cellular and extracellular components and resolve them for their chemical structure. In line with data from non-canonical amino-acid tagging, this should investigate the differences of protein production between various hydrogel compositions. Work with the Raman set-up is going to be performed by collaborating PhD student Anders Runge Walther (University of Southern Denmark). Credit for experimental execution and data analysis goes to him.

2 Materials & Methods

2.1 Materials and equipment

Unless otherwise stated, chemicals purchased were all of analytical grade. Materials used for cell culture were either purchased sterile or sterile filtered using a 0.22 µm syringe filter.

Table 1: Reagents and material for synthesis and characterisation of acellular hydrogels

Reagent/Material	Abbreviation; Specification	Manufacturer; Country of Origin
1,4-dithiothreitol	DTT	Sigma-Aldrich
2′,4′,5′,7′-Tetrabromofluorescein	Eosin-Y	Fisher Scientific
3-(4,5-Dimethyl-2-thiazolyl)-2,5-diphenyl-2H-tetrazolium bromide	MTT	Sigma-Aldrich
Anti-biotic/anti-mycotic solution	ABAM	Gibco Life Technologies
Borosilicate cylindrical glass moulds, 4 mm inner diameter		SciQuip Ltd
Carbazole		Sigma-Aldrich
D-glucuronic acid sodium salt monohydrate		Sigma-Aldrich
Dopamine hydrochloride		Sigma-Aldrich
high molecular weight hyaluronic acid sodium salt (1 MDa)	HA (1 MDa)	Sigma-Aldrich
hyaluronic acid sodium salt	HA; 100 - 150 kDa; 1 g per batch	LifeCore Biomedical; Chaska, USA
hyaluronidase (HAse, type I-S, from bovine testes)	HAse; 400-1000 $U \cdot mg^{-1}$	Sigma-Aldrich
Linear dithiol-Poly(ethylene glycol) (1 kDa)	PEG; 1 g	JenKem Technology
Magnesium Fluoride slides	MgF_2 slides	Crystran Ltd., Dorset, UK
methacrylic anhydride		Santa Cruz Biotechnology
N-(3-Dimethylaminopropyl)-N′-ethylcarbodiimide hydrochloride	EDC	Sigma-Aldrich

N-hydroxysuccinimide	NHS	Sigma-Aldrich
Pur-A-Lyzer (Mega 3500)		Sigma-Aldrich
Sigmacote® siliconizing reagent		Sigma-Aldrich

Table 2: List of equipment used

Equipment	Specification	Manufacturer; Country of Origin
532 nm laser	Torus 532	Laser Quantum, Stockport, UK
Bruker Avance NMR spectrometer	400 MHz	Bruker
Charge coupled device	PIXIS100B	Teledyne Princeton Instruments, Birmingham, UK
CLARIOstar 430-0768		BMG Labtech
Confocal laser scanning microscope	DM16000	Leica
Dichroic mirror		Semrock
Fiber collimator		Thorlabs Inc., Ely, UK
Fiber coupler	50 µm core, low OH optical fiber	Thorlabs Inc., Ely, UK
Fluorescent microscope	CSE2100	Thorlabs Inc., Ely, UK
Holographic spectrometer	HS-HSG-532-LF, Andor HoloSpec	Andor, Belfast, UK
Laser fibre	125 µm cladding single mode fiber	Laser Quantum, Stockport, UK
Magnesium Fluoride glass slides		Global Optics UK
OmniCure light system S1500		Lumen Dynamics
QHL75 dental curing light		Dentsply
Thermomixer		Eppendorf
Water immersion objective	60x/1.0NA, CFI Apo NIR 60X W	Nikon, Melville, USA

Table 3: Reagents and components for characterisation of cell-encapsulated hydrogels

Cells/Reagent	Abbreviation; Specification	Manufacturer; Country of Origin
17IA4 cell line	mouse dental pulp cells	
Alpha MEM medium	#BE0-002F	Lonza
Click-iT™ HPG Alexa Fluor™ 594 Protein Synthesis Assay Kit	#C10429	Invitrogen
DMEM medium	#31053-028; high glucose, no glutamine, no phenol red	Gibco Life Technologies
Fibronectin	From bovine plasma	Sigma-Aldrich
Foetal bovine serum	FBS; heat inactivated	Gibco Life Technologies
hMSC (also: hMSC)	Human primary bone marrow aspirate	
HCS CellMask blue staining	#H32720	Invitrogen
MEM Alpha medium	#41061-029	Gibco Life Technologies
Recombinant human fibroblast growth-factor	rhFGF; 175 aa	R&D Systems
Insulin-Transferrin-Selenium-solution	ITS-G; 100x; #41400045	Gibco Life Technologies
Recombinant human transforming growth-factor β3	TGF-β3; #100-36E	Peprotech

2.2 Development and characterisation of MA-HA-Dopa hydrogels

2.2.1 MA-HA and MA-HA-Dopa macromer synthesis

MA-HA-Dopa was synthesised using two sequential reactions. For MA-HA, the second synthesis step was omitted, and the protocol followed from dialysis onwards. The methacrylation reaction (MA-HA) was adapted from previous reports (see Figure 8).[124] Briefly, HA (100 – 150 kDa) was reacted with a 20-fold excess of methacrylic anhydride relative to primary HA hydroxyl groups in an aqueous environment (pH 8). The pH was monitored continuously for 4 h at room temperature (RT) and adjusted by addition of NaOH, every 20 minutes. The reaction was then allowed to proceed for a further 20 h at 4 ˚C. Degree of modification was controlled by varying the amount of methacrylic anhydride (1:1 to 1:3, HA to methacrylic anhydride). HA was precipitated with ice-cold ethanol (5-fold excess) and the solution incubated on a tube roller for 10 minutes at RT. Precipitated HA was spun down at 2,025 g for 15 minutes and the resultant pellet washed excessively with ice-cold ethanol. MA-HA was dried under vacuum and resuspended in dH_2O (pH 5).

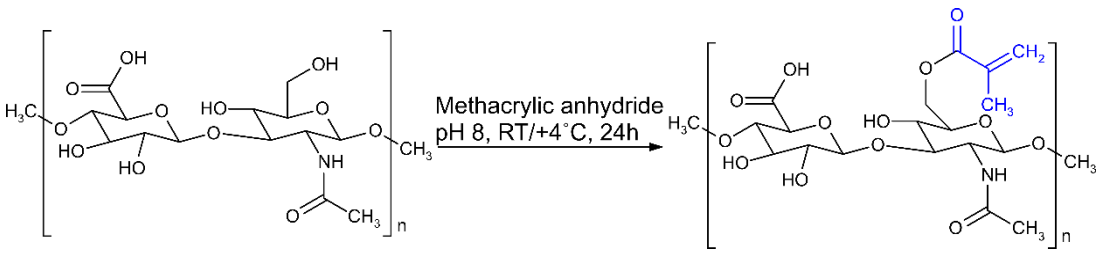

Figure 8: MA-HA synthesis.
Synthesis of MA-HA macromers through reaction of HA with methacrylic anhydride at a basic pH 8.

The degree of methacrylation was confirmed by proton NMR and defined as the number of substituents per 100 hydroxyl groups in HA. This was determined by integrating the signals at δ 5.68 and 6.13 ppm ($C=CH_2$ of the conjugated methacrylate) and comparing to the peak at δ 2.1 ppm ($C(=O)CH_3$ in HA).

$$\text{Degree of methacrylation } [\%] = \left(\frac{I^{\delta H\ 5.68} + I^{\delta H\ 6.13}}{2} \div \frac{I^{\delta H\ 2.10}}{3} \right) \times 100$$

The dopamination reaction (MA-HA-Dopa) was carried out using a modified protocol to that reported previously (see Figure 9).[161] Briefly, MA-HA was dopaminated via a carbodiimide coupling reaction using EDC/NHS. The degree of dopamination was controlled by varying the MA-HA dopamine hydrochloride ratio from 1:0.5 to 1:2 and was allowed to proceed for 4 h (pH 5) in the dark. The double-modified macromer was purified via dialysis using 3.5 kDa MWCO tubing in acidic buffer (pH 5, HCl) for 48 h, followed by dH_2O for 24 h. Buffers were replaced twice a day. The final product was lyophilized and stored at -20 ˚C, protected from light.

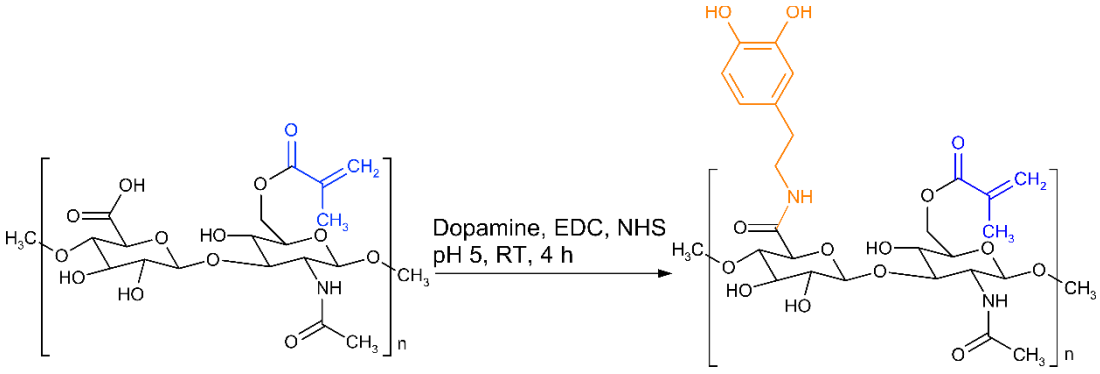

Figure 9: MA-HA-Dopa synthesis.
Synthesis of MA-HA-Dopa macromers through EDC/NHS facilitated reaction of MA-HA with dopamine at an acidic pH 5.

The degree of dopamination was analysed by proton NMR to confirm the presence of characteristic peaks of catechol at δ 6.5 - 7.2 ppm, which correspond to the ortho and meta coupling position of the ring. The degree of dopamination was defined as the number of substituents per 100 carboxyl groups in HA and determined by integrating the signals at δ 6.5 - 7.2 ppm compared to that of the peak at δ 2.1 ppm ($C(=O)CH_3$ in HA).

$$\text{Degree of dopamination } [\%] = \left(\frac{I^{\delta H6.5\text{-}7.2}}{3} \div \frac{I^{\delta H2.1}}{3} \right) \times 100$$

MA-HA reaction is strongly pH dependent, whereby the driving force is a basic pH. The amount of MA moieties bound to HA is thereby determined by the total amount of excess hydroxyl radicals provided throughout the overall reaction time of 24 h. During the binding process, those free radicals are exhausted, returning the pH towards neutral. As shown in Figure 10, the reaction is based on an acyl substitution mechanism. Hereby, the nucleophilic hydroxyl group of HA targets a carbonyl group of methacrylic anhydride. The subsequent deprotonation of methacrylic anhydride leads to a collapse of this intermediate state. This results in one part of the methacrylic anhydride being linked to the former hydroxyl group of the HA macromer. The availability and amount of free hydroxide is driving the reaction forward, directly influencing the resulting DOM. Subsequently, performing this reaction step under controlled alkaline conditions is critical. pH 8 was chosen as optimum, as higher pH values tend to induce hydrolytic degradation of HA.[162]

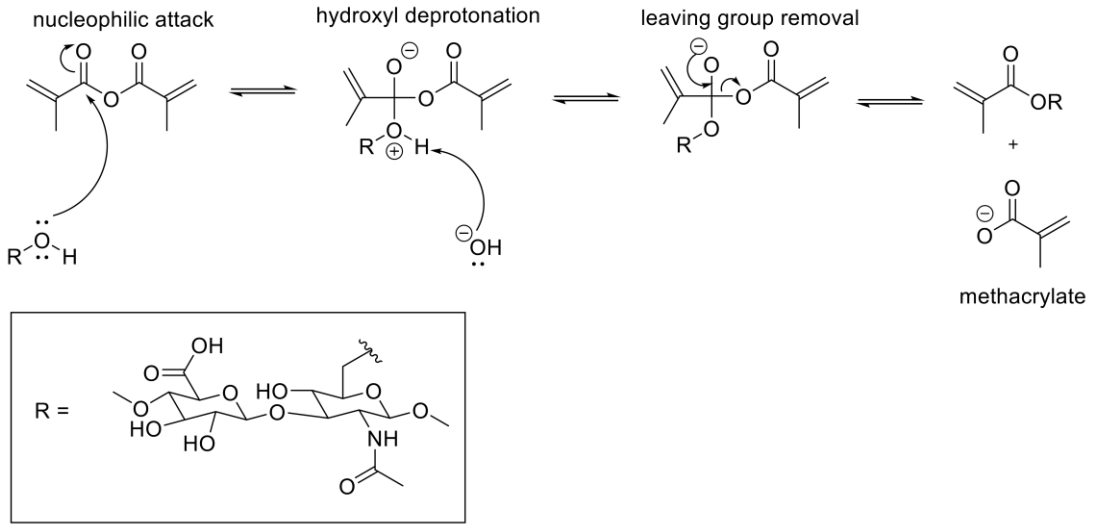

Figure 10: The nucleophilic acyl substitution mechanism for methacrylation reaction. The reactive OH-group on HA is proposed to be the primary alcohol at the 6-position of the N-acetylglucosamine sub-unit.

In order to create a reproducible protocol for the methacrylation reaction (see Figure 11), pH was adjusted to 8 with NaOH every 20 minutes during the first 4 h of incubation at RT (dashed lines). Following incubation at RT with repeated pH adaption, pH 8 was set before 20 h of reaction at +4 ˚C was carried out without further pH adjustment.

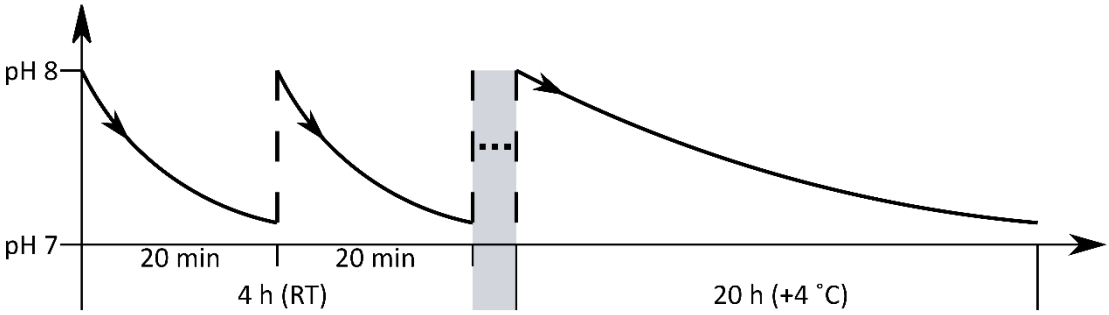

Figure 11: Timeline for macromer synthesis with manual pH adjustment. Methacrylation reaction was performed in deionised water with the pH being manually adjusted to 8.0 using NaOH solution. Adaption of pH (dashed line) was done every 20 minutes for 4 h at RT, following 20 h at +4 ˚C without further pH adjustment. pH levels tended to decrease towards a neutral level over time (full line).

To optimise the handling of pH adjustment, buffer solutions were tested.

Using 1 M MOPS buffer (3-(N-morpholino)propanesulfonic acid; pKa = 8.07), MOPS (23.12 g) was dissolved in deionised water (90 mL). The pH was titrated to pH 8 by addition of HCl and topped up with dH_2O to a total of 100 mL.

Using 0.6 M tris buffer (tris(hydroxymethyl)aminomethane; pKa = 8.06), Tris base (7.27 g) was dissolved in deionised water (90 mL). The pH was titrated to pH 8 by addition of HCl and topped up with dH_2O to a total of 100 mL. For 0.3 M tris buffer, 0.6 M tris buffer was diluted 1:1 with dH_2O.

The following HA-HA-Dopa reaction is catalysed via EDC/NHS coupling reaction (see Figure 12). EDC is known to facilitate coupling reaction of carboxyl groups with primary amines, by forming a reactive O-acylisourea intermediate of a carboxyl group.

This intermediate stage tends to be unstable and benefits from further reaction with NHS, which forms a more stable NHS ester group. Consequently, this amine-reactive form can react with a primary amine (of the dopamine), allowing sufficient coupling.

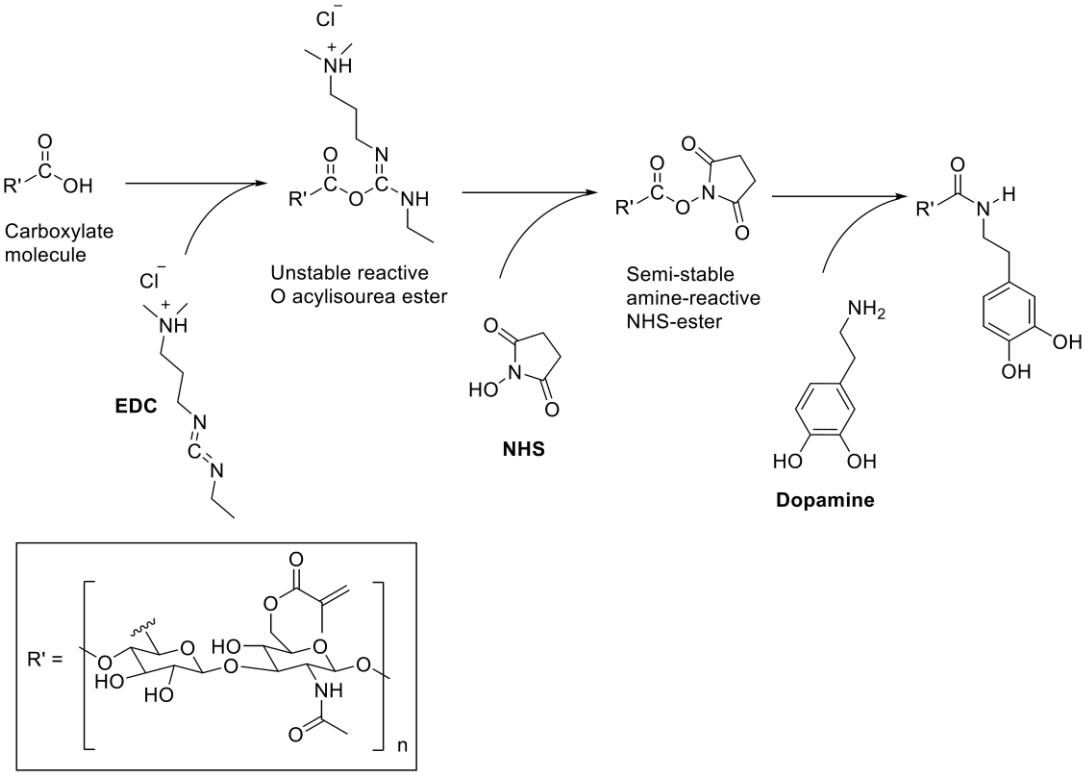

Figure 12: EDC/NHS coupling reaction for dopamination.
EDC reacting with carboxylic acid of HA to form an unstable intermediate that was further stabilised with NHS. This complex can react further with the primary amine of dopamine to conjugate HA and dopamine together.

Although EDC/NHS reaction could be performed under neutral pH conditions, the catechol groups of the dopamine tend to oxidise upon exposure to free protons (i.e. pH level or light). Carrying out the reaction under pH 5 and protected from light, preserves the reduced state of these reactive groups.[163]

Corresponding to the degree of modification, macromers were classified as no/low/high Dopa and low/high MA (see Table 7 page 71). All macromers have been modified with MA groups resulting in low or high DOM. For Dopa, there is also low or high DOM, with some macromers not being dopaminated at all. These allowed to

investigate any influence and characteristics caused by the Dopa. However, as MA-HA hydrogels do not provide sites to stably interact with cells or tissues, MA-HA-Dopa hydrogels exclusively were considered for biological experiments.

2.2.2 Fabrication of acellular hydrogels

MA-HA-Dopa and MA-HA macromers aliquoted in amber glass vials got sterilised with 54 kGy gamma irradiation and stored at -20 ˚C until further use. Hydrogels were formed via step-growth polymerisation by blue light (400 - 500 nm, 500 $mW \cdot cm^{-2}$), facilitated by dithiol-PEG or DTT (65 mM) and Eosin-Y (154 µM; 0.01 wt%) in phenol-free cell culture media (660 µL). Dithiol/ Eosin solution was sterilised using 0.22 µm syringe filters. Macromers (1 or 3 %) were dissolved in dithiol/Eosin solution on an Eppendorf Thermomixer (1,400 rpm) at 37 ˚C. In some samples, unmodified 1 MDa HA (2 %) was added, to increase the viscosity. Hydrogels were then cast into cylindrical glass moulds that had been pre-coated with Sigmacote® (following the manufacturer's protocol) and exposed to blue light (4 minutes).

2.2.3 Viscosity

To determine the viscosity of the macromer solutions, measurements were carried out in triplicates on a HAAKE™ CaBER™ 1 Capillary Breakup Extensional Rheometer. Sample volumes of 100 µL were loaded and data acquisition was performed at RT. Measurements were done from 0 to 20 Pa·s. Values are reported at strain 9 Pa·s.

2.2.4 Gelation kinetics and bulk stiffness

The time until gelation upon application of blue light (gelation kinetics) and bulk stiffness reached after certain time of exposure was measured on a strain-controlled ARES rheometer (TA Instruments).

150 µL viscous macromer solution was loaded onto an 8 mm parallel plate geometry (see Figure 13). Dynamic time-sweep experiments were performed at a fixed frequency (6.28 rad·s^{-1}) and strain amplitude (0.5 %) and a temperature of 25 °C controlled by a Peltier unit. The solution was placed on the rheometer plate, and after 60 seconds, the sample got exposed to light using the OmniCure system with a 5 mm fibre-optical light guide and an intensity of 500 mW·cm^{-2}. Measurements were carried out for a total of 10 minutes. Gelation time was determined by the cross-over between the storage modulus (G') and the loss modulus (G''). G' was determined from time-sweep curves. Bulk stiffness got analysed for 4 minutes light exposure (set as clinically relevant time) and 9 minutes light exposure (maximum bulk stiffness).

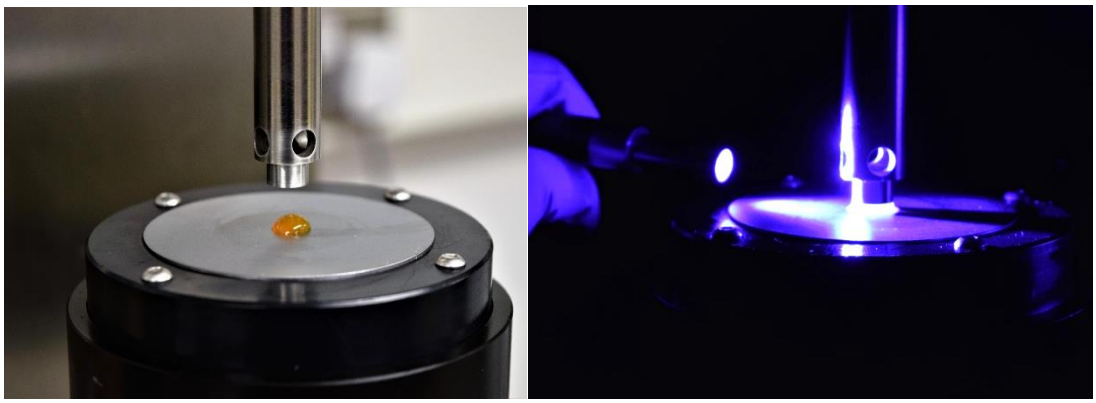

Figure 13: Rheology set-up to evaluate gelation kinetics and bulk stiffness.

2.2.5 Shelf-life

Shelf-life of viscous precursor solution was determined via dynamic time-sweep rheology. The bulk stiffness has been set as indicator to reflect shelf-life, comparing the change of stiffness over time. Solutions of 3 % MA-HA and MA-HA-Dopa (low/high MA, no/low/high Dopa, see Table 7 page 71) without 1 MDa HA, were prepared and stored either at either RT or in the fridge (4 ˚C). Samples have been taken after 1 day and 8 days, respectively, and measurements were performed as previously described (see 0 page 56), with a total of 9 minutes blue light exposure. Values recorded got normalised to values of freshly prepared solutions at day 0 (Table 12 page 140) and reported as % of initial stiffness G'. Data (n = 3) was analysed via two-tailed Mann-Whitney test.

2.2.6 Mass swelling ratio

Hydrogel mass swelling was evaluated via gravimetry. 50 µL cylindrical hydrogels were formed in pre-weighed 10 mm petri dishes, submerged in PBS containing 1X anti-biotic/anti-mycotic solution (ABAM), and incubated at 37 ˚C for 72 h. PBS was removed at 2, 6, 24, 48 and 72 h, wells blotted dry and the sample weighed. Experiment has been performed under sterile conditions. Swelling (Q_W) was quantified using the following equation where W_t is the weight of the swollen hydrogel and W_0, the initial dry weight.

$$Q_W[\%] = \left(\frac{W_t - W_0}{W_0}\right) \times 100$$

2.2.7 Enzymatic degradation

To assess enzymatic degradability, swollen hydrogels were placed in 48-well suspension plates in a hyaluronidase (HAse) solution (10 $U \cdot mL^{-1}$) in PBS with ABAM (1 %) and incubated at 37 ˚C under standard conditions. HAse was replaced with freshly prepared solution every 24 h. Samples have been stored at -20 ˚C. Degradation products of HA were quantified by carbazole assay.[164] Briefly, 50 µL of the degradation solution got added to a solution of sodium tetraborate decahydrate (25 mM) in concentrated sulfuric acid (200 µL) and heated to 99 °C for 15 minutes. Carbazole (0.125 %) in absolute ethanol (50 µL) was then added and solutions briefly vortexed. After heating to 99 ˚C for 15 minutes, absorbance of the solution was measured on a colorimetric plate reader at 530 nm. The amount of D-glucuronic acid has been determined using solutions of known concentrations of the D-glucuronic acid sodium salt monohydrate in PBS.

2.2.8 In aqua application

To demonstrate the hydrogels ability be applied and solidify under aqueous conditions, viscous solution (3 %, high MA, low Dopa, no 1 MDa HA) was pipetted into a cylindrical mould while fully submerged in water. The material settled to the base of the mould and was gelled with blue light. The hydrogel was removed from the mould after 4 minutes light exposure.

2.2.9 Dopa oxidation

MA-HA-Dopa and MA-HA macromers were dissolved in cell culture media (phenol red-free) and incubated at 37 ˚C under standard or hypoxic (5 % O_2) conditions for 72 h. Aliquots were taken at 4, 24, 48 and 72 h. Oxidation was assessed by measuring absorbance at 250 - 550 nm. All samples were blanked against PBS or cell culture media (no phenol red).

2.3 Cell and tissue interaction

2.3.1 Cytotoxicity

To determine cytotoxicity of components freely available in the viscous precursor solution (before solidification), Eosin-Y as well as PEG and DTT were tested with a direct cytotoxicity assay. Therefore, 17IA4 dental pulp cells were grown in Alpha-MEM media, supplemented with ABAM (1 %) and FBS (10 %).[165] Cells were cultured to 80 % confluency and then seeded in 96-well plates at a density of 22,000 cells·cm^{-2}. Eosin-Y was tested from 0 - 0.3 wt%, PEG and DTT from 0 - 10 mM. Reagents were dissolved in cell culture media and applied to cells. 3-(4,5-dimethylthiazol-2-yl)-2,5-diphenyltetrazolium bromide (MTT) assay was performed 20 h later, according to the manufacturer's instructions.

To evaluate cell compatibility with solid hydrogels (after solidification), indirect cytotoxicity tests were carried out according to ISO10993-12:2009.[166] Hydrogels were prepared using either DTT or dithiol PEG, immersed in cell culture medium with a surface to volume ratio of 0.5 cm²·mL^{-1}, and incubated for 72 h under standard cell culture conditions to create conditioned media. 17IA4 dental pulp cells were seeded in 96-well plates at a density of 22,000 cells·cm^{-2}. Conditioned media was applied to the cells, and an MTT assay has been performed after 20 h, according to the manufacturer's instructions.

2.3.2 hMSC expansion and maintenance

Human tissues were obtained from the Imperial College Healthcare Tissue Bank (HTA license 12275), which is supported by the National Institute for Health research Biomedical Research Centre at Imperial College London (12/WA/0196). Samples have been issued from sub-collection R16052. hMSC were isolated from bone marrow aspirates collected from the iliac crest of healthy paediatric donors with informed consent of their parents.[142] Cells were cultured in αMEM cell culture

media with FBS (10 %) and rhFGF (5 ng·mL^{-1}) under standard conditions. At approximately 80 % confluency cells were trypsinised and expanded up to passage 7.

2.3.3 Fabrication of cell encapsulated hydrogels

In order to form hydrogels that contained encapsulated cells, a viscous solution was prepared according to 2.2.2, with double the concentration of macromer (2 or 6 %) and dithiol/Eosin solution (130 mM/308 µM). Cells were trypsinised, counted and diluted accordingly so the viscous solution and cell solution could be mixed 1:1. Cells added to the dissolved macromer were homogenised on an Eppendorf Thermomixer with 180 g for 15 minutes at 37 ˚C.

Chondrogenic induction media was composed of DMEM (high glucose, no phenole-Red, no glutamine, no methionine, no cystine) supplemented with L-glutamine (2 mM), Dexamethasome (100 nM), Insulin-Transferrin-Selenium-solution (1 %), ABAM (1 %), ascorbic-acid-2-phosphate (50 µg·mL^{-1}), L-proline (40 µg·mL^{-1}) and TGF-β3 (10 ng·mL^{-1}).

In order to increase chondrogenesis of hMSCs, DMOG (200 µM; 35 µg·mL^{-1}) has been added to the induction media.[21]

2.3.4 2D cell attachment

MA-HA and MA-HA-Dopa hydrogels were formed with additional 5 mg fibronectin per mL hydrogel solution, to provide RGD binding sites for cellular integrin interaction. 150 µL hydrogels were cast in 6-well suspension plates and Sigmacote®-treated coverslips placed over them. 17IA4 mouse dental pulp cells (2.5×10^5 cells·cm^{-2}) were seeded on top of each hydrogel and incubated for 2 h at 37 ˚C under standard conditions (normoxia; 18 – 21 % oxygen) before being topped up with 2 mL media. After 16 h, gels were rinsed with pre-warmed media to remove non-attached cells. Samples were observed under a light microscope.

2.3.5 3D cell survival

Live/dead assay was performed to determine whether cells would withstand the process of mixing them into the viscous HA solution, application through a narrow needle, exposure to the blue light and short-term survival within the solid hydrogel. hMSCs (5×10^6 cells·mL^{-1}) were mixed with MA-HA-Dopa or MA-HA solution and solidified in cylindrical moulds (see 2.2.2 page 88). Gels were topped up with media and incubated for 24 h under standard cell culture conditions before being stained with a live/dead kit (Molecular Probes, Invitrogen). Samples got imaged in glass-bottom slides (MatTek, CCS-8) on a Leica DM16000 confocal laser scanning microscope equipped with a physiological chamber set to 37 °C. Red and green channels were split in ImageJ. Maxima were counted in the separate channels (as described by BRTILifeScience [167]). A minimum of 100 cells have been counted per z-stack per sample. Three z-stacks per gel were analysed.

2.3.6 Qualitative tissue interaction

Qualitative evaluation of the interaction of MA-HA (high MA, no Dopa) and MA-HA-Dopa (high MA, low Dopa) hydrogels (3 %) with fresh tissue was carried out using mouse hind limbs (wild type C57BL/6 mouse strain). Hind limbs were skinned, and an incision was made in the hamstring muscle with a scalpel. Samples were either incubated with sodium periodate solution (8.33 $mg \cdot mL^{-1}$ in PBS + 0.4 M NaOH in a 10:1 ratio; active Dopa oxidation, 1 h) or in cell culture media (passive Dopa oxidation, 72 h).

For active Dopa oxidation, the hind limb was then dipped in a sodium periodate solution. This solution was freshly prepared by mixing sodium periodate (8.33 $mg \cdot mL^{-1}$ in PBS) with NaOH (0.4 M) in a 10:1 ratio. The viscous hydrogel solution was then applied to the cut surfaces and exposed to blue light for 4 minutes. After 30 minutes, the cut muscle tissue was pulled apart using forceps and pictures as well as videos were captured. Hind limbs were then submerged in PBS + ABAM (1 %) and stored under standard cell culture conditions for 5 days before an additional movie was captured.

For passive Dopa oxidation, viscous solution was applied onto the fresh incision and exposed to blue light for 4 minutes. Samples were transferred into cell culture media and incubated for 72 h at 37 ˚C. Following, samples were pulled apart using forceps and pictures were taken.

Videos were recorded on a on a Leica MZ95 microscope.

2.3.7 Quantitative tissue adhesion

Quantitative evaluation of the interaction of MA-HA-Dopa hydrogels with fresh tissue was carried out using porcine articular cartilage (adult animals). In order to quantify adhesion forces, 3 % MA-HA (high MA, no Dopa) and MA-HA-Dopa (high MA, low Dopa) hydrogels were prepared. Porcine articular cartilage was harvested from front legs and hind legs of adult animals. Cartilage samples were washed in sterile PBS and tissue was removed using a biopsy punch (Ø 8 mm; see Figure 14). HA solutions were applied and solidified by 4 minutes blue light exposure. Samples were either treated with sodium periodate (8.33 $mg \cdot mL^{-1}$ in PBS + 0.4 M NaOH in a 10:1 ratio; active Dopa oxidation) or incubated in cell culture media for 72 h (passive Dopa oxidation). Hydrogel-cartilage samples were mechanically fixed, and weight was applied on top of the gel.

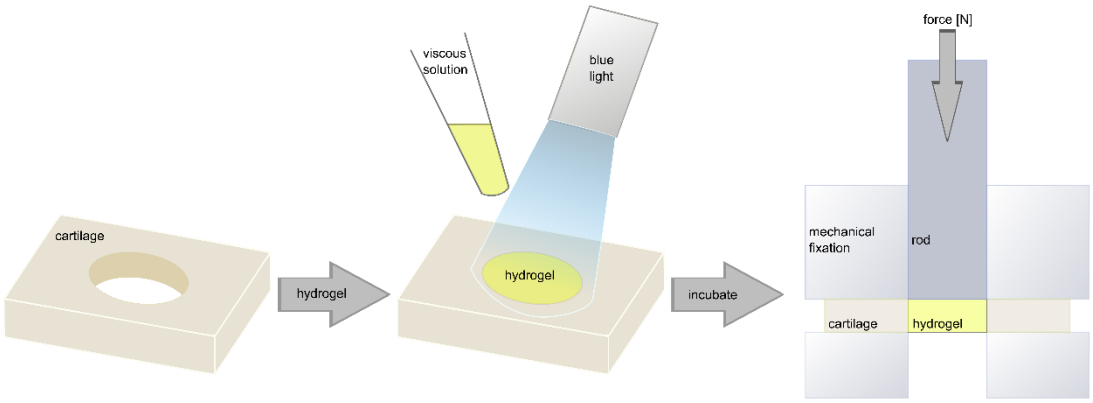

Figure 14: Set-up of quantitative adhesion analysis.
Fresh cartilage samples with MA-HA or MA-HA-Dopa hydrogel were mechanically fixed and a push out test was done by applying force on top of the hydrogel. The force at which the hydrogel-cartilage-interface failed was recorded.

The weight [m] at which the hydrogel-cartilage-interface ruptured, was recorded via gravimetry. Total adhesion force was calculated as followed:

$$F\ [N] = m\ [kg] \times a\ [m \cdot s^{-2}]$$

With [N] = $[kg \cdot m \cdot s^{-2}]$ and acceleration set as 9.81 $m \cdot s^{-2}$.

2.4 Intra- and extracellular matrix formation

Analysing cell specific protein synthesis and the influence of HIF-1α stabilising factor DMOG and different gel formulations was investigated with various techniques.

2.4.1 Non-canonical amino-acid tagging (FUNCAT)

Cell-encapsulated hydrogels were prepared as described in chapter 2.3.3 (page 61). To visualise newly synthesised peptides and proteins, a Click-iT HPG Alexa Fluor 594 kit was used, following the manufacturer's instructions. In short, the methionine-substitute L-homopropargylglycine (HPG) was added to the cell culture media. Cells incorporated HPG into the newly synthesised peptide/protein. After incubation, hydrogels were rinsed in dH_2O and permeabilised with 0.5 % TritonX in PBS for 15 minutes at RT. Following, Alexa Fluor 594 azide was added for 30 minutes at RT. During this reaction time the azide group could bind to the modified alkyne group on the HPG via a copper-catalysed click-reaction. Nuclei were stained with an HSC NuclearMask blue stain for 30 minutes at RT. Samples were rinsed thoroughly in PBS, transferred onto a glass slide and cover slipped. Samples were imaged on a DM16000 confocal laser scanning microscope.

From each group, 4 cell images were selected. Image processing is shown in Figure 15. First, the cell membrane was identified by Differential Interference Contrast (DIC) imaging using a 488 nm laser. ECM was evaluated for distance and detectable protein density by generating 20 random lines (blue lines Figure 15) from the membrane to the end of the ECM. Protein density, as determined by fluorescence intensity of the labelled secreted protein, was measured by analysing the brightness (arbitrary units A.U.) of each pixel in radii extending from the cell surface. The fluorescence signals were normalised to a line within the cell (positive Alexa signal) and a line in the hydrogel (negative background signal), of equal length. Values reported are mean (±S.D.).

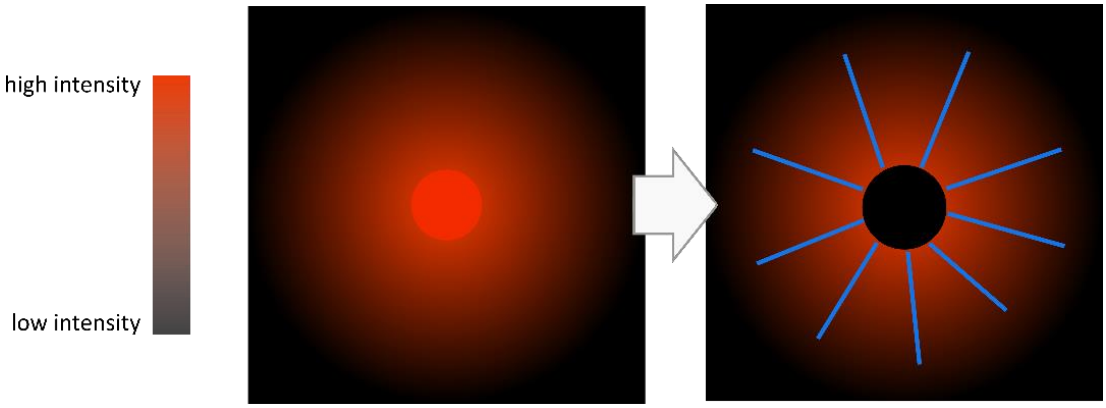

Figure 15: FUNCAT image processing
Intracellular signals were removed by overlapping fluorescent image with differential interference contrast (DIC) images to identify cell membrane; extracellular signal intensity and distance was quantified by line plots (n = 80 lines, 4 cells per group with 20 lines per cell); radial intensity profile represent mean values (with S.D.) as a function of distance from the cell membrane.

2.4.2 Raman spectroscopy

Work with the Raman set-up was performed by collaborating PhD student Anders Runge Walther (University of Southern Denmark). Credit for data acquisition, analysis and interpretation goes to him. His contribution is summarised in the following chapter and was generated together, following his instructions.

Cell-encapsulated hydrogels were prepared as described in chapter 2.3.3 (page 61). Hydrogel samples were thoroughly rinsed with dH_2O and transferred onto a MgF_2 glass slide and fully submerged in dH_2O. Samples were stored in the fridge over night before measurements were taken. Raman imaging was performed on an in-house built Raman confocal micro-spectroscope. A 532 nm laser light source (Torus 532) was coupled into the microscope (CSE2100) via a 125 µm cladding single mode fiber and a fiber collimator. The collimated laser beam was filtered through a laser line filter and directed onto a dichroic mirror before being guided a 60x/1.0NA water immersion objective (CFI Apo NIR 60X W). The Raman emission collected by the objective was guided back through the dichroic mirror and filtered through a long pass filter to

remove scattered light before entering the fibre coupler and 50 µm core, low OH optical fibre acting as a pinhole to provide confocality. Following, the Raman signal was directed to the holographic spectrometer (HS-HSG-532-LF) and detected on a thermoelectrically cooled back-illuminated charge coupled device (CCD) spanning a spectral range from 0 - 2,500 cm^{-1}. For scanning purposes, a piezoelectric stage was used, with a step size of 500 nm and a total acquisition time of 0.3 – 0.8 seconds. For 3D imaging, a piezo objective mount has been utilised and 2D images were collected at parallel planes every 5 µm spanning the entire cell.

Analysing the raw data was done via spectral processing, using in-house written algorithms in MatLab programming environment. Pre-processing of Raman spectra involved baseline correction using asymmetric least squares smoothing, cosmic ray removal and spectral smoothing by a second order Savitzy-Golay filter with a 9-point window in the spectral range 750 - 1,760 cm^{-1}. All individual spectra were normalized using the Euclidean vector norm to remove instrument effects. The spectra from all Raman 2D and 3D hyperspectral images were unfolded into a single matrix comprising more than 160,000 spectra. The N-FINDR algorithm [14] was used to unmix the Raman spectra in the dataset and identify pseudo pure biochemical components (endmembers). Amount of components (4) has been chosen, that maximised the number of biochemically meaningful spectra through peak assignment and correlation with literature.[15, 16] The pixels in the hyperspectral images were assigned 4 abundance values from 0 to 1 according to their spectral similarities with the endmembers using a nonnegative alternating least squares algorithm. Each of the 4 abundance value matrices for each image were min-max normalised and refolded back into the original shape. The images were plotted by assigning a false colour to each endmember channel.

Relative area quantification for each spectral endmember in an image was performed by counting the number of pixels with an abundance value larger than a chosen

threshold and calculating the percentage to total area (in pixels) of the cells. A threshold larger than the average abundance value of all images was chosen for our application.[17]

2.5 Statistical analysis

Unless stated otherwise, all values reported are means and error bars represent standard deviations (S.D.). Analysis was performed using GraphPad Prism statistical software (GraphPad Software Inc., California, USA). Comparisons of the variables were performed with the one-way ad hoc ANOVA. When evaluating only 2 groups, a t-test was applied. Statistical significance was considered when $p \leq 0.05$.

3 Results & Discussion

3.1 Development and characterisation of MA-HA-Dopa hydrogels

3.1.1 MA-HA and MA-HA-Dopa macromer synthesis

HA was modified with various degrees of MA. Qualitative and quantitative analysis of the resulting MA-HA and MA-HA-Dopa macromers was evaluated via Proton-NMR (find plots in Appendix 5.4 page 127 following).

Table 4 summarises the achieved DOMs. Manual adaption of pH with NaOH resulted in a series of methacrylations, ranging from 21 to 65 % of available hydroxyl groups modified (see MA21-Dopa0 to MA65-Dopa0). This corresponds to molar feeding ratios of HA hydroxyl to methacrylic anhydride from 1:1 to 1:6. Molar feeding ratio and achieved level of methacrylation did not follow a linear pattern.

Table 4: DOMs (pH manually adjusted)

	Molar feeding ratio				
Sample ID	HA:MA	HA:Dopa	Degree of methacrylation [%]	Degree of dopamination [%]	Total Degree of modification [%]
MA21-Dopa0	1:1	-	21	-	11
MA30-Dopa0	1:2	-	30	-	15
MA40-Dopa0	1:2.6	-	40	-	20
MA47-Dopa0	1:3	-	47	-	24
MA65-Dopa0	1:6	-	65	-	33

Buffer solutions were tested to maintain the pH at an alkaline level. Starting with a feeding ratio of 1:3 (HA:MA), tris buffer resulted in 1 % degree of methacrylation (see Table 5). Comparable levels with manual pH adaption (see Table 4) would be at 47 %.

Table 5: DOMs (Tris buffer)

	Molar feeding ratio			
Sample ID	HA:MA	buffer concentration [M]	Degree of methacrylation [%]	Total Degree of modification [%]
MA1-Dopa0	1:3	0.3	1	< 1
MA1-Dopa0	1:3	0.6	1	< 1

MOPS buffer resulted in various degrees of methacrylation (see Table 6), with molar feeding ratios from 1:3 (= 18 % methacrylation) up to 1:13 (= 33 % methacrylation). This is less than half the DOM achieved with manual pH adaption (see Table 4 page 69) using the same molar feeding ratio of HA:MA.

Table 6: DOMs (MOPS buffer)

	Molar feeding ratio			
Sample ID	HA:MA	buffer concentration [M]	Degree of methacrylation [%]	Total Degree of modification [%]
MA18-Dopa0	1:3	1.0	18	9
MA24-Dopa0	1:6		24	12
MA33-Dopa0	1:13		33	17

The manual adaption of pH for methacrylation was favoured for further experiments.

Following methacrylation, dopamination reactions were carried out with molar feeding ratios of 1:2.6 of HA:MA, leading to 36 % degree of methacrylation (MA36-Dopa23 and MA36-Dopa46), which again, is comparable to previous synthesis (MA40-Dopa0). Levels of dopamination reached from 23 - 46 %.

As methacrylation and dopamination proven to be a stable and repetitive synthesis, a range of different DOMs were created to conduct all further *in vitro* experiments (see MA18-Dopa0 to MA38-Dopa31, Table 7). For low methacrylation MA18-Dopa0 and high methacrylation MA38-Dopa0 were synthesised. Splitting therefrom, each batch was further modified with a low level of dopamination (MA18-Dopa18 and MA38-Dopa20), with 18 and 20 % DOM or a high level of dopamination (MA18-Dopa29 and MA38-Dopa31), with 29 and 31 % DOM.

Table 7: DOMs double-modification

		Molar feeding ratio				
Reference	Sample ID	HA:MA	HA:Dopa	Degree of methacrylation [%]	Degree of dopamination [%]	Total Degree of modification [%]
-	MA36-Dopa23	1:2.6	1:0.5	36	23	30
-	MA36-Dopa46	1:2.6	1:2	36	46	41
Low MA No Dopa	MA18-Dopa0	1:1	-	18	-	9
Low MA Low Dopa	MA18-Dopa18	1:1	1:0.5	18	18	18
Low MA High Dopa	MA18-Dopa29	1:1	1:2	18	29	23
High MA No Dopa	MA38-Dopa0	1:2.6	-	38	-	19
High MA Low Dopa	MA38-Dopa20	1:2.6	1:0.5	38	20	29
High MA High Dopa	MA38-Dopa31	1:2.6	1:2	38	31	35

3.1.2 Viscosity

Hydrogels produced were composed of either 1 % or 3 % modified HA (wt%), as summarised in Figure 16. Those reached extensional viscosities of 2.9 ±0.2 Pa·s (1 % solution) and 2.9 ±1.2 Pa·s (3 % solution). To increase viscosity, unmodified HA (1 MDa, 2 %) was added. These solutions were measured as 19.8 ±1.2 Pa·s (1 % solution + 2 % 1 MDa HA) and 34.0 ±9.5 Pa·s (3 % solution + 2 % 1 MDa HA) extensional viscosity. One-way Anova analysis showed that both solutions 1 % and 3 % exerted statistical significantly ($p = 0.0114$ and $p = 0.0002$) increased viscosity due to the addition of unmodified HA (1 MDa, 2 wt%). 1 % and 3 % precursor solutions without 2 % 1 MDa HA did not show any statistically significant different viscosity ($p > 0.9999$), whereby addition of 2 % unmodified 1 MDa HA resulted in higher viscosity for the 3 % solution ($p = 0.0281$).

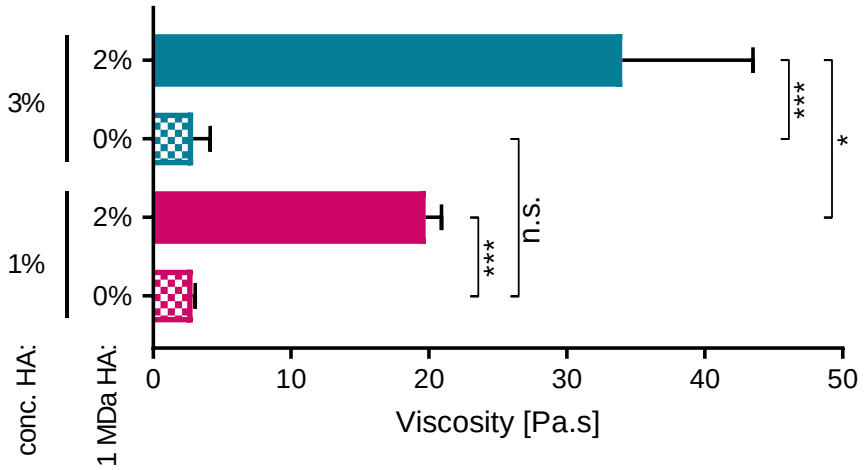

Figure 16: Extensional viscosity of pre-solidified macromer solutions
Extensional viscosity of 1 and 3 % (wt%) precursor solutions with and without the addition of 2 % (wt%) unmodified 1 MDa HA. 1 % and 3 % precursor solutions did not show any statistically significant different viscosity ($p > 0.9999$ (n.s.)), whereby addition of 2 % unmodified 1 MDa HA resulted in higher viscosity for the 3 % solution ($p = 0.0281$ (*)). 1 % without/with 2 % unmodified HA ($p = 0.0114$ (*)) and 3 % without/with 2 % unmodified HA ($p = 0.0002$ (***)). One-way Anova; Plot shows means and S.D., n = 3.

3.1.3 Gelation kinetics and bulk stiffness

As indicated in Figure 17, MA-HA and MA-HA-Dopa formulations with low degrees of dopamination gelled in less than 4 minutes (taken as the cross-over between G' and G''). Apart from 1 % formulation without unmodified HA. Non-dopaminated formulations gelled within 3 - 16 seconds, low dopaminated took 10 - 145 seconds and high dopaminated compositions required 153 - 175 seconds to gel (see Table 10 page 138, for exact values). Several formulations did not solidify within 4 minutes. MA-HA-Dopa with high degrees of Dopa gelled more slowly (> 4 minutes) or not at all. For all MA-HA and MA-HA-Dopa (low) formulations, adding 2 % 1 MDa HA did not have an adverse effect on gelation time.

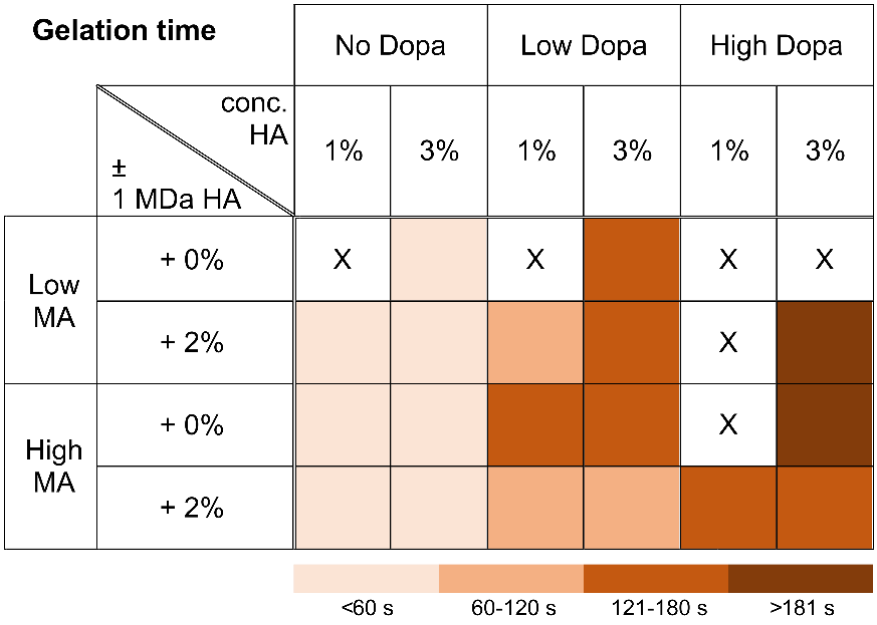

Figure 17: Gelation time of different hydrogel formulations
Gelation times for different hydrogel compositions. Gelation times were grouped so that light colour indicates fast gelation and darker colours show slower gelation. X indicates compounds that did not solidify.

Bulk stiffness G' reached after 4 minutes of light exposure is summarised in Figure 18. Similarly to the observation made with the gelation time (Figure 17), hydrogels with no Dopa were stiffer than those with double-modification. Subsequently, 3 %

hydrogels appeared stiffer than 1 % hydrogels. The addition of 2 % 1 MDa HA has further increased the overall stiffness of the hydrogel, in comparison to the samples without. Bulk stiffness for non-dopaminated formulations were 343 - 11,107 Pa, low dopaminated reached 173 - 600 Pa and high dopaminated compositions achieved 37 - 337 Pa (for exact values see Table 11 page 139).

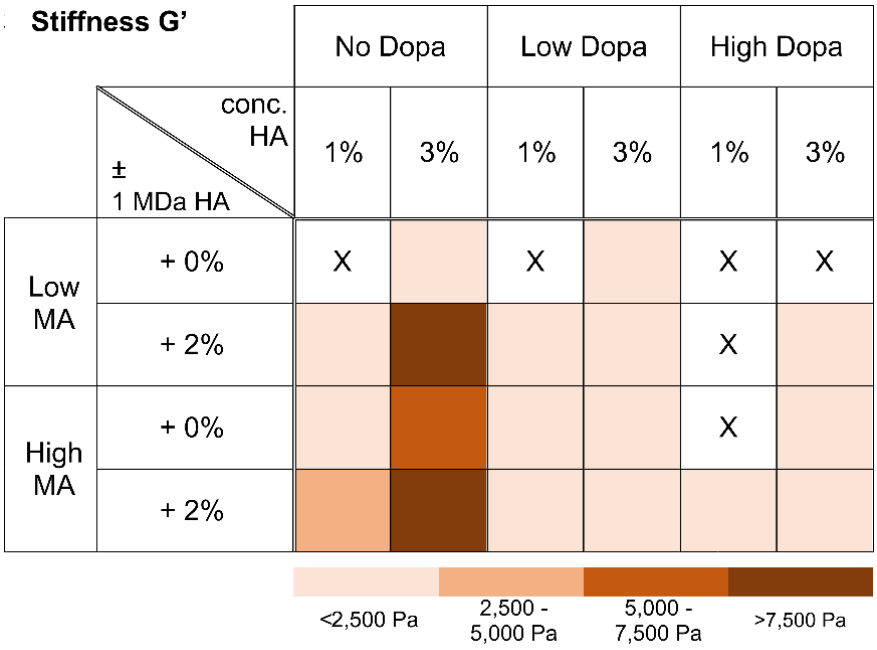

Figure 18: Bulk stiffness of different hydrogel formulations after 4 minutes light exposure

Bulk stiffness for different hydrogel compositions. Values were grouped so that light colour indicates softer gels and darker colours show harder gels. X indicates compounds that did not solidify.

In order to investigate whether there was full cross-linking achieved, samples were exposed to blue light for a total of 9 minutes. Values recorded (Table 12 page 129) indicate higher stiffness values for all hydrogel formulations, than after 4 minutes of light exposure (Table 11 page 128). Although total kinetic chain formation was achieved later, 4 minutes were considered as sufficient time to solidify the hydrogels tested. Consistent with observations of gelling time, more extensive Dopa modification tended to result in lower values of bulk stiffness G'.

3.1.4 Shelf-life

Shelf-life as a matter of stiffness was investigated via rheology. Storage conditions were set to either RT or 4 ˚C, mimicking temperatures required in case drugs or other medications are mixed with the precursor solution. In order to measure maximum stiffness, hydrogels were exposed to a total of 9 minutes of blue light, as previously described (see 0 page 56). G' after storage was normalised to G' of freshly prepared material (no storage) (see Figure 19 page 76).

Low MA, no Dopa formulations showed reduced bulk stiffness after 1 day of storage, reaching 44 % (RT) and 74 % (4 ˚C). Storing the solutions for 8 days resulted in 30 % (RT) and 70 % (4 ˚C). Low MA, low Dopa achieved 30 % (RT and 4 ˚C) after 1 day of storage and did not solidify when stored for 8 days. High MA, no Dopa compositions reached 61 % (RT) and 70 % (4 ˚C) after 1 day of storage, and 50 % (RT) and 75 % (4 ˚C) after 8 days. High MA, low Dopa hydrogels were at 98 % (RT) and 93 % (4 ˚C) after 1 day and resulted in 47 % (RT) and 92 % (4 ˚C) after 8 days of storage.

Overall, solutions stored in the fridge showed higher stiffness' than those stored at RT. Furthermore, most conditions were significantly different from their respective control ($p<0.05$). High MA, low Dopa best preserved G' over 8 days of storage, particularly when kept at 4 ˚C. This formulation showed no statistically significant difference compared to its controls (no storage) (#, Mann-Whitney, two-tailed, $p = 0.1$), indicating that a precursor solution of this composition can be stored for at least 8 days prior to use.

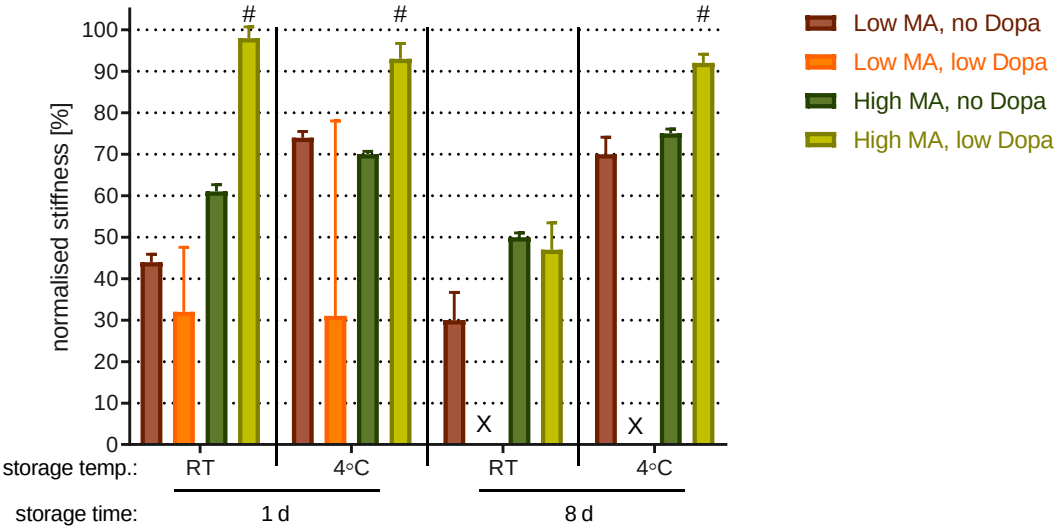

Figure 19: Shelf-life, G' normalised to G' of freshly prepared material (no storage) n = 3, mean values with S.D., # = no statistically significant difference (Mann-Whitney, two-tailed, p = 0.1). X indicates compounds that did not solidify.

3.1.5 Mass swelling ratio

Mass swelling ratios were determined via gravimetry, where increases in weight over time was recorded as swelling. Time dependent weight changes (Figure 61 page 149) were summarised according their plateau swelling behaviour (Figure 20 page 77).

Significant changes in weight occurred within 2 h after hydrogel formation (One-way Anova, $p<0.001$). Swelling reached a plateau level for all hydrogel formulations between 2 - 6 h, except of high MA, high Dopa, which took 24 h to reach maximum swelling. Comparing the plateau swelling ratios in Figure 20, low methacrylated hydrogels swell about 102 - 255 %, whereby high methacrylated hydrogels tend to swell less than 36 - 241 %.

Increase in dopamination also increased the swelling ratios, especially with the addition of 2 % 1 MDa HA. High dopaminated hydrogels showed swelling ratios greater than 300 %, which were excluded from further studies. Low dopamination increased the swelling ratio for 3 % hydrogel formulations by 35/41 % (+0/2 % 1 MDa

HA) for low MA hydrogels, and 210/111 % (+0/2 % 1 MDa HA) for high MA hydrogels, compared to the non-dopaminated formulations. Although they solidified during rheological bulk stiffness experiments, formulations with 3 % low MA, high Dopa (+2 % 1 MDa HA) and 1 % high MA, high Dopa (+2 % 1 MDa HA) disintegrated during the swelling experiments and therefore were excluded from the results.

Overall swelling ratios were between 100 - 250 % for low MA hydrogels, and 50 - 250 % high MA hydrogels. The swelling behaviour observed is in parallel with the materials behaviour for gelation time and stiffness (see 3.1.3).

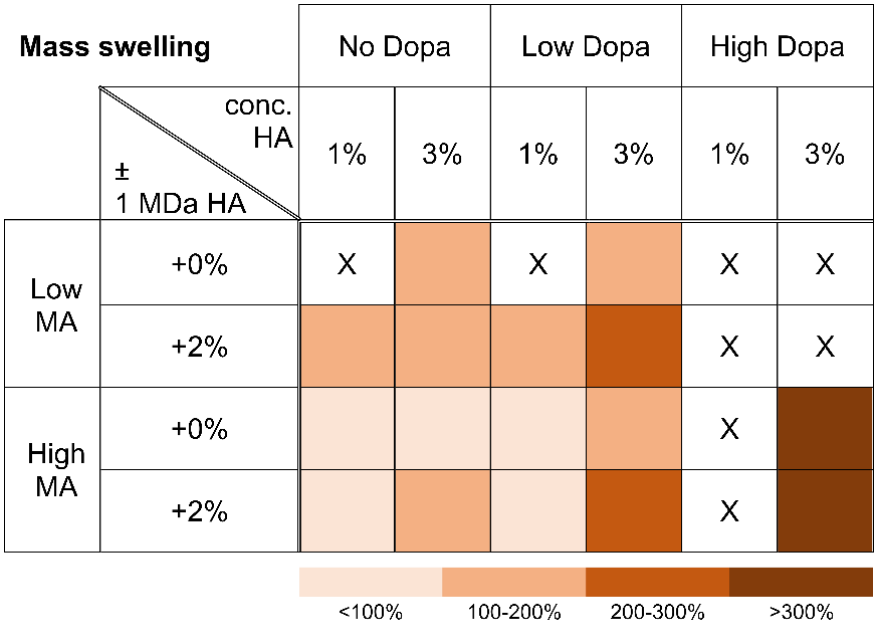

Figure 20: Summary of mass swelling ratios
Mass swelling ratios for different hydrogel compositions. Values were grouped so that light colour indicates less swelling and darker colours show more swelling. X indicates compounds that did not solidify.

3.1.6 Enzymatic degradation

Enzymatic degradation of HA occurs by cellular synthesis and release of hyaluronidase (HAse).[168-170] Investigating hydrogel degradability in the presence of HAse Type I, confirmed that all compositions are degradable (see Figure 21 and Figure 62 page 151).

Non-dopaminated 3 % hydrogel formulations fully degraded after 48/72 h (+0/2 % 1 MDa HA) for low MA hydrogels, and 168/216 h (+0/2 % 1 MDa HA) for high MA hydrogels. 1 % hydrogels of low MA (+2 % 1 MDa HA) degraded within 24 h (+0 % as well 2 % 1 MDa HA) whereas high MA hydrogels took 48 h (+0/2 % 1 MDa HA). Degradation times were shorter for dopaminated hydrogels. Low Dopa formulations of 1 and 3 % hydrogels degraded within 24 h, except high MA (both 1 % formulations and 3 % without 1 MDa HA). All high Dopa hydrogels degraded within 24h.

Degradation tended to be slower in formulations with higher levels of methacrylation, lower levels of dopamination and in the presence of unmodified 1 MDa HA.

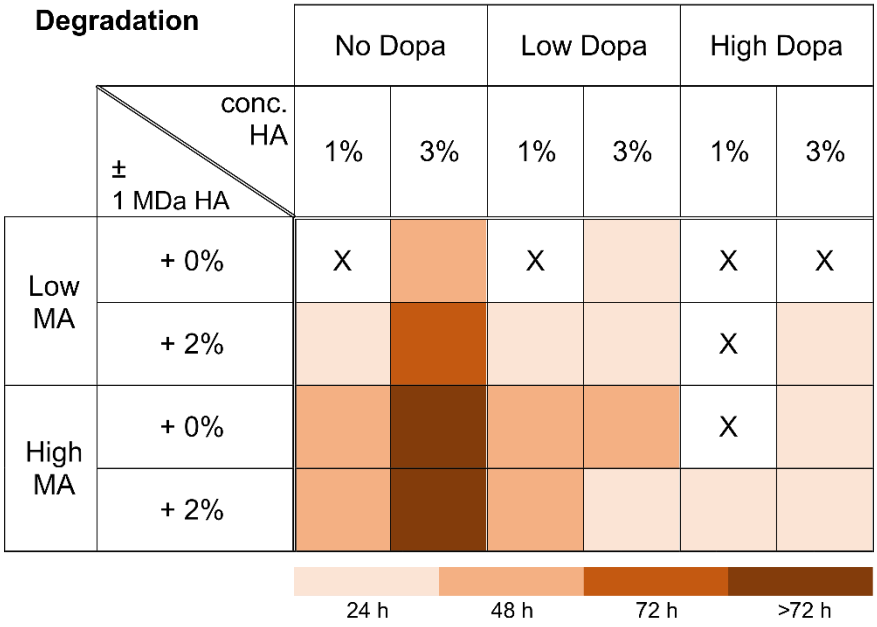

Figure 21: Summary of enzymatic degradation
Time for full enzymatic degradation of different hydrogel formulations. Lighter colours indicate fast degradation and darker colours show slower degradation. X indicates the absence of gel solidification.

3.1.7 In aqua application

The non-thickened hydrogel solution (3 % high MA, low Dopa; no 1 MDa HA) settled down into a ring submerged under water and remained in place for the time of the experiment (Figure 22, see also Movie 1). Upon 4 minutes blue light application, the material successfully solidified into a hydrogel. As described in 1.3.2 (page 31), a change from red to colourless was noticeable after light exposure, indicating Eosin-mediated cross-linking.

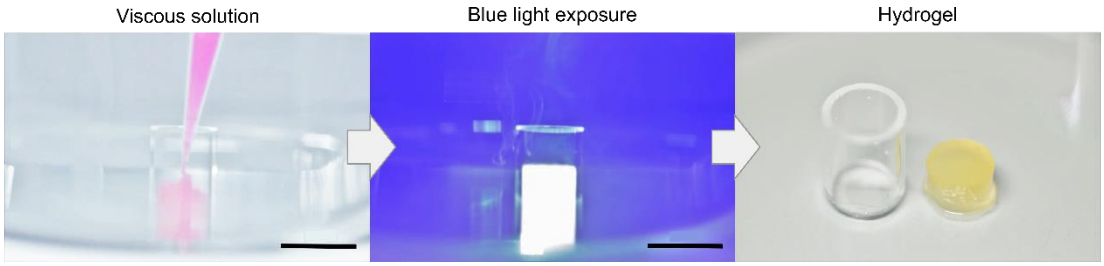

Figure 22: In aqua application.
Images showing in aqua application of non-thickened viscous solution and gelation upon blue light exposure; Scale bar = 10 mm.

3.1.8 Dopa oxidation

After 24 h in cell culture medium, MA-HA-Dopa hydrogels (3 %, high MA, low Dopa, no 1 MDa HA) changed from colourless to brown, indicating Dopa oxidation (see Figure 23).[56]

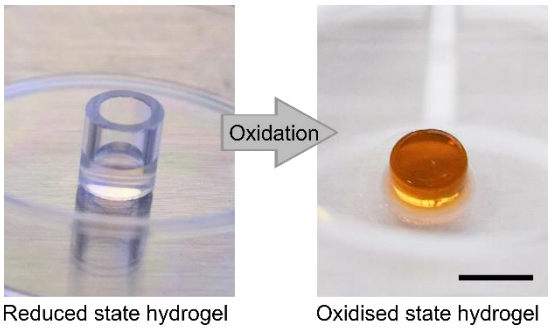

Figure 23: Oxidation of MA-HA-Dopa hydrogel
Images of hydrogels captured directly after gelation (left) or after 24 h incubation in cell culture media (right) showing that the hydrogel converts brown, indicating oxidation of the Dopa; Scale bar = 10 mm.

Comparing PBS and cell culture media for incubation, hydrogels showed that only MA-HA-Dopa formulations incubated in media turned brownish after 24 h incubation (Figure 24). Non-dopaminated hydrogels as well as MA-HA-Dopa hydrogels incubated in PBS were lacking this effect.

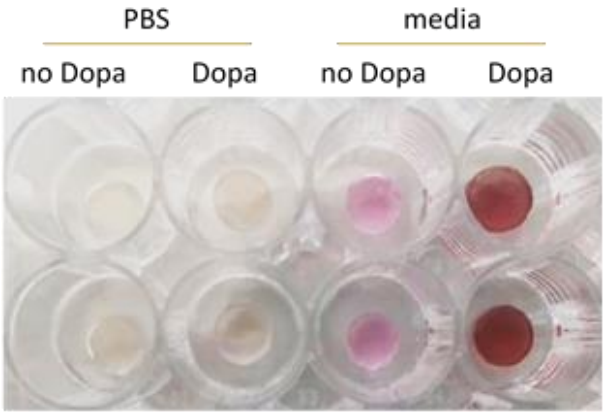

Figure 24: Oxidation of hydrogels in PBS or cell culture media
Images of hydrogels incubated in PBS (left) or cell culture media (right) for 24 h; MA-HA-Dopa hydrogels in media are the only group showing the indicative brown colour.

This characteristic change was confirmed by colorimetric measurements (Figure 25, left), for MA-HA-Dopa hydrogels in cell culture media. Here, absorption between 250 - 500 nm continued to increase over 72 h (data point not shown). Oxidation under hypoxic conditions (5 % O_2), as can be found in less vascularised tissues, could be slowed by maintaining hydrogels under hypoxic conditions, confirming that atmospheric oxygen was sufficient to oxidise the Dopa moiety; however, lower, tissue-like levels of O_2, could also foster the process. Maximum oxidation for both oxygenated conditions could be detected after 120 h. Incubating MA-HA-Dopa hydrogels in PBS did not show a comparable increase in Dopa oxidation over the same period of time (Figure 25, right).

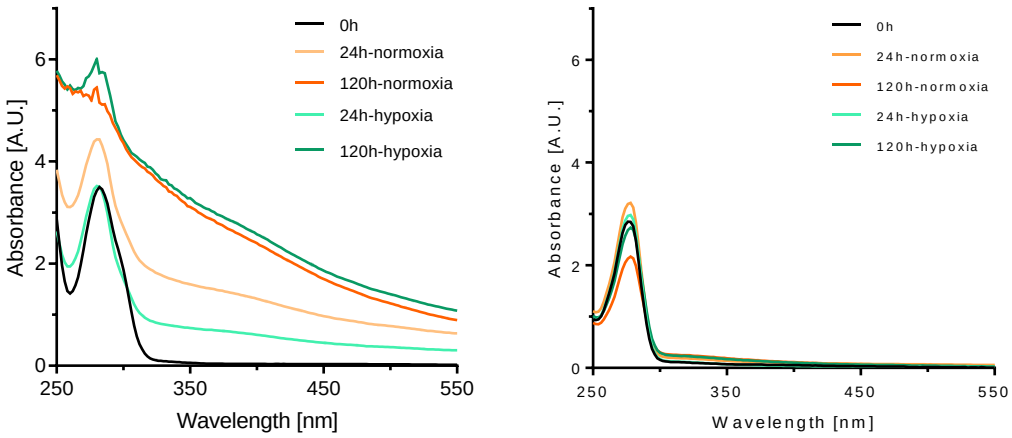

Figure 25: Time course of Dopa oxidation
Colorimetric measurements of Dopa oxidation in hydrogels maintained in cell culture media (left) or PBS (right) under standard or hypoxic (5 % O_2) conditions.

3.1.9 Discussion

Developing MA-HA-Dopa hydrogels has strongly focused on clinical application and translation into human patients. Therefore, chemical and physical properties have been tailored accordingly, with the input of maxillofacial surgeons, dentists and ENT specialists.

Chemical synthesis is primarily done with organic solvents, which are later removed via extensive purification processes. However, this requires additional procedures which are bearing the risk of contamination or solvents remaining in the final product. Chlorinated solvents are amongst the most common to synthesise and modify macromers for TE purposes. Such solvents, particularly dichloromethane, which has been used by Guvendiren et al.[171] and Lee et al.[56] to create Dopa-modified hydrogels, has been associated with neural toxicity. Indeed, exposure to dichloromethane has been linked to facial nerve palsy, which is an important concern in temporomandibular joint applications, which are in close proximity to the facial nerve. The hydrogel system described in this work is based on an aqueous system which completely avoids such organic solvents, precluding the need for purification or potential toxicity. In order to optimise handling and reproducibility of the MA-HA and MA-HA-Dopa macromers, several buffers were tested. Resulting DOMs revealed that tris buffer was not sufficient to sustain a stable methacrylation reaction (see Table 5 page 70), whereby MOPS buffer resulted in increasing DOMs (see Table 6 page 70), depending on the molar feeding ratio of methacrylic anhydride. The quantity of methacrylic anhydride to achieve comparable DOMs as with manual pH calibration was several factors higher. Although using MOPS buffer allowed an easy reaction, the high amount of methacrylic anhydride necessary was deemed a downside. Besides requiring a higher amount of reagent, removal of unreacted compounds has to be done much more thoroughly, which is time consuming and costly. Consequently, manual pH adaption was chosen for methacrylation reaction as

proposed in Figure 11 page 53. Therefrom HA macromers were produced with low and high levels of methacrylation. Portions of those were further dopaminated with low and high levels of Dopa moieties, creating a total of 6 differently modified HA macromers (low MA, no Dopa; low MA, low Dopa; low MA, high Dopa; high MA, no Dopa; high MA, low Dopa; high MA, high Dopa), which are summarised in Table 7 page 71. Those were submitted to further experiments and analysis.

When preparing the hydrogel pre-curser solution, lyophilised HA macromers (MA-HA, MA-HA-Dopa) were dissolved in an Eosin/PEG solution by shaking. Increasing the content of HA made those solutions more viscous, whereby, adding more than 2 % (wt%) unmodified HA (1 MDa) appeared to be not fully dissolvable. This might be overcome by using stirring tools. However, this bears the risk of contamination and increases the shear forces within the solution. In case cells are going to be encapsulated, high shear forces might damage or destroy those cells. Therefore, 2 % unmodified 1 MDa HA was set as maximum to increase viscosity. The viscosities reached with the addition of 2 % unmodified HA is comparable to commercially available clinical products (see Figure 16 page 72).[158] A number of clinicians from different backgrounds (dentists, ENT specialists, maxillofacial surgeons) randomly applied and solidified those solutions *ex vivo* and rated the material as easy to handle, with not much introduction necessary. Of course, this is relative and might be assessed differently by other end users.

Hydrogels produced from those precursor solutions possessed a range gelation behaviours, which are summarised in Figure 17 page 73. To determine the maximum stiffness achievable, the solutions were exposed to a total of 9 minutes of blue light. However, timing plays a crucial role during surgical operations as patients are supposed to be under anaesthesia for shortest period possible. Consulting with clinicians, maximum time for gelation was set to 4 minutes.

Step-growth light-activated cross-linking of dithiol-PEG molecules with the MA moieties of HA macromers is a time dependent reaction. The longer blue light exposure is activating this reaction, the more PEG molecules manage to reach close proximity towards a MA group to react with it. Accordingly, hydrogels exposed to 4 minutes of blue light appeared to form fewer kinetic chains, and therefore were softer, than hydrogels of the same precursor solution being irradiated for 9 minutes (see Table 11 page 139 and Table 12 page 140). The amount of kinetic chains formed was not only limited by the time active cross-linking molecules were available, but also by the quantity of MA moieties to react with. Subsequently, 3 % hydrogels appeared stiffer than 1 % hydrogels (see Table 11 page 139 and Table 12 page 140), which is to be expected as there are fewer MA moieties present within the same volume. This effect was also detectable when comparing the degree of methacrylation. Here, low MA hydrogels were comparably softer than same formulations with high MA levels (see Table 11 page 139 and Table 12 page 140). Interestingly, increase of dopamination leads to a later gelation and softer hydrogels (see Figure 17 page 73). This suggests that the Dopa group does not contribute to cross-linking, but instead hinders it. This seems counterintuitive at first, as Dopa is known to react with a variety of functional groups and should result in a shorter gelation time and stiffer gels, as there are more contributing moieties present. However, this phenomenon is actually an expected result. Because the Dopa-Dopa and Dopa-thiol covalent interactions that would potentially contribute to hydrogel cross-linking require the Dopa to be oxidised.[52] In studies in which Dopa is used to covalently cross-link hydrogels, sodium periodate or similar oxidising agents are used to enable this reaction. However, this hydrogel system cross-links within minutes, before the Dopa is oxidised. Under these conditions, the Dopa groups are unlikely to participate in any cross-linking reactions and on the contrary are inhibiting them instead. In MA-HA-Dopa hydrogels presented in this work, cross-linking is mainly expected to occur through thiol-ene radical addition. Therefore,

catechol ability of scavenging free radicals directly inhibits thiol-ene type cross-links, while the regeneration of free catechol after a radical scavenging cycle assures no alternative cross-links are formed in this process.[172] Although Dopa can also react with free thiols upon oxidation to its quinone form, Dopa exists predominantly in its reduced catechol form when hydrogels are formed, which is known to be non-thiol-reactive.[52] Consequently, the increased free radical scavenging ability at higher degree of dopamination is expected to effectively reduce the overall formation of elastically active crosslinks and therefore stiffness G'. A similar effect has been observed for tough adhesives based on catechol-functionalised thiol–ene polymer networks.[173]

As previously discussed, time and resources are limited inside an operating theatre, which renders shelf-life an important factor for a material to be considered practical in clinical application. Shelf-life was determined by the ability of a precursor solution to form the same amount of kinetic chains, which results in similar stiffness, after being stored compared to when freshly produced. Solutions kept in the fridge showed higher stiffness' than those stored at RT, following the assumption that a lower temperature slows down natural macromer degradation and reaction of moieties with each other (see Figure 19 page 76). Most conditions were significantly different from their respective controls, suggesting that those are suitable when prepared freshly. High MA, low Dopa formulation best preserved bulk stiffness over 8 days of storage, particularly when kept at 4 ˚C. This formulation showed no statistically significant difference compared to its controls (no storage), concluding that it is appropriate to store for several days after preparation.

As the nomenclature reveals, hydrogels have a high affinity towards water accumulation. Comparing swelling ratios, low methacrylated hydrogels swell about 100 - 200 %, whereby high methacrylated hydrogels tend to swell less than 100 %. This is to be expected, as the higher degree of MA allows a superior interconnection

of single methacrylated HA-macromers into the polymeric network. The same effect is perceptible with increase in dopamination, as there are less kinetic chains formed, which would mechanically restrict the hydrogels network to expand upon influx of water. Although an important factor for characterising hydrogel materials, swelling might be of less importance for a clinical application in TMD treatments. Performing partial surface reconstruction of the fibrous cartilage in TMJ, the hydrogel would be surrounded by neighbouring tissue. This mechanically rigid obstruction would hinder the gel from swelling in a fashion recorded with *in vitro* experiments.

For treatments to be able to achieve a complete tissue regeneration, implants are supposed to be degradable. This can be due to chemical cleavage (i.e. hydrolytic degradation), mechanical erosion or enzymatic degradation. All hydrogel compositions were entirely enzymatically degradable (see Figure 21 page 78). These observations were in line with previous reports of degradability in HA with similar degrees of modification.[170] Comparing swelling data with degradation behaviour, it appears that softer gels tend to degrade on a faster rate. This might be due to less material to be degraded (1 % versus 3 %) or higher swelling rates enabling increased influx of enzymes into the hydrogel network. Although they solidified during rheological bulk stiffness experiments, formulations with 3 % low MA, high Dopa (+2 % 1 MDa HA) and 1 % high MA, high Dopa (+2 % 1 MDa HA) disintegrated during the swelling experiments. Following the trend seen, those formulations might have formed only few kinetic chains, which could be broken by movement of the surrounding fluid (mechanical erosion).

As for clinical application, minimally invasive techniques in the TMJ are utilising water-based buffers to inflate the joint space. Precursor solutions without increased viscosity (no addition of 2 % unmodified 1 MDa HA) settled into a levelled volume. Solutions of low viscosity appear to settle easily even in liquid environments and could be utilised for applications filling more complex shapes. Whereby higher viscosities

might permit application in non-horizontal defects. This could be explored further with actual minimal-invasive tools, to confirm the effect detected here.

After being applied and solidified *in vivo*, Dopa is supposed to be oxidised in order to support cell and tissue interactions.[52, 56] Oxidation can be achieved by adding active oxidants like sodium periodate or hydrogen peroxide.[56] Unfortunately, these are fairly rapid in action and limit the timeframe for application as well as represent potential biological toxicity. The mechanism the approach proposed here is that redox reactions are occurring spontaneously under physiological conditions, allowing Dopa to form a partially oxidised semi-quinone or fully oxidised quinone state. To mimic such *in vivo* conditions, hydrogels were incubated in cell culture media under normoxia or hypoxia, showing that only MA-HA-Dopa hydrogels incubated in media turned brownish after 24 h incubation (see Figure 24 page 80). This suggests that, although molecular oxygen being present, other components like sugars or proteins might be necessary to facilitate the necessary redox potential. Concluding, Dopa is capable to auto-oxidise under physiological conditions found in cartilage tissue. Although this effect takes a few hours to appear, tissue interaction and cell adhesion to the injected hydrogel is unlikely to be necessary immediately after application.

Overall, the MA-HA-Dopa hydrogel system proposed here could resist the liquid surrounding it would be exposed during minimally invasive TMJ surgery. The hydrogel can be tailored in viscosity, depending on the nature of the defect and is capable of supporting primary cell encapsulation. As for clinical applicability, MA-HA-Dopa precursor solutions are stable for several days when stored at 4 ˚C and solidify in less than 4 minutes when exposed to standard clinical blue light.

3.2 Cell and tissue interaction

3.2.1 Cytotoxicity

Cytotoxicity is a key factor when designing medical implants. This includes synthesis of the single ingredients, as well as toxicity before and after gelation.

Direct cytotoxicity assays show no reduction in metabolic activity with the working concentration of 0.01 wt% Eosin (see Figure 26). Increasing the levels to 0.04 wt% lowers the activity to approximately 50 %, which amounts to 4x the working concentration. Metabolic activity was almost not detectable above 0.08 wt%.

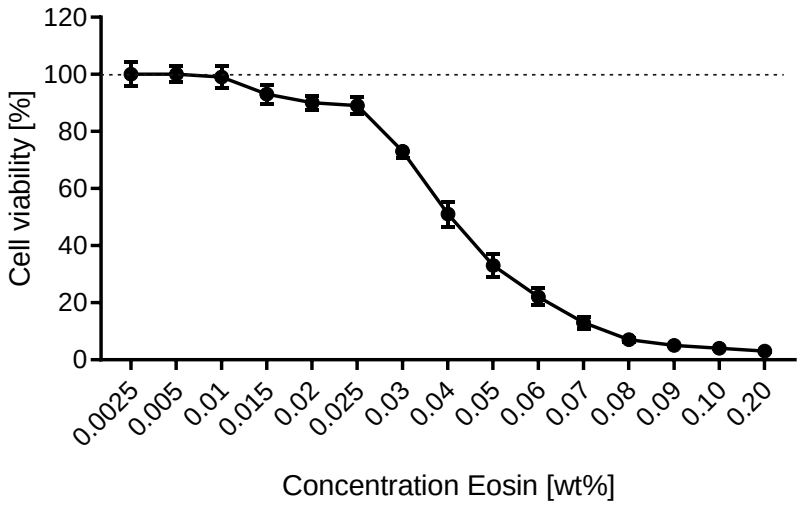

Figure 26: Direct cytotoxicity of Eosin
Direct cytotoxicity of a range of Eosin concentrations. n = 3, mean values with S.D. Working concentration of 0.01 wt% did not show a reduction in metabolic activity, measured via MTT assay.

Further, 1,4-dithiothreitol (DTT) and dithiolated PEG have been tested via direct cytotoxicity assays. As illustrated in Figure 27, DTT and PEG indicate cytocompatibility at the working concentration of 0.01 mM. At a concentration of 0.6 mM DTT lowers cell activity to ~50 %, whereby PEG is tolerated more than 2.25 mM before halving metabolic activity. This equals 60x the working concentration of DTT and 225x the working concentration of PEG, suggesting that PEG is better tolerated *in vitro*. Absolute cell toxicity is attained for DTT at 3.2 mM and PEG at 5 mM.

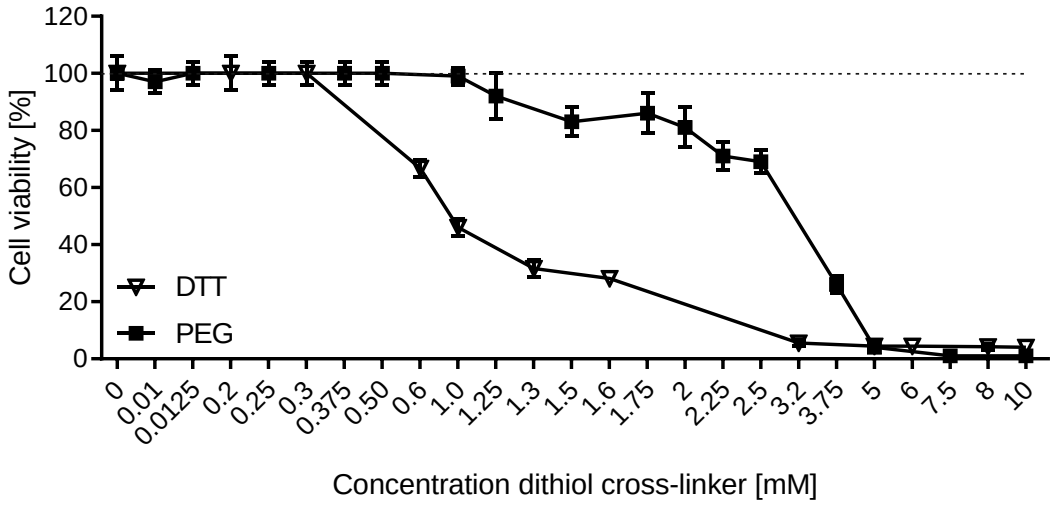

Figure 27: Direct cytotoxicity of dithiol cross-linking molecules (PEG and DTT)
Direct cytotoxicity of a range of DTT and PEG concentrations. n = 3, mean values with S.D. Working concentration of 0.01 mM did not show any reduction in metabolic activity for either components, measured via MTT assay.

Indirect cytotoxicity testing has been performed to exclude the possibility of toxic products formed during the hydrogel solidification process. Comparing metabolic activity to media only controls, cells treated with PEG cross-linked hydrogel media reached 106 %, those incubated with DTT cross-linked hydrogel media resulted in 89 % (see Figure 28 page 90). As such, both do not exhibit any statistically significant toxicity compared to media only controls, however, cells treated with PEG cross-linked hydrogel media had a statistically significant higher metabolic activity then those treated with DTT cross-linked hydrogel media (n = 5, multiple comparison, Kruskal Wallis, p = 0.001(***)). These results are in line with the outcomes of the single component analysis in Figure 27.

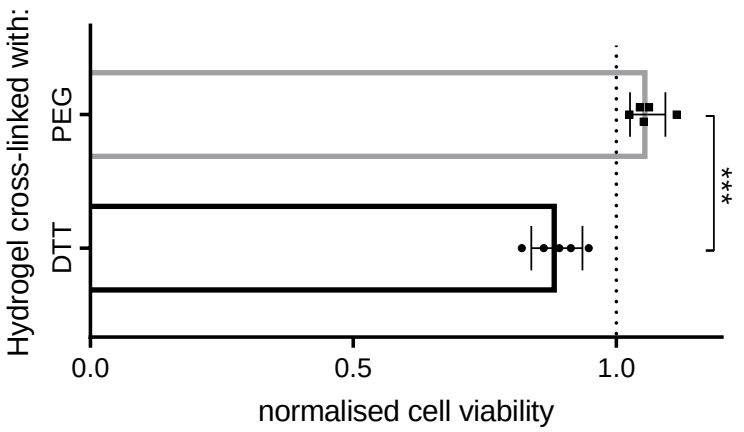

Figure 28: Indirect cytotoxicity of hydrogels formed with PEG or DTT
Indirect cytotoxicity assays of hydrogels formed with PEG or DTT. n = 5, mean values with S.D. Multiple-comparison analysis (Kruskal Wallis, p = 0.001(***)) shows significantly higher metabolic activity in cells treated with PEG-hydrogel media.

3.2.2 2D cell attachment

Confirming previous observations [108, 142], cells do not adhere to MA-HA hydrogels (Figure 29, left) (3 %, high MA, no Dopa). However, cells do adhere to MA-HA-Dopa hydrogels, 16 h after seeding (Figure 29, right) (3 %, high MA, low Dopa). As HA has no sites required for integrin-mediated cell attachment, cells are unable to stably attach to it, even in the presence of soluble RGD-presenting proteins (i.e. fibronectin).

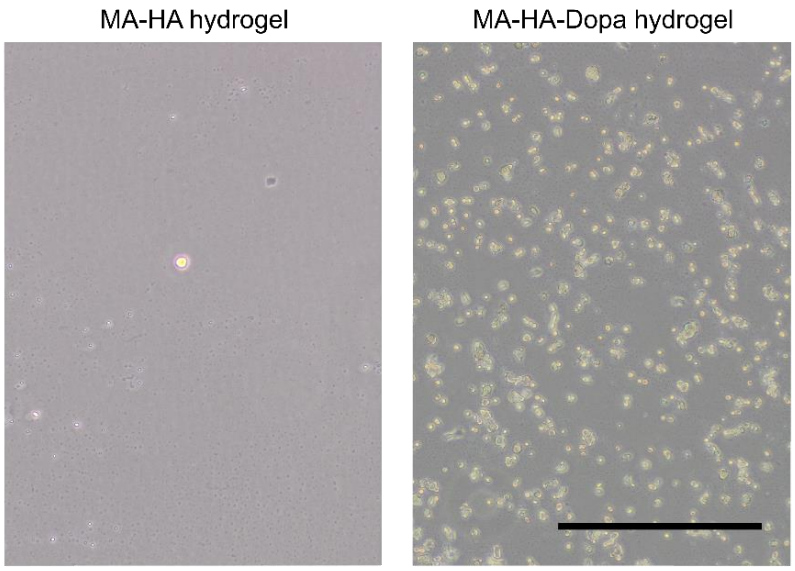

Figure 29: 2D cell attachment to hydrogel.
Bright-field images of 17IA4 cells attached to MA-HA (3 %, high MA, no Dopa) and MA-HA-Dopa (3 %, high MA, no Dopa) hydrogels after 16 h of culture. Very few cells were observed attached to MA-HA hydrogels, compared to the MA-HA-Dopa hydrogels. Scale bar = 200 µm.

3.2.3 3D cell survival

Encapsulating hMSCs in various hydrogel compositions showed high tolerance of cells towards preparation and application process , with an overall cell survival of 73 - 96 % 24 h post-encapsulation (Figure 30 and Figure 63 page 152). 1 % hydrogel formulations reported 80/82 % (high MA, no Dopa/high MA, low Dopa) cell survival. 3 % hydrogels reached 76/93 % (low MA, no Dopa/low MA, low Dopa) and 73/84 % (high MA, no Dopa/high MA, low Dopa). All formulations showed increased cell

survival for dopaminated hydrogels versus their non-dopaminated compounds. 1 % hydrogels and 3 % High MA formulations did not result in statistical significant increased survival rate; however, cell survival in 3 % low MA formulations was statistically significant between no/low Dopa (Fisher's exact test, n = 3 (total 300 cells per condition), p = 0.0014 (**)).

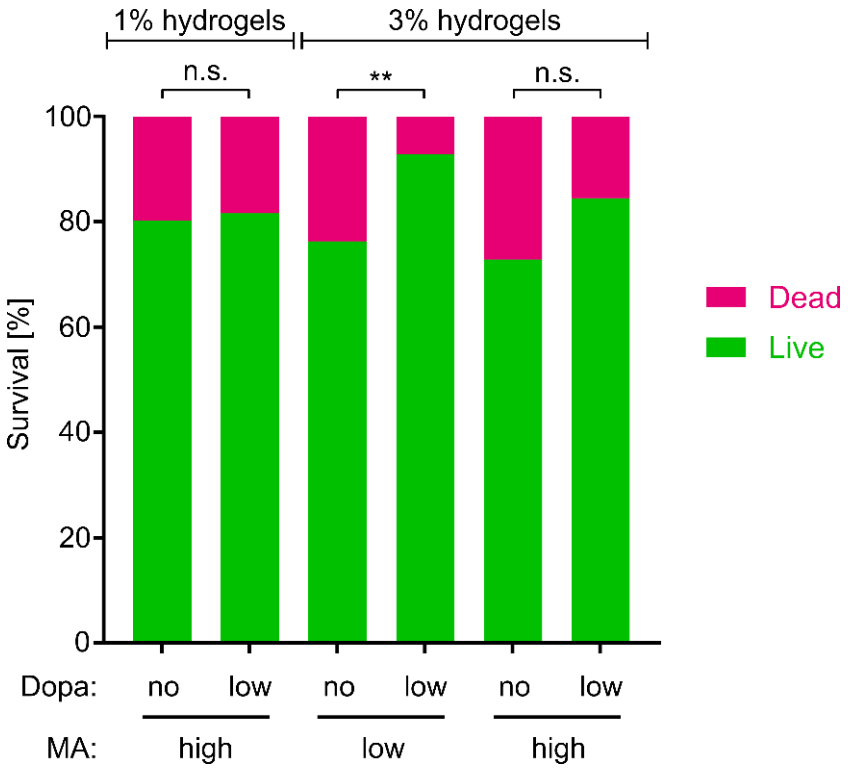

Figure 30: hMSC survival after 24 h encapsulation within hydrogels
In 3 % hydrogels, cells show significantly higher viability in MA-HA-Dopa hydrogels compared to MA-HA hydrogels. Fisher's exact test, n = 3, total of 300 cells per condition.

3.2.4 Qualitative tissue interaction

Qualitative tissue interaction experiments were performed in order to visualise the adhesive properties of MA-HA-Dopa (high MA, low Dopa) hydrogels, and the lack of such in MA-HA (high MA, no Dopa) hydrogels, respectively.

Active oxidation resulted in MA-HA-Dopa hydrogels undergoing the characteristic brown colour change within several minutes, indicating Dopa being present in its

oxidised form (see Table 8, top row). As the surrounding muscle tissue was moved, MA-HA-Dopa hydrogels followed the change and remained adherent (see movie 2). This adhesion effect was still visible after 5 days incubation in PBS (see movie 3). Non-dopaminated hydrogels on the other hand, were sliding along the tissue, showing no significant interaction with the muscle (see Table 8, bottom row). Those were floating in the cell culture media after the incubation.

Table 8: Images hydrogel-tissue interaction via active Dopa oxidation
3 % MA-HA-Dopa (high MA, low Dopa) and MA-HA (high MA, no Dopa) hydrogels adherent/in contact with muscle tissue after treatment to actively oxidise Dopa. As the muscle tissue is being pulled apart, the MA-HA-Dopa hydrogel remains adherent to the tissue surfaces (see also Movies 2). The MA-HA hydrogel does not stay adherent when the tissue is manipulated. Hydrogel borders are indicated in blue.

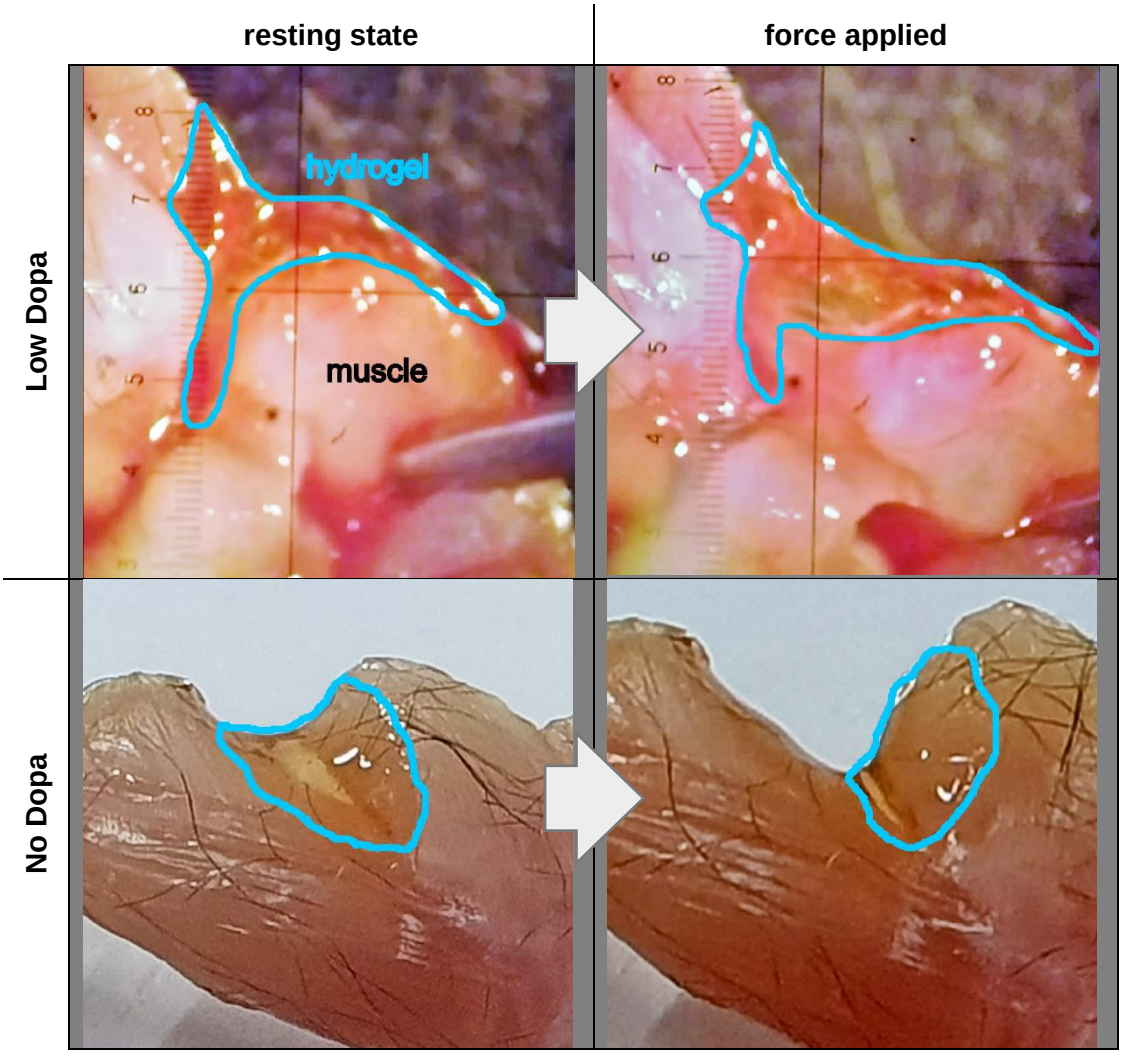

Passive Dopa oxidation via incubation in cell culture media, followed the pattern observed with active oxidation. Dopaminated hydrogels interacted with the muscle, in parallel to the movement of the tissue (Table 9). Changes visible during movement applied to the bulk hydrogel deforming, with the hydrogel-tissue interface appearing stable. However, as non-dopaminated hydrogels did not interact with the muscle, they were floating in the cell culture media after incubation. This effect could be seen already a few hours after starting the incubation.

Table 9: Images hydrogel-tissue interaction via passive Dopa oxidation
3 % MA-HA-Dopa (high MA, low Dopa) hydrogels adherent to muscle tissue after passive Dopa oxidation. As the muscle tissue is being pulled apart, the MA-HA-Dopa hydrogel remains adherent to the tissue surfaces. The MA-HA hydrogel did not interact with the tissue and so after 72 h in cell culture media had lost contact with the tissue. Hydrogel borders are indicated in blue.

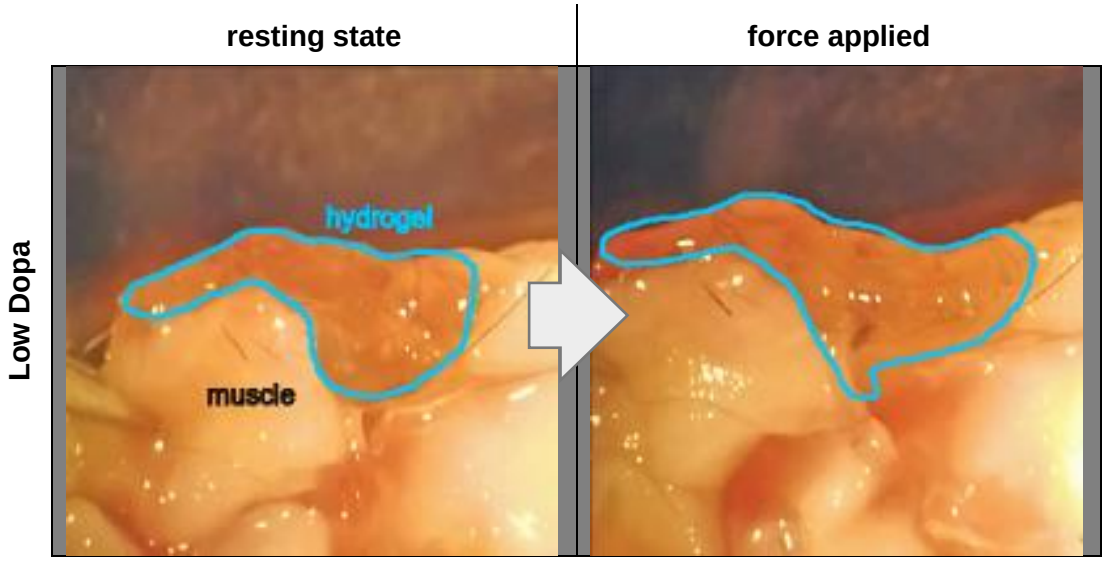

Although, active Dopa oxidation is not considered in the design of this system, it demonstrated an interaction between MA-HA-Dopa hydrogels and tissue and excluded any impacts of swelling. This effect was not detectable with MA-HA hydrogels. Passive Dopa oxidation experiments reported the same effect but were limited due to the swelling of the hydrogels, especially the MA-HA control group. As the hydrogels are rather soft, repeated movement eventually lead to a rupture of the gel itself, leaving hydrogel residues on the hydrogel-tissue-interface.

3.2.5 Quantitative tissue adhesion

To determine if the Dopa moiety enabled stable tissue interactions, MA-HA and MA-HA-Dopa hydrogels were formed within circular defects punched out of mature porcine articular cartilage explants. Catechol moieties were either actively oxidised ($NaIO_4$) or allowed to undergo passive oxidation (cell culture media) before quantifying the force required to push the hydrogel out of the tissue. For active oxidation, this resulted in 141 ± 6 µN (MA-HA-Dopa) and 8 ± 1 µN (MA-HA) of force needed (see Figure 31), which is 17x higher force required to push out MA-HA-Dopa hydrogel. Passive oxidation reached necessary push-out forces of 61 ± 8 µN (MA-HA-Dopa) and 5 ± 1 µN (MA-HA), which is 12x higher force necessary to push out MA-HA-Dopa hydrogel. Both, actively and passively oxidised Dopa-modified hydrogels required significantly higher push out forces than their MA-HA counterparts (Unpaired t-test with mean values and S.D., n = 3, p = 0.0035(**) and p < 0.0001(****)), confirming tissue adhesive properties of MA-HA-Dopa hydrogels.

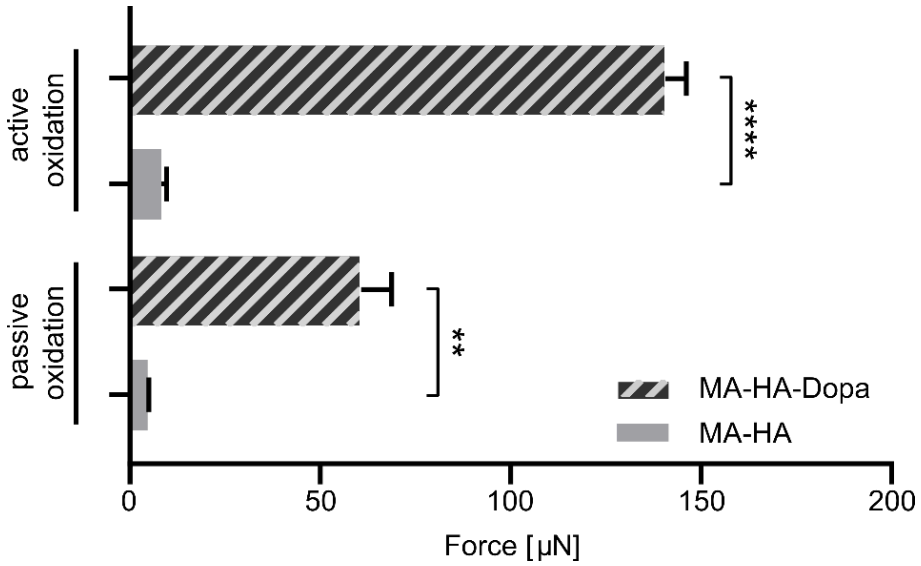

Figure 31: Quantitative tissue adhesion
Force required to push hydrogel (3 %; high MA, low Dopa; high MA, no Dopa) out of circular defect created in porcine articular cartilage, either after being actively oxidised with $NaIO_4$ or passively oxidised in cell culture media over 72 h. Unpaired t-test with mean values and S.D., n = 3, p = 0.0035(**) and p < 0.0001(****).

3.2.6 Discussion

Besides physical and chemical properties discussed in 3.1.9 (page 82), biological characteristics of MA-HA-Dopa hydrogels have been explored. Here, the immediate effect of hydrogel formulations upon cells as well as interaction with fresh tissue explants has been investigated.

Cytotoxicity is a major factor throughout this project and has been focused on during synthesis of MA-HA and MA-HA-Dopa macromers. MA-HA and HA-Dopa constructs have been used by previous groups, which have shown that they do not emit any cytotoxic components.[108, 174] Additional soluble components are Eosin-Y, as well as the dithiol cross-linking molecules (PEG and DTT). These could potentially be available to cells before undergoing a covalent reaction with the HA-macromers, or if not consumed during the solidification process. Held et al. have previously explored cytotoxic effects of DTT in cell culture experiments, confirming 0.01 mM as non-toxic concentration.[175] DTT is known to facilitate additive reactions via Michael-addition, which has been utilised to produce self-assembling hydrogel networks.[176, 177] These networks form within a few minutes under physiological pH conditions.[177] Considering the significantly higher cytotoxicity, it appears that the reactive thiol groups of DTT are more active than those linked to the PEG. This was further backed up by the fact that solutions with PEG did not spontaneously gel. Testing a wide range of concentrations with the single components as well as fully solidified hydrogels has proven to be well tolerated by cells, without reduction of cellular viability (see 3.2.1 page 88).

Besides the cytocompatibility, gelling behaviour might be a significant factor when evaluating a cross-linker. DTT is a short molecule that connects MA groups which are near each other. PEG, in contrast, is a longer and more flexible cross-linker which could connect MA moieties that are located further away from one another. During the cross-linking process HA macromeres will be trapped in position, leaving

more flexible PEG molecules to reach out and connect the MA groups. Concluding, further experiments have been performed using only PEG as cross-linking molecule.

Comparing 2D cell interaction with MA-HA and MA-HA-Dopa hydrogels, it became obvious that cells managed to interact with MA-HA-Dopa formulations within a short period of time. Following auto-oxidation of the catechol group, dopaminated hydrogel compositions should decorate themselves with soluble proteins in an *in vitro* setting. Once a semi-quinone or quinone has covalently attached to a protein, it is no longer susceptible to redox reactions and therefore firmly bind to each other. This ultimately leaves all catechol groups in MA-HA-Dopa hydrogels attached to a soluble or tissue-bound protein over time in *in vitro* or *in vivo* conditions. Serum proteins could foster integrin-based cell interactions with the hydrogel.[52, 178] Consequently, having no RGD-containing soluble protein to interact with would not permit a swift integrin-based cell interaction with MA-HA-Dopa hydrogels. The same effect was seen for cells 3D encapsulated in hydrogel formulations. Cells did survive in MA-HA as well as in MA-HA-Dopa hydrogels which confirms previous reports that hMSC can thrive within HA-based hydrogels lacking adhesive motifs.[179-181] In fact, cells have demonstrated to rather swiftly create their own proteinaceous matrix which they can actively probe via cell receptors like integrins.[63, 182] Additionally, Vining and colleagues have proven that this effect is genuine even in the absence of serum proteins.[183] Nevertheless, for a clinical setting it can be expected for soluble proteins to be present to some extend within the surrounding of the applied hydrogel. This could be due proteinaceous components originating from the synovial fluid, the microfracture procedure and tissue residuals of abrasive processes. In addition, 3D encapsulation experiments are suggesting that the presence of Dopa in hydrogel constructs might enhance overall cell survival. Taken together, these observations show that by providing sites for protein interaction and thus integrin-mediated interactions, MA-HA-

Dopa hydrogels can potentially deliver viable cells or be infiltrated by endogenous cells made available using procedures such as microfracture.[184-186]

Integration of neo-cartilage into the surrounding host tissue is an important factor for a material to succeed in cartilage regeneration.[49] Lacking a vascular network combined with limited self-repair remains challenging for regeneration to occur via hMSCs or chondrogenic cell types. However, loading the cartilage might increase influx of water and nutrients. This could be further enhanced by the swelling of the hydrogel network itself, however, expansion of the applied material might be restricted due to the surrounding host tissue (see Figure 4 page 30). This swelling could further support firm interaction of the hydrogel with the native cartilage, enhancing adhesive connections via catechol groups. Adhesive strategies utilising components other than mussel-inspired catechols have been explored for arthroscopic approaches (see 1.3.3 page 35). Those have limited to no application in arthroscopic approaches as they either have to be applied as a liquid, and would be washed away within the liquid environment of the inflated TMJ space, or require the addition of potentially toxic components.[130-135]

When interacting with a tissue-bound protein, Dopa is supposed to facilitate tissue adhesion. Qualitative results demonstrated a fairly stable connection for MA-HA-Dopa hydrogels when actively or passively oxidised (see 3.2.4 page 92, and movies 2 and 3). Even though the mechanical strain applied here is not what would to be expected in a clinical setting, the results indicate a tissue-hydrogel interaction, stronger than the actual kinetic chains within the hydrogel. Quantifying strength of adhesives is largely validated via lap-shear tests [187, 188] or peel tests [189, 190]. Such tests require a thin layer of adhesive agent in comparison to a large interface area. Those approaches should minimise the influence of the materials property, and only focus on the material-tissue interaction. Qualitative tissue interaction experiments concluded, that the MA-HA-Dopa hydrogel is posing a weaker physical

resistance then the hydrogel-tissue interface. Approaching the quantification of adhesion forces between MA-HA-Dopa hydrogels and tissue has proven challenging. The application of light was a limiting factor, as the hydrogel layer was too thin and uneven for the light to properly penetrate and therefore cross-link the viscous gel solution. Consequently, and in line with the proposed clinical application (see 1.3.1 page 29), a push-out test was utilised to quantify adhesion of MA-HA and MA-HA-Dopa hydrogels to mature porcine cartilage. Results clearly indicate a catechol-dependent adhesion of MA-HA-Dopa hydrogels to cartilage tissue explants when exposed to physiological conditions, without the addition of further oxidising agents (see Figure 31 page 95).

Summarising, MA-HA-Dopa hydrogel systems proposed in this project represent a highly cyto-compatible material, that is likely to be suitable for maxillofacial applications. Cellular and tissue adhesion is supported in wet environment without the addition of potentially harmful oxidising agents and would not require secondary adhesive agents to be applied.

3.3 Intra- and extracellular matrix formation

3.3.1 Non-canonical amino-acid tagging (FUNCAT)

After 21 days in culture, newly synthesised peptides/proteins were visible intracellularly as well as in the pericellular space under all conditions (representative images in Figure 32A, B, C and D). To better understand the distribution and density of the secreted matrix, radial fluorescence intensity profiles of the HPG signals extending from the cell membrane of encapsulated cells have been plotted as mean intensity over distance (Figure 32A', B', C' and D').

hMSCs encapsulated in 1 % hydrogels indicated HPG positive signals up to 42/31 µm (without/with DMOG) from the plasma membrane. In 3 % hydrogel compositions, HPG positive signals were detected up to 31/37 µm (without/with DMOG) from the cell membrane.

Quantitatively comparing the overall intensities from each group via two-tailed Mann-Whitney test, showed no statistically significant increase in fluorescence intensity when treating hMSCs with DMOG in 1 % hydrogels ($p = 0.5101$). hMSCs in 3 % hydrogels revealed a statistically significant increase in HPG positive signal when being treated with DMOG ($p = 0.0042$). Comparing the different hydrogel compositions without DMOG, hMSCs in 1 % hydrogels released significantly more HPG positive peptides/proteins into the pericellular space then cells in 3 % hydrogels ($p = 0.0002$). The same response was detectable for DMOG treated groups, where 1 % hydrogels also exhibited significantly higher intensities over 3 % hydrogels ($p = 0.0222$). For 3 % hydrogel compositions, hMSCs treated with DMOG resulted in HPG-signal intensities, which are comparable levels to those in 1 % hydrogels without DMOG ($p = 0.9792$), but significantly less than in 1 % hydrogels with DMOG ($p = 0.0222$).

Those observations showed that in all conditions, pericellular matrix PCM formation was concentrated immediately around the cell membrane. DMOG showed limited

impact upon peptide/protein secretion in 1 % hydrogels. However, in 3 % hydrogel compositions the presence of DMOG resulted in production of more HPG signal and at larger distances from the cell membrane as the control group without DMOG. In total, hMSCs encapsulated in 1 % hydrogels treated with DMOG resulted in highest HPG-positive signals after 21 days in incubation.

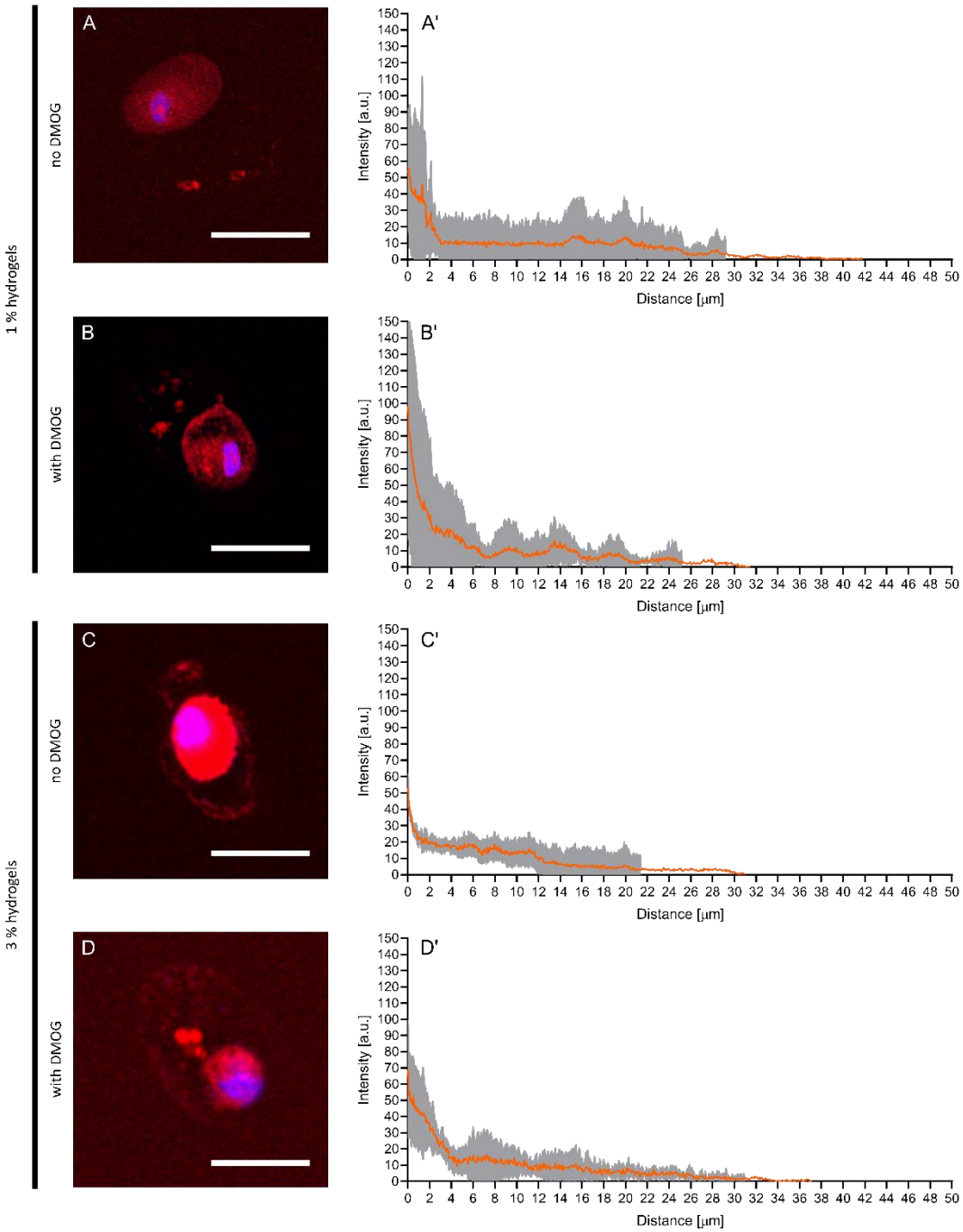

Figure 32: Fluorescent non-canonical amino acid tagging to visualise secreted peptide and protein contents. (figure legend continuing on next page)

FUNCAT analysis on 1 % and 3 % MA-HA-Dopa hydrogels (no 1 MDa HA) 21 days post encapsulation. Each group shows a representative cell image (A, B, C and D) with HPG signal in red and nuclei in blue. Error bar = 40 µm. Summarising FUNCAT plot of n = 4 cells (A', B', C' and D') show mean values in orange with S.D. in grey. ***(A)*** *1 % hydrogel without DMOG; HPG signal was detected as far as 42 µm from the cell membrane;* ***(B)*** *1 % hydrogel with DMOG; HPG positive signals were detected up to 31 µm from the cell membrane;* ***(C)*** *3 % hydrogel without DMOG; HPG positive proteins were detected up to 31 µm from the cell membrane;* ***(D)*** *3 % hydrogel with DMOG at 21 days; HPG positive signals were detected up to 37 µm from the cell membrane; no statistical significant difference was detected for the 1 % hydrogel groups (A) and (B) (Mann-Whitney test, p = 0.5101); for 3 % hydrogels, DMOG treated group (D) compared to group without DMOG (C) confirmations a statistical significantly higher amount of HPG positive peptides/proteins in the DMOG group (Mann-Whitney test, p-value = 0.0042); hMSCs in 1 % hydrogel compositions (A) and (B) secreted more peptides/proteins into their pericellular space, compared to 3 % groups (C) and (D). Overall, 1 % hydrogel with DMOG (B) developed the highest HPG-positive signal intensities.*

3.3.2 Raman spectroscopy

Work with the Raman set-up was performed together with collaborating PhD student Anders Runge Walther (University of Southern Denmark). Following experimental design and preparation of hydrogel samples, remaining credit for data acquisition and analysis goes to him.

Raman micro-spectroscopy was utilised to visualise hMSCs after cultured in MA-HA-Dopa hydrogels (3 %; high MA, low Dopa; no 1 MDa HA) for 21 days with and without the addition of HIF-1α stabilising factor DMOG. Multivariate image processing of the entire hyperspectral dataset produced 4 pseudo pure spectra (endmembers) describing the biochemical composition of the cells and their immediate surrounding (see Figure 33B). Cell image reconstruction were conducted by assigning abundance values to each pixel in the images according to their spectral similarity with the endmembers (see Figure 33A).

The endmembers (Figure 33B) show typical protein Raman bands for Amide I (~1,654 cm^{-1}), Amide III (~1,255 cm^{-1}), Phenylalanine (1,034 cm^{-1} and 1,003 cm^{-1}). The spectra representing the proteinaceous contents (Figure 33B, cyan and blue) show some dissimilarities. The cyan endmember exhibits a broad and intense peak in the Amide III region with high intensity in the range 1,250 - 1,300 cm^{-1} relative to the amide I band calculated using the respective band areas. Previously published work have shown this to be associated with α-helix secondary structure in proteins such as collagen.[191] The blue endmember shows an Amide I shoulder around 1,610 cm^{-1} usually assigned to cytosine, tyrosine and tryptophan and has a lower intensity in the Amide III region 1,250 - 1,300 cm^{-1} relative to the Amide I band. The nucleus spectrum contains additional bands associated with DNA and RNA around 1,340 cm^{-1} (Nucleic acid mode) and 828 cm^{-1} (O-P-O stretch).[192] The final endmember (yellow) contains spectral features associated with lipids around 1,130 cm^{-1}, 1,303 cm^{-1} and 1,674 cm^{-1}.[191] Movie 4 demonstrates a 3D Raman image of a primary human mesenchymal stromal cell encapsulated in a MA-HA-Dopa hydrogel, showing the spectra discussed.

Differences due to the influence of DMOG was determined by relative area quantification in which the number of pixels associated with the respective endmembers are counted and related to the total number of pixels in each cell. Results show that the largest difference is found in the cytoplasmic content of the cells where hMSCs exposed to DMOG exhibit more of the cyan coloured proteinaceous endmember although not statistically significant (Mann-Whitney test, p-value = 0.11). This suggests that DMOG has increased the production of proteins 21 days post encapsulation.

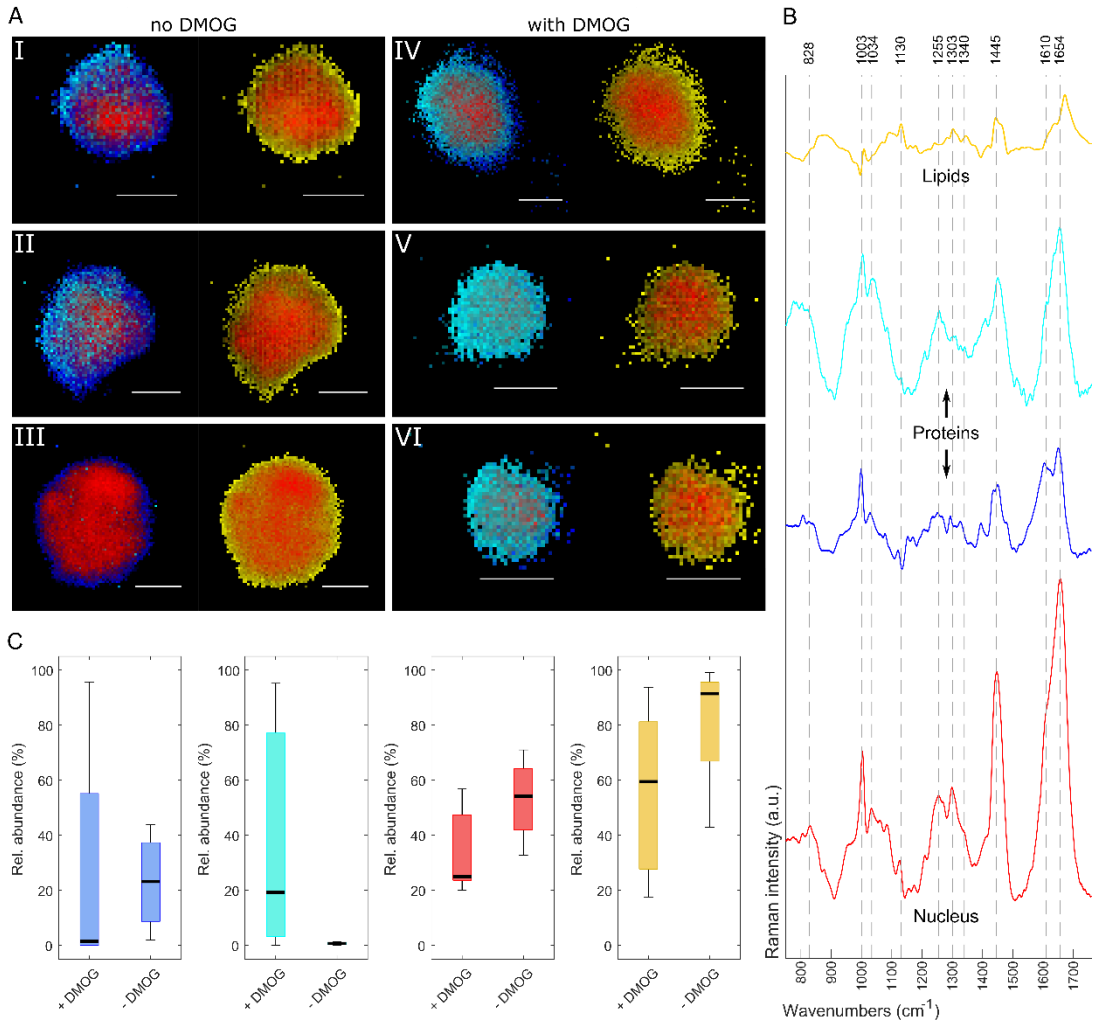

Figure 33: Raman imaging and quantitative analysis of encapsulated hMSC biochemical composition.

(A) *Representative Raman images of hMSCs cultured without (I-III) and with DMOG (IV-VI); Pairs of images (I-VI) represents the same cell showing nucleus (red) along with proteins (cyan, blue) and nucleus with lipid content (yellow); Scale bar = 10 µm.* ***(B)*** *The corresponding Raman spectral endmembers of subcellular components extracted using the NFINDR algorithm (showing 4 components); from top to bottom lipids (yellow), proteins (cyan, blue) and nucleus (red).* ***(C)*** *Relative area quantification and comparison of the subcellular composition for cells cultured with (n = 5) and without DMOG (n = 4). Mann-Whitney test resulted in no statistically significant difference between the groups.*

3.3.3 Discussion

Observations suggested that a combination of FUNCAT and Raman spectral imaging could provide unbiased *in situ* visualisation of both cells within 3D hydrogels and their secreted matrix. In detail, FUNCAT data provided quantitative insight about secretion and distance of newly synthesised peptides/proteins from the cellular plasma membrane, which indirectly gives feedback about hydrogel behaviour. Raman imaging supplements that with qualitative input about the properties of this newly formed ECM.

Overall, quantity and distance of HPG-positive signals is comparable to similar systems published by our team as well as other groups.[63, 160] 1 % hydrogel formulations enabled hMSCs to produce vast quantities of peptides/proteins and to secret them into their pericellular space. Here, DMOG did not seem to have significant effects on quantity or distance of HPG-positive signals. In 3 % hydrogel formulations on the other hand, DMOG statistically significantly increased both distance and intensity of stained peptides/proteins in the extracellular space. This effect might be resulting from the higher density of hydrogel being present in 3 % compositions, as the hydrogel might sterically restrict secretion to a greater extent than in 1 % hydrogels, which is also more easily amendable by cells. Cell-active components like DMOG have been deemed potentially valuable for chondrogenic TE approaches.[193-196] DMOG has shown to strongly target chondrogenic gene expression, suggesting that it might support hMSCs to undergo differentiation. Taheem and colleagues[21] have shown that DMOG could be utilised for cartilage regeneration by inhibiting FIH and PHD2 hydroxylases, upregulating HIF-mediated transcription to support chondrogenesis. They added that DMOG reduced expression of hypertrophy associated type X collagen. Furthermore, early DMOG administration appeared to strongly induce chondrogenesis, however, it also reduced expression of collagen type II when administered initially. Exposure of DMOG 14 days after hMSCs

encapsulation resulted in elevated chondrogenic expression profile, with no negative impact on cartilage-like ECM formation. This concludes that a delayed release of DMOG might increase the secretion of cellular proteins.

As both HA-based hydrogels and DMOG are known to enhance hMSC chondrogenesis, next steps planned are to confirm these unbiased visualisation techniques by carrying out immunostaining for collagen type I and II. Fibrocartilage of TMJ articular surface is mainly composed of those two collagen types. Therefore, examining the proteinaceous content and presence of glycosaminoglycans of matrix secreted by those encapsulated hMSCs should allow to make more competitive assumptions about what formulation has the highest probability of restoring fibro-cartilage *in vivo*.

Work with the Raman set-up was performed together with collaborating PhD student Anders Runge Walther (University of Southern Denmark). Discussion of Raman results is kept general and focused on the benefits it gained for this project: Utilising Raman spectral imaging has proven as quick and versatile technique to investigate 3D encapsulated cells within MA-HA-Dopa hydrogels. Compared to conventional techniques, samples did not require time consuming preparation like sectioning or further staining. Raman imaging resembles a non-invasive, non-destructive method for *in vitro* purposes. Data collected allows unbiased as well as biased analysis of chemical compositions.[197-199] N-FINDER algorithms like the one used in this approach can discover various chemically different components within a small spot. Searching for a specific chemical component allows biased, targeted investigation of materials present. However, specificity that can be achieved with i.e. immunohistochemistry cannot be accomplished with Raman and FUNCAT alone and would benefit from supporting techniques. Analysing for elements of native cartilage components, immunohistochemistry allows to further chemically characterise the neo-tissue formed. This will allow to draw conclusions about what type of cartilage-

like ECM is being produced. In addition, overlapping with the non-canonical amino-acid tagging data, this can give information about what portion of the newly synthesised matrix is located at what distance to the producing cell.

In summary, hMSCs encapsulated in MA-HA-Dopa hydrogels do synthesise and secrete peptide/proteins into their pericellular space. DMOG is capable of significantly increasing protein secretion for 3 % hydrogels. Exploring new techniques to evaluate the formation of such ECM components, Raman spectral imaging combined with FUNCAT analysis bears great potential to serve as a multitalented and high-throughput system to visualise and evaluate hydrogels for TE purposes.

4 Conclusion & future directions

Summarising results and discussion, the aims of this project are considered as achieved successfully. Presented here is a double-modified hydrogel system, which can be synthesised without any potentially neurotoxic reagents, in a highly controlled environment. Chemical, physical and biological properties have been tailored for usage in arthroscopic surgery in maxillofacial applications, specifically the articular cartilage of the TMJ. As such, a range of different precursor solutions with various viscosities can be created, to permit application within a liquid environment and solidify rapidly when exposed to standard clinical blue light. These hydrogels also promote survival of primary human cells and enable delivery of cyto-active agents (i.e. DMOG). As a result, cells not only survive application and solidification of the hydrogel material but also produce and secrete matrix components into their immediate pericellular space. This was evaluated as first *in vitro* indication for potential tissue regeneration. Besides allowing easy handling and no specialised equipment necessary, hydrogel precursor solutions can be applied, moulded and if required removed and reapplied, before solidifying, making it an exceedingly adaptable material to work with. Precursor solutions can also be prepared upfront and stored for several days before use, rendering this system even more suitable for clinical translation. This novel material, its synthesis and characterisation has been published in Advanced Healthcare Materials (see 5.1(1) page 124). Currently, Raman and FUNCAT data is being drafted into a follow-up publication, to be considered soon for submission to a suitable journal (see 5.1(2) page 124).

At the current stage of this project, there have been hydrogel compositions identified that could potentially facilitate formation of articular fibro-cartilage. Hence, the next stage is aimed to be an *in vivo* study. This should give further insights into clinical applicability of the precursor solution and its potential for neo-tissue formation. In order to investigate optimal tissue development conditions, it would be of interest

to compare different cell sources like BM-MSCs from microfracturing, as well as directly incorporated primary cells like mature chondrocytes. MSCs would allow administration via microfracturing techniques, minimising the need of additional procedures. Furthermore, those are available in large quantities and do recovery naturally.[200] They can be driven towards tissue-specific lineages, which here was investigated by the administration of HIF-1α stabilising factor DMOG. Mature chondrocytes on the other hand are considered to have a high potential for ECM synthesis and secretion.[201] Repeating 2D adhesion experiments with serum versus serum-free cell culture media should demonstrate that cells are lacking capability of interaction with either MA-HA or MA-HA-Dopa gels. Specifically blocking integrin-interactions could further prove the role of integrins in these adhesion processes.[202, 203] When encapsulated, comparing serum with serum-free conditions could confirm previous observations, that cells within 3D hydrogels are capable of secreting their own proteinaceous matrix, even when serum proteins are absent.[63, 182, 183] Analysing these two conditions, FUNCAT combined with Raman might give detailed insight into the time course of matrix secretion as well as potential differences in their composition. Furthermore, complexity of the hydrogel environment is changed drastically in *in vivo* studies contrasted to *in vitro* surroundings. Besides chemical differences like growth factors and oxygen gradients occurring[204], cellular components like immune cells[205] and neighbouring tissue-specific cells can influence the behaviour of cells present within the hydrogel. This will further be affected by mechanical compression forces, which are considered to be a major driving factor for osteochondral reconstruction.[206]

Extending the impact of this project beyond the immediate aims, contributions to other projects have led to various co-authorships (see 5.2 page 124).

Bibliography

1. Lories, R.J. and F.P. Luyten, *The bone-cartilage unit in osteoarthritis.* Nat Rev Rheumatol, 2011. **7**(1): p. 43-9.

2. Makris, E.A., et al., *Repair and tissue engineering techniques for articular cartilage.* Nat Rev Rheumatol, 2015. **11**(1): p. 21-34.

3. Garcia-Gareta, E., M.J. Coathup, and G.W. Blunn, *Osteoinduction of bone grafting materials for bone repair and regeneration.* Bone, 2015. **81**: p. 112-121.

4. Langer, R. and J.P. Vacanti, *Tissue engineering.* Science, 1993. **260**(5110): p. 920-6.

5. Urist, M.R., et al., *Inductive substrates for bone formation.* Clin Orthop Relat Res, 1968. **59**: p. 59-96.

6. Laskin, R.S., *Unicompartmental tibiofemoral resurfacing arthroplasty.* J Bone Joint Surg Am, 1978. **60**(2): p. 182-5.

7. Haasper, C., et al., *Tissue engineering of osteochondral constructs in vitro using bioreactors.* Injury, 2008. **39 Suppl 1**: p. S66-76.

8. Jacobi, M., et al., *MACI - a new era?* Sports Med Arthrosc Rehabil Ther Technol, 2011. **3**(1): p. 10.

9. Marlovits, S., et al., *Clinical and radiological outcomes 5 years after matrix-induced autologous chondrocyte implantation in patients with symptomatic, traumatic chondral defects.* Am J Sports Med, 2012. **40**(10): p. 2273-80.

10. Zheng, M.H., et al., *Matrix-induced autologous chondrocyte implantation (MACI): biological and histological assessment.* Tissue Eng, 2007. **13**(4): p. 737-46.

11. Kon, E., et al., *Scaffold-based cartilage treatments: with or without cells? A systematic review of preclinical and clinical evidence.* Arthroscopy, 2015. **31**(4): p. 767-75.

12. Oda, K., et al., *Comparison of repair between cartilage and osteocartilage defects in rabbits using similarly manipulated scaffold-free cartilage-like constructs.* J Orthop Sci, 2014. **19**(4): p. 637-45.

13. Costa, E., et al., *Maintenance of chondrocyte phenotype during expansion on PLLA microtopographies.* J Tissue Eng, 2018. **9**: p. 2041731418789829.

14. Lafont, J.E., et al., *Hypoxia potentiates the BMP-2 driven COL2A1 stimulation in human articular chondrocytes via p38 MAPK.* Osteoarthritis Cartilage, 2016. **24**(5): p. 856-67.

15. Lafont, J.E., et al., *Hypoxia promotes the differentiated human articular chondrocyte phenotype through SOX9-dependent and -independent pathways.* J Biol Chem, 2008. **283**(8): p. 4778-86.

16. Suzuki, T., et al., *Regeneration of defects in the articular cartilage in rabbit temporomandibular joints by bone morphogenetic protein-2.* Br J Oral Maxillofac Surg, 2002. **40**(3): p. 201-6.

17. Takafuji, H., et al., *Regeneration of articular cartilage defects in the temporomandibular joint of rabbits by fibroblast growth factor-2: a pilot study.* Int J Oral Maxillofac Surg, 2007. **36**(10): p. 934-7.

18. Jeon, J.E., et al., *Perspectives in multiphasic osteochondral tissue engineering.* Anat Rec (Hoboken), 2014. **297**(1): p. 26-35.

19. Dormer, N.H., et al., *Osteochondral interface regeneration of rabbit mandibular condyle with bioactive signal gradients.* J Oral Maxillofac Surg, 2011. **69**(6): p. e50-7.

20. Fernandez-Torres, J., et al., *Hypoxia-Inducible Factors (HIFs) in the articular cartilage: a systematic review.* Eur Rev Med Pharmacol Sci, 2017. **21**(12): p. 2800-2810.

21. Taheem, D.K., et al., *Differential Regulation of Human Bone Marrow Mesenchymal Stromal Cell Chondrogenesis by Hypoxia Inducible Factor-1alpha Hydroxylase Inhibitors.* Stem Cells, 2018. **36**(9): p. 1380-1392.

22. Sathy, B.N., et al., *Hypoxia mimicking hydrogels to regulate the fate of transplanted stem cells.* Acta Biomater, 2019. **88**: p. 314-324.

23. Chan, M.C., et al., *Tuning the Transcriptional Response to Hypoxia by Inhibiting Hypoxia-inducible Factor (HIF) Prolyl and Asparaginyl Hydroxylases.* J Biol Chem, 2016. **291**(39): p. 20661-73.

24. Nguyen, L.K., et al., *A dynamic model of the hypoxia-inducible factor 1alpha (HIF-1alpha) network.* J Cell Sci, 2013. **126**(Pt 6): p. 1454-63.

25. Sridharan, B., et al., *In vivo evaluation of stem cell aggregates on osteochondral regeneration.* J Orthop Res, 2017. **35**(8): p. 1606-1616.

26. Ishihara, K., et al., *Simultaneous regeneration of full-thickness cartilage and subchondral bone defects in vivo using a three-dimensional scaffold-free autologous construct derived from high-density bone marrow-derived mesenchymal stem cells.* J Orthop Surg Res, 2014. **9**: p. 98.

27. Radhakrishnan, J., et al., *Injectable and 3D Bioprinted Polysaccharide Hydrogels: From Cartilage to Osteochondral Tissue Engineering.* Biomacromolecules, 2017. **18**(1): p. 1-26.

28. Wang, W., et al., *An anti-inflammatory cell-free collagen/resveratrol scaffold for repairing osteochondral defects in rabbits.* Acta Biomater, 2014. **10**(12): p. 4983-4995.

29. Sofu, H., et al., *Results of Hyaluronic Acid-Based Cell-Free Scaffold Application in Combination With Microfracture for the Treatment of Osteochondral Lesions of the Knee: 2-Year Comparative Study.* Arthroscopy, 2017. **33**(1): p. 209-216.

30. Brix, M., et al., *Successful osteoconduction but limited cartilage tissue quality following osteochondral repair by a cell-free multilayered nano-composite scaffold at the knee.* Int Orthop, 2016. **40**(3): p. 625-32.

31. Hindle, P., et al., *Autologous osteochondral mosaicplasty or TruFit plugs for cartilage repair.* Knee Surg Sports Traumatol Arthrosc, 2014. **22**(6): p. 1235-40.

32. Zhang, L., et al., *Three-dimensional (3D) printed scaffold and material selection for bone repair.* Acta Biomaterialia, 2019. **84**: p. 16-33.

33. Gu, B.K., et al., *3D Bioprinting Technologies for Tissue Engineering Applications.* Adv Exp Med Biol, 2018. **1078**: p. 15-28.

34. Daly, A.C., et al., *3D Bioprinting for Cartilage and Osteochondral Tissue Engineering.* Adv Healthc Mater, 2017. **6**(22).

35. Guo, T., et al., *3D printed biofunctionalized scaffolds for microfracture repair of cartilage defects.* Biomaterials, 2018. **185**: p. 219-231.

36. Zeng, L., et al., *Effect of microcavitary alginate hydrogel with different pore sizes on chondrocyte culture for cartilage tissue engineering.* Mater Sci Eng C Mater Biol Appl, 2014. **34**: p. 168-75.

37. Fonseca, K.B., et al., *Injectable MMP-sensitive alginate hydrogels as hMSC delivery systems.* Biomacromolecules, 2014. **15**(1): p. 380-90.

38. Choi, B., et al., *Cartilaginous extracellular matrix-modified chitosan hydrogels for cartilage tissue engineering.* ACS Appl Mater Interfaces, 2014. **6**(22): p. 20110-21.

39. Muhonen, V., et al., *Recombinant human type II collagen hydrogel provides a xeno-free 3D micro-environment for chondrogenesis of human bone marrow-derived mesenchymal stromal cells.* J Tissue Eng Regen Med, 2017. **11**(3): p. 843-854.

40. Toh, W.S., et al., *Modulation of mesenchymal stem cell chondrogenesis in a tunable hyaluronic acid hydrogel microenvironment.* Biomaterials, 2012. **33**(15): p. 3835-45.

41. Vega, S.L., M.Y. Kwon, and J.A. Burdick, *Recent advances in hydrogels for cartilage tissue engineering.* Eur Cell Mater, 2017. **33**: p. 59-75.

42. Censi, R., A. Dubbini, and P. Matricardi, *Bioactive hydrogel scaffolds - advances in cartilage regeneration through controlled drug delivery.* Curr Pharm Des, 2015. **21**(12): p. 1545-55.

43. Ma, Q., J. Liao, and X. Cai, *Different Sources of Stem Cells and their Application in Cartilage Tissue Engineering.* Curr Stem Cell Res Ther, 2018. **13**(7): p. 568-575.

44. Pereira, H., et al., *Hyaluronic Acid.* Adv Exp Med Biol, 2018. **1059**: p. 137-153.

45. Tanaka, E., M.S. Detamore, and L.G. Mercuri, *Degenerative disorders of the temporomandibular joint: etiology, diagnosis, and treatment.* J Dent Res, 2008. **87**(4): p. 296-307.

46. Yuan, T., et al., *Collagen hydrogel as an immunomodulatory scaffold in cartilage tissue engineering.* J Biomed Mater Res B Appl Biomater, 2014. **102**(2): p. 337-44.

47. Ahsan, T. and R.L. Sah, *Biomechanics of integrative cartilage repair.* Osteoarthritis Cartilage, 1999. **7**(1): p. 29-40.

48. Boushell, M.K., et al., *Current strategies for integrative cartilage repair.* Connect Tissue Res, 2017. **58**(5): p. 393-406.

49. Moroni, L. and J.H. Elisseeff, *Biomaterials engineered for integration.* Materials Today, 2008. **11**(5): p. 44-51.

50. Wang, D.A., et al., *Multifunctional chondroitin sulphate for cartilage tissue-biomaterial integration.* Nat Mater, 2007. **6**(5): p. 385-92.

51. Zhu, W., J. Iqbal, and D.-A. Wang, *A DOPA-functionalized chondroitin sulfate-based adhesive hydrogel as a promising multi-functional bioadhesive.* Journal of Materials Chemistry B, 2019. **7**(10): p. 1741-1752.

52. Kord Forooshani, P. and B.P. Lee, *Recent approaches in designing bioadhesive materials inspired by mussel adhesive protein.* J Polym Sci A Polym Chem, 2017. **55**(1): p. 9-33.

53. Lee, B.P., et al., *Mussel-Inspired Adhesives and Coatings.* Annu Rev Mater Res, 2011. **41**: p. 99-132.

54. Kim, J.Y., S.B. Ryu, and K.D. Park, *Preparation and characterization of dual-crosslinked gelatin hydrogel via Dopa-Fe3+ complexation and fenton reaction.* Journal of Industrial and Engineering Chemistry, 2018. **58**: p. 105-112.

55. Han, L., et al., *Mussel-Inspired Adhesive and Tough Hydrogel Based on Nanoclay Confined Dopamine Polymerization.* ACS Nano, 2017. **11**(3): p. 2561-2574.

56. Lee, B.P., J.L. Dalsin, and P.B. Messersmith, *Synthesis and gelation of DOPA-modified poly(ethylene glycol) hydrogels.* Biomacromolecules, 2002. **3**(5): p. 1038-47.

57. Moreira Teixeira, L.S., et al., *Self-attaching and cell-attracting in-situ forming dextran-tyramine conjugates hydrogels for arthroscopic cartilage repair.* Biomaterials, 2012. **33**(11): p. 3164-74.

58. Cui, X., et al., *Rapid Photocrosslinking of Silk Hydrogels with High Cell Density and Enhanced Shape Fidelity.* Adv Healthc Mater, 2020. **9**(4): p. e1901667.

59. Naahidi, S., et al., *Biocompatibility of hydrogel-based scaffolds for tissue engineering applications.* Biotechnology Advances, 2017. **35**(5): p. 530-544.

60. Drury, J.L. and D.J. Mooney, *Hydrogels for tissue engineering: scaffold design variables and applications.* Biomaterials, 2003. **24**(24): p. 4337-51.

61. Hu, W., et al., *Advances in crosslinking strategies of biomedical hydrogels.* Biomater Sci, 2019. **7**(3): p. 843-855.

62. Hedberg, E.L., et al., *In vitro degradation of porous poly(propylene fumarate)/poly(dl-lactic-co-glycolic acid) composite scaffolds.* Biomaterials, 2005. **26**(16): p. 3215-3225.

63. Ferreira, S.A., et al., *Bi-directional cell-pericellular matrix interactions direct stem cell fate.* Nat Commun, 2018. **9**(1): p. 4049.

64. Shah, R. *Temporomandibular Joint (TMJ) Disorders: An Overview*. 2020; Available from: https://www.pain-health.com/conditions/facial-pain/temporomandibular-joint-tmj-disorders-overview.

65. Hansson, T., et al., *Thickness of the soft tissue layers and the articular disk in the temporomandibular joint.* Acta Odontol Scand, 1977. **35**(2): p. 77-83.

66. Shibukawa, Y., et al., *Temporomandibular joint formation and condyle growth require Indian hedgehog signaling.* Dev Dyn, 2007. **236**(2): p. 426-34.

67. Ochiai, T., et al., *Indian hedgehog roles in post-natal TMJ development and organization.* J Dent Res, 2010. **89**(4): p. 349-54.

68. Shen, G., *The role of type X collagen in facilitating and regulating endochondral ossification of articular cartilage.* Orthod Craniofac Res, 2005. **8**(1): p. 11-7.

69. Singh, M. and M.S. Detamore, *Biomechanical properties of the mandibular condylar cartilage and their relevance to the TMJ disc.* J Biomech, 2009. **42**(4): p. 405-17.

70. Chai, Y., et al., *Fate of the mammalian cranial neural crest during tooth and mandibular morphogenesis.* Development, 2000. **127**(8): p. 1671-9.

71. Bouaziz, W., et al., *Loss of sclerostin promotes osteoarthritis in mice via beta-catenin-dependent and -independent Wnt pathways.* Arthritis Res Ther, 2015. **17**: p. 24.

72. Funck-Brentano, T., et al., *Dkk-1-mediated inhibition of Wnt signaling in bone ameliorates osteoarthritis in mice.* Arthritis Rheumatol, 2014. **66**(11): p. 3028-39.

73. Baron, R. and M. Kneissel, *WNT signaling in bone homeostasis and disease: from human mutations to treatments.* Nat Med, 2013. **19**(2): p. 179-92.

74. Strobel, S., et al., *Anabolic and catabolic responses of human articular chondrocytes to varying oxygen percentages.* Arthritis Res Ther, 2010. **12**(2): p. R34.

75. Hunter, D.J., *Risk stratification for knee osteoarthritis progression: a narrative review.* Osteoarthritis Cartilage, 2009. **17**(11): p. 1402-7.

76. Chisnoiu, A.M., et al., *Factors involved in the etiology of temporomandibular disorders - a literature review.* Clujul Med, 2015. **88**(4): p. 473-8.

77. Gage, J.P., *Collagen biosynthesis related to temporomandibular joint clicking in childhood.* J Prosthet Dent, 1985. **53**(5): p. 714-7.

78. Sidebottom, A.J., *Current thinking in temporomandibular joint management.* Br J Oral Maxillofac Surg, 2009. **47**(2): p. 91-4.

79. Wilkes, C.H., *Internal derangements of the temporomandibular joint. Pathological variations.* Arch Otolaryngol Head Neck Surg, 1989. **115**(4): p. 469-77.

80. Chen, Y.J., et al., *Individualized oblique-axial magnetic resonance imaging for improved visualization of mediolateral TMJ disc displacement.* J Orofac Pain, 2000. **14**(2): p. 128-39.

81. Chen, F., et al., *Bone graft in the shape of human mandibular condyle reconstruction via seeding marrow-derived osteoblasts into porous coral in a nude mice model.* J Oral Maxillofac Surg, 2002. **60**(10): p. 1155-9.

82. Von Korff, M., L. Le Resche, and S.F. Dworkin, *First onset of common pain symptoms: a prospective study of depression as a risk factor.* Pain, 1993. **55**(2): p. 251-8.

83. Maixner, W., et al., *Orofacial pain prospective evaluation and risk assessment study--the OPPERA study.* J Pain, 2011. **12**(11 Suppl): p. T4-11 e1-2.

84. List, T. and S. Axelsson, *Management of TMD: evidence from systematic reviews and meta-analyses.* J Oral Rehabil, 2010. **37**(6): p. 430-51.

85. Nitzan, D.W. and A. Price, *The use of arthrocentesis for the treatment of osteoarthritic temporomandibular joints.* J Oral Maxillofac Surg, 2001. **59**(10): p. 1154-9; discussion 1160.

86. Laskin, D.M.G., C.S.; Hylander, W.L., *TMDs: an evidence-based approach to diagnosis and treatment*. 2006: British Dental Journal.

87. Liu, F., et al., *Retrospective study of facial nerve function following temporomandibular joint arthroplasty using the endaural approach.* Craniomaxillofac Trauma Reconstr, 2015. **8**(2): p. 88-93.

88. Sindelar, B.J. and S.W. Herring, *Soft tissue mechanics of the temporomandibular joint.* Cells Tissues Organs, 2005. **180**(1): p. 36-43.

89. Sun, Z., Z.J. Liu, and S.W. Herring, *Movement of temporomandibular joint tissues during mastication and passive manipulation in miniature pigs.* Arch Oral Biol, 2002. **47**(4): p. 293-305.

90. Almarza, A.J., et al., *Preclinical Animal Models for Temporomandibular Joint Tissue Engineering.* Tissue Eng Part B Rev, 2018. **24**(3): p. 171-178.

91. Zhu, S., et al., *NEL-like molecule-1-modified bone marrow mesenchymal stem cells/poly lactic-co-glycolic acid composite improves repair of large osteochondral defects in mandibular condyle.* Osteoarthritis Cartilage, 2011. **19**(6): p. 743-50.

92. Wang, L., M. Lazebnik, and M.S. Detamore, *Hyaline cartilage cells outperform mandibular condylar cartilage cells in a TMJ fibrocartilage tissue engineering application.* Osteoarthritis Cartilage, 2009. **17**(3): p. 346-53.

93. Murakami, K., *Rationale of arthroscopic surgery of the temporomandibular joint.* J Oral Biol Craniofac Res, 2013. **3**(3): p. 126-34.

94. McCain, J.P., *Principles and Practice of Temporomandibular Joint*. 1996.

95. Quinn, J.H., *Arthroscopic management of temporomandibular joint disc perforations and associated advanced chondromalacia by discoplasty and abrasion arthroplasty: preliminary results.* J Oral Maxillofac Surg, 1994. **52**(8): p. 800-6; discussion 806-7.

96. BAOMS, *Annual meeting of British Association of Oral and Maxillofacial Surgeons 2016.* 2016.

97. Maytin, E.V., *Hyaluronan: More than just a wrinkle filler.* Glycobiology, 2016. **26**(6): p. 553-9.

98. Walker, K., et al., *Hyaluronic Acid*, in *StatPearls*. 2020: Treasure Island (FL).

99. Holmes, M.W., M.T. Bayliss, and H. Muir, *Hyaluronic acid in human articular cartilage. Age-related changes in content and size.* Biochem J, 1988. **250**(2): p. 435-41.

100. Iturriaga, V., et al., *Effect of hyaluronic acid on the regulation of inflammatory mediators in osteoarthritis of the temporomandibular joint: a systematic review.* Int J Oral Maxillofac Surg, 2017. **46**(5): p. 590-595.

101. Akmal, M., et al., *The effects of hyaluronic acid on articular chondrocytes.* J Bone Joint Surg Br, 2005. **87**(8): p. 1143-9.

102. Evans, N.D., et al., *Substrate stiffness affects early differentiation events in embryonic stem cells.* Eur Cell Mater, 2009. **18**: p. 1-13; discussion 13-4.

103. Olivares-Navarrete, R., et al., *Substrate Stiffness Controls Osteoblastic and Chondrocytic Differentiation of Mesenchymal Stem Cells without Exogenous Stimuli.* PLoS One, 2017. **12**(1): p. e0170312.

104. Walters, N.J. and E. Gentleman, *Evolving insights in cell-matrix interactions: elucidating how non-soluble properties of the extracellular niche direct stem cell fate.* Acta Biomater, 2015. **11**: p. 3-16.

105. Huebsch, N., et al., *Harnessing traction-mediated manipulation of the cell/matrix interface to control stem-cell fate.* Nat Mater, 2010. **9**(6): p. 518-26.

106. Khetan, S., et al., *Degradation-mediated cellular traction directs stem cell fate in covalently crosslinked three-dimensional hydrogels.* Nat Mater, 2013. **12**(5): p. 458-65.

107. Lutolf, M.P., *Biomaterials: Spotlight on hydrogels.* Nat Mater, 2009. **8**(6): p. 451-3.

108. Guvendiren, M. and J.A. Burdick, *Stiffening hydrogels to probe short- and long-term cellular responses to dynamic mechanics.* Nat Commun, 2012. **3**: p. 792.

109. Burdick, J.A., et al., *Controlled degradation and mechanical behavior of photopolymerized hyaluronic acid networks.* Biomacromolecules, 2005. **6**(1): p. 386-91.

110. Cam, C. and T. Segura, *Chemical sintering generates uniform porous hyaluronic acid hydrogels.* Acta Biomater, 2014. **10**(1): p. 205-13.

111. Pedron, S., et al., *Extracellular Hyaluronic Acid Influences the Efficacy of EGFR Tyrosine Kinase Inhibitors in a Biomaterial Model of Glioblastoma.* Adv Healthc Mater, 2017. **6**(21).

112. Khoshakhlagh, P. and M.J. Moore, *Photoreactive interpenetrating network of hyaluronic acid and Puramatrix as a selectively tunable scaffold for neurite growth.* Acta Biomater, 2015. **16**: p. 23-34.

113. Wei, Z., et al., *Dual Cross-Linked Biofunctional and Self-Healing Networks to Generate User-Defined Modular Gradient Hydrogel Constructs.* Adv Healthc Mater, 2017. **6**(16).

114. Nair, D.P., et al., *The Thiol-Michael Addition Click Reaction: A Powerful and Widely Used Tool in Materials Chemistry.* Chemistry of Materials, 2014. **26**(1): p. 724-744.

115. Pfeifer, G.P., Y.H. You, and A. Besaratinia, *Mutations induced by ultraviolet light.* Mutat Res, 2005. **571**(1-2): p. 19-31.

116. Ruskowitz E.R., D.C.A., *Proteome-wide Analysis of Cellular Response to Ultraviolet Light for Biomaterial Synthesis and Modification.* ACS Biomater. Sci., 2019: p. 2111-2116.

117. Yadav, R. and M. Kumar, *Dental restorative composite materials: A review.* J Oral Biosci, 2019. **61**(2): p. 78-83.

118. Chesterman, J., et al., *Bulk-fill resin-based composite restorative materials: a review.* Br Dent J, 2017. **222**(5): p. 337-344.

119. Fugolin, A.P.P. and C.S. Pfeifer, *New Resins for Dental Composites.* J Dent Res, 2017. **96**(10): p. 1085-1091.

120. Kaastrup, K. and H.D. Sikes, *Using photo-initiated polymerization reactions to detect molecular recognition.* Chem Soc Rev, 2016. **45**(3): p. 532-45.

121. Shih, H. and C.C. Lin, *Visible-light-mediated thiol-ene hydrogelation using eosin-Y as the only photoinitiator.* Macromol Rapid Commun, 2013. **34**(3): p. 269-73.

122. Karami, P., et al., *Composite Double-Network Hydrogels To Improve Adhesion on Biological Surfaces.* ACS Appl Mater Interfaces, 2018. **10**(45): p. 38692-38699.

123. Poldervaart, M.T., et al., *3D bioprinting of methacrylated hyaluronic acid (MeHA) hydrogel with intrinsic osteogenicity.* PLoS One, 2017. **12**(6): p. e0177628.

124. Bian, L., et al., *The influence of hyaluronic acid hydrogel crosslinking density and macromolecular diffusivity on human MSC chondrogenesis and hypertrophy.* Biomaterials, 2013. **34**(2): p. 413-21.

125. Renard, J.L., D. Felten, and D. Bequet, *Post-otoneurosurgery aluminium encephalopathy.* Lancet, 1994. **344**(8914): p. 63-4.

126. Bale, A.S., et al., *A review of potential neurotoxic mechanisms among three chlorinated organic solvents.* Toxicol Appl Pharmacol, 2011. **255**(1): p. 113-26.

127. Jacubovich, R.M., et al., *Facial nerve palsy after acute exposure to dichloromethane.* Am J Ind Med, 2005. **48**(5): p. 389-92.

128. Leng, Y., et al., *Hyaluronic acid, CD44 and RHAMM regulate myoblast behavior during embryogenesis.* Matrix Biol, 2019. **78-79**: p. 236-254.

129. Dowthwaite, G.P., J.C. Edwards, and A.A. Pitsillides, *An essential role for the interaction between hyaluronan and hyaluronan binding proteins during joint development.* J Histochem Cytochem, 1998. **46**(5): p. 641-51.

130. Penoff, J., *Skin closures using cyanoacrylate tissue adhesives. Plastic Surgery Educational Foundation DATA Committee. Device and Technique Assessment.* Plast Reconstr Surg, 1999. **103**(2): p. 730-1.

131. Sung, H.W., et al., *Gelatin-derived bioadhesives for closing skin wounds: an in vivo study.* J Biomater Sci Polym Ed, 1999. **10**(7): p. 751-71.

132. Iwata, H., et al., *A novel surgical glue composed of gelatin and N-hydroxysuccinimide activated poly(L-glutamic acid):: Part 1. Synthesis of activated poly(L-glutamic acid) and its gelation with gelatin.* Biomaterials, 1998. **19**(20): p. 1869-1876.

133. Ono, K., et al., *Photocrosslinkable chitosan as a biological adhesive.* (0021-9304 (Print)).

134. Noori, A., et al., *A review of fibrin and fibrin composites for bone tissue engineering.* Int J Nanomedicine, 2017. **12**: p. 4937-4961.

135. Roberts, I.V., et al., *Fibrin Matrices as (Injectable) Biomaterials: Formation, Clinical Use, and Molecular Engineering.* Macromol Biosci, 2020. **20**(1): p. e1900283.

136. Kan, Y., et al., *Boronate complex formation with Dopa containing mussel adhesive protein retards ph-induced oxidation and enables adhesion to mica.* PLoS One, 2014. **9**(10): p. e108869.

137. Krogsgaard, M., et al., *Self-healing mussel-inspired multi-pH-responsive hydrogels.* Biomacromolecules, 2013. **14**(2): p. 297-301.

138. Chan Choi, Y., et al., *Human gelatin tissue-adhesive hydrogels prepared by enzyme-mediated biosynthesis of DOPA and Fe3+ ion crosslinking.* Journal of Materials Chemistry B, 2014. **2**(2): p. 201-209.

139. Meng, H., et al., *Hydrogen peroxide generation and biocompatibility of hydrogel-bound mussel adhesive moiety.* Acta Biomater, 2015. **17**: p. 160-9.

140. Trusek-Holownia, A. and A. Noworyta, *Efficient utilisation of hydrogel preparations with encapsulated enzymes - a case study on catalase and hydrogen peroxide degradation.* Biotechnol Rep (Amst), 2015. **6**: p. 13-19.

141. Blache, U., et al., *Notch-inducing hydrogels reveal a perivascular switch of mesenchymal stem cell fate.* EMBO Rep, 2018. **19**(8).

142. Ferreira, S.A., et al., *Bi-directional cell-pericellular matrix interactions direct stem cell fate.* Nat. Commun., 2018. **9**(1): p. 4049.

143. Loebel, C., R.L. Mauck, and J.A. Burdick, *Local nascent protein deposition and remodelling guide mesenchymal stromal cell mechanosensing and fate in three-dimensional hydrogels.* Nat. Mater., 2019. **18**(8): p. 883-891.

144. Coons, A.H., H.J. Creech, and R.N. Jones, *Immunological properties of an antibody containing a fluorescent group.* Exp Biol Med, 1941. **47**(2): p. 200-202.

145. Ferreira, S.A., et al., *Neighboring cells override 3D hydrogel matrix cues to drive human MSC quiescence.* Biomaterials, 2018. **176**: p. 13-23.

146. Wiseman, J.M., et al., *Desorption electrospray ionization mass spectrometry: Imaging drugs and metabolites in tissues.* Proc Natl Acad Sci USA, 2008. **105**(47): p. 18120-5.

147. Marx, V., *A dream of single-cell proteomics.* Nat Methods, 2019. **16**(9): p. 809-812.

148. McLeod, C.M. and R.L. Mauck, *High fidelity visualization of cell-to-cell variation and temporal dynamics in nascent extracellular matrix formation.* Sci Rep, 2016. **6**: p. 38852.

149. Autefage, H., et al., *Sparse feature selection methods identify unexpected global cellular response to strontium-containing materials.* Proc Natl Acad Sci USA, 2015. **112**(14): p. 4280-5.

150. Tarnowski, C.P., M.A. Ignelzi, Jr., and M.D. Morris, *Mineralization of developing mouse calvaria as revealed by Raman microspectroscopy.* J Bone Miner Res, 2002. **17**(6): p. 1118-26.

151. Autefage, H., et al., *Multiscale analyses reveal native-like lamellar bone repair and near perfect bone-contact with porous strontium-loaded bioactive glass.* Biomaterials, 2019. **209**: p. 152-162.

152. Loaiza, S., et al., *An engineered, quantifiable in vitro model for analysing the effect of proteostasis-targeting drugs on tissue physical properties.* Biomaterials, 2018. **183**: p. 102-113.

153. Gentleman, E., et al., *Comparative materials differences revealed in engineered bone as a function of cell-specific differentiation.* Nat. Mater., 2009. **8**(9): p. 763-70.

154. Volponi, A.A., et al., *Composition of Mineral Produced by Dental Mesenchymal Stem Cells.* J Dent Res, 2015. **94**(11): p. 1568-74.

155. Evans, N.D., et al., *Gene-expression analysis reveals that embryonic stem cells cultured under osteogenic conditions produce mineral non-specifically compared to marrow stromal cells or osteoblasts.* Eur Cell Mater, 2012. **24**: p. 211-23.

156. Thorre, K., et al., *New antioxidant mixture for long term stability of serotonin, dopamine and their metabolites in automated microbore liquid chromatography with dual electrochemical detection.* J Chromatogr B Biomed Sci Appl, 1997. **694**(2): p. 297-303.

157. Hong, S., et al., *Hyaluronic Acid Catechol: A Biopolymer Exhibiting a pH-Dependent Adhesive or Cohesive Property for Human Neural Stem Cell Engineering.* Advanced Functional Materials, 2013. **23**(14): p. 1774-1780.

158. Nie, J., A. Yap, and X. Wang, *Influence of Shrinkage and Viscosity of Flowable Composite Liners on Cervical Microleakage of Class II Restorations: A Micro-CT Analysis.* Operative Dentistry, 2018. **43**(6): p. 656-664.

159. *ISO 10993: Biological evaluation of medical devices*. International Organization for Standardization: https://www.iso.org/home.html.

160. McLeod, C.M. and R.L. Mauck, *High fidelity visualization of cell-to-cell variation and temporal dynamics in nascent extracellular matrix formation.* Scientific Reports, 2016. **6**(1): p. 38852.

161. Lee, Y., et al., *Thermo-sensitive, injectable, and tissue adhesive sol–gel transition hyaluronic acid/pluronic composite hydrogels prepared from bio-inspired catechol-thiol reaction.* Soft Matter, 2010. **6**(5): p. 977-983.

162. Nystrom, B., et al., *Characterization of polyelectrolyte features in polysaccharide systems and mucin.* Adv Colloid Interface Sci, 2010. **158**(1-2): p. 108-18.

163. Thorré K, P.M., Sarre S, Ebinger G, Michotte Y, *New antioxidant mixture for long term stability of serotonin, dopamine and their metabolites in automated microbore liquid chromatography with dual electrochemical detection.* Journal of Chromatography B: Biomedical Sciences and Applications, 1997.

164. Bitter, T. and H.M. Muir, *A modified uronic acid carbazole reaction.* Anal Biochem, 1962. **4**: p. 330-4.

165. Keller, L., et al., *Tooth engineering: searching for dental mesenchymal cells sources.* Front Physiol, 2011. **2**: p. 7.

166. Brauer, D.S., et al., *Benefits and drawbacks of zinc in glass ionomer bone cements.* Biomed Mater, 2011. **6**(4): p. 045007.

167. BRTILifeScience, *Quantification of Live/Dead Staining Using Fiji Software*. 2019: https://brtilifesciences.com/PDF/Quantification%20of%20Live_Dead%20Staining%20Using%20Fiji%20software.pdf.

168. Girish, K.S. and K. Kemparaju, *The magic glue hyaluronan and its eraser hyaluronidase: a biological overview.* Life Sci, 2007. **80**(21): p. 1921-43.

169. Hahn, S.K., et al., *Synthesis and degradation test of hyaluronic acid hydrogels.* Int J Biol Macromol, 2007. **40**(4): p. 374-80.

170. Park, Y.D., N. Tirelli, and J.A. Hubbell, *Photopolymerized hyaluronic acid-based hydrogels and interpenetrating networks.* Biomaterials, 2003. **24**(6): p. 893-900.

171. Guvendiren, M., P.B. Messersmith, and K.R. Shull, *Self-assembly and adhesion of DOPA-modified methacrylic triblock hydrogels.* Biomacromolecules, 2008. **9**(1): p. 122-8.

172. Galano, A.P.-G., A., *On the free radical scavenging mechanism of protocatechuic acid, regeneration of the catechol group in aqueous solution.* Theor. Chem. Acc., 2012.

173. Donovan, B.R., et al., *Thiol–ene adhesives from clove oil derivatives.* RSC Advances, 2014. **4**(106): p. 61927-61935.

174. Lih, E., et al., *Optimal conjugation of catechol group onto hyaluronic acid in coronary stent substrate coating for the prevention of restenosis.* J Tissue Eng, 2016. **7**: p. 2041731416683745.

175. Held, K.D. and D.C. Melder, *Toxicity of the sulfhydryl-containing radioprotector dithiothreitol.* Radiat Res, 1987. **112**(3): p. 544-54.

176. Zhao, T., et al., *Tunable, Injectable Hydrogels Based on Peptide-Cross-Linked, Cyclized Polymer Nanoparticles for Neural Progenitor Cell Delivery.* Biomacromolecules, 2017. **18**(9): p. 2723-2731.

177. Liu, Z.Q., et al., *Dextran-based hydrogel formed by thiol-Michael addition reaction for 3D cell encapsulation.* Colloids Surf B Biointerfaces, 2015. **128**: p. 140-148.

178. Liu, H.Y., et al., *Enzyme-mediated stiffening hydrogels for probing activation of pancreatic stellate cells.* Acta Biomater, 2017. **48**: p. 258-269.

179. Bian, L., et al., *Hydrogels that mimic developmentally relevant matrix and N-cadherin interactions enhance MSC chondrogenesis.* Proc Natl Acad Sci U S A, 2013. **110**(25): p. 10117-22.

180. Lisignoli, G., et al., *Hyaluronan-based polymer scaffold modulates the expression of inflammatory and degradative factors in mesenchymal stem cells: Involvement of Cd44 and Cd54.* J Cell Physiol, 2006. **207**(2): p. 364-73.

181. Zhu, H., et al., *The role of the hyaluronan receptor CD44 in mesenchymal stem cell migration in the extracellular matrix.* Stem Cells, 2006. **24**(4): p. 928-35.

182. Li, B., et al., *Mesenchymal stem cells exploit extracellular matrix as mechanotransducer.* Sci Rep, 2013. **3**: p. 2425.

183. Vining, K.H., et al., *Synthetic Light-Curable Polymeric Materials Provide a Supportive Niche for Dental Pulp Stem Cells.* Adv Mater, 2018. **30**(4).

184. Frehner, F. and J.P. Benthien, *Microfracture: State of the Art in Cartilage Surgery?* Cartilage, 2018. **9**(4): p. 339-345.

185. Gottschalk, O., et al., *Functional Medium-Term Results After Autologous Matrix-Induced Chondrogenesis for Osteochondral Lesions of the Talus: A 5-Year Prospective Cohort Study.* J Foot Ankle Surg, 2017. **56**(5): p. 930-936.

186. Sommerfeldt, M.F., et al., *Microfracture of Articular Cartilage.* JBJS Rev, 2016. **4**(6).

187. Zhao, X., et al., *Antibacterial anti-oxidant electroactive injectable hydrogel as self-healing wound dressing with hemostasis and adhesiveness for cutaneous wound healing.* Biomaterials, 2017. **122**: p. 34-47.

188. Han, L., et al., *Mussel-Inspired Tissue-Adhesive Hydrogel Based on the Polydopamine-Chondroitin Sulfate Complex for Growth-Factor-Free Cartilage Regeneration.* ACS Appl Mater Interfaces, 2018. **10**(33): p. 28015-28026.

189. Kao, F.J., G. Manivannan, and S.P. Sawan, *UV curable bioadhesives: copolymers of N-vinyl pyrrolidone.* J Biomed Mater Res, 1997. **38**(3): p. 191-6.

190. Shen, M., et al., *Rheology and adhesion of poly(acrylic acid)/laponite nanocomposite hydrogels as biocompatible adhesives.* Langmuir, 2014. **30**(6): p. 1636-42.

191. Rygula, A., et al., *Raman spectroscopy of proteins: a review.* J RAMAN SPECTROSC, 2013. **44**(8): p. 1061-1076.

192. Movasaghi, Z., S. Rehman, and I.U. Rehman, *Raman Spectroscopy of Biological Tissues.* Appl. Spectrosc. Rev., 2007. **42**(5): p. 493-541.

193. Duval, E., et al., *Molecular mechanism of hypoxia-induced chondrogenesis and its application in in vivo cartilage tissue engineering.* Biomaterials, 2012. **33**(26): p. 6042-51.

194. Thoms, B.L. and C.L. Murphy, *Inhibition of hypoxia-inducible factor-targeting prolyl hydroxylase domain-containing protein 2 (PHD2) enhances matrix synthesis by human chondrocytes.* J Biol Chem, 2010. **285**(27): p. 20472-80.

195. Niebler, S., et al., *Hypoxia-Inducible Factor 1 Is an Inductor of Transcription Factor Activating Protein 2 Epsilon Expression during Chondrogenic Differentiation.* Biomed Res Int, 2015. **2015**: p. 380590.

196. Gelse, K., et al., *Role of hypoxia-inducible factor 1 alpha in the integrity of articular cartilage in murine knee joints.* Arthritis Res Ther, 2008. **10**(5): p. R111.

197. von Erlach, T.C., M.A. Hedegaard, and M.M. Stevens, *High resolution Raman spectroscopy mapping of stem cell micropatterns.* Analyst, 2015. **140**(6): p. 1798-803.

198. Hedegaard, M.A., et al., *Model based variable selection as a tool to highlight biological differences in Raman spectra of cells.* Analyst, 2014. **139**(18): p. 4629-33.

199. Hedegaard, M.A., M.S. Bergholt, and M.M. Stevens, *Quantitative multi-image analysis for biomedical Raman spectroscopic imaging.* J Biophotonics, 2016. **9**(5): p. 542-50.

200. Savkovic, V., et al., *Mesenchymal stem cells in cartilage regeneration.* Curr Stem Cell Res Ther, 2014. **9**(6): p. 469-88.

201. Akkiraju, H. and A. Nohe, *Role of Chondrocytes in Cartilage Formation, Progression of Osteoarthritis and Cartilage Regeneration.* J Dev Biol, 2015. **3**(4): p. 177-192.

202. Park, E.J., et al., *Structural basis of blocking integrin activation and deactivation for anti-inflammation.* J Biomed Sci, 2015. **22**: p. 51.

203. Gahmberg, C.G., et al., *Regulation of integrin activity and signalling.* Biochim Biophys Acta, 2009. **1790**(6): p. 431-44.

204. O'Reilly, A. and D.J. Kelly, *Role of oxygen as a regulator of stem cell fate during the spontaneous repair of osteochondral defects.* J Orthop Res, 2016. **34**(6): p. 1026-36.

205. Smith, B., I.R. Sigal, and D.A. Grande, *Immunology and cartilage regeneration.* Immunol Res, 2015. **63**(1-3): p. 181-6.

206. Heuijerjans, A., et al., *Osteochondral resurfacing implantation angle is more important than implant material stiffness.* J Orthop Res, 2018. **36**(11): p. 2911-2922.

5 Supplementary information

5.1 Project publications

1) **Salzlechner C.**, Haghighi T., Huebscher I., Walther A.R., Schell S., Gardner A., Undt G., da Silva R.M.P., Dreiss C.A., Fan K., Gentleman E.; *Adhesive Hydrogels for Maxillofacial Tissue Regeneration Using Minimally Invasive Procedures*; Advanced Healthcare Materials, Volume 9, Issue 4; First published 14 January 2020; https://doi.org/10.1002/adhm.201901134

2) **Salzlechner C.**, Walther A.R., Schell S., Haghighi T., Huebscher I., Merrild N.G., Undt G., Bergholt M., Hedegaard M., Fan K., Gentleman E.; *Complementary techniques to analyse pericellular matrix formation by human MSC within hyaluronic acid hydrogels.;* manuscript in preparation

5.2 Associated publications

1) da Silva J.G., Babb R., **Salzlechner C.**, Sharpe P.T., Brauer D.S., Gentleman E.; *Optimisation of lithium-substituted bioactive glasses to tailor cell response for hard tissue repair.*; Journal of Materials Science, First published 9 February 2017, 2017;52(15):8832-8844; https://doi.org/10.1007/s10853-017-0838-7

2) Ferreira S.A., Motwani M.S., Faull P.A., Seymour A.J., Yu T.T.L., Enayati M., Taheem D.K., **Salzlechner C.**, Haghighi T., Kania E.M., Oommen O.P., Ahmed T., Loaiza S., Parzych K., Dazzi F., Varghese O.P., Festy F., Grigoriadis A.E., Auner H.W., Snijders A.P., Bozec L., Gentleman E.; *Bi-directional cell-pericellular matrix interactions direct stem cell fate.*; Nature Communications, First published 3 October 2018, (1):4049; https://doi.org/10.1038/s41467-018-06183-4

3) Zaugg L.K., Banu A., Walther A.R., Chandrasekaran D., Babb R.C., **Salzlechner C.**, Hedegaard M.A.B., Gentleman E., Sharpe P.T.; *Translation Approach for Dentine Regeneration Using GSK-3 Antagonists.*; Journal of Dental Research, March 2020, 10:22034520908593; https://doi.org/10.1177/0022034520908593

4) Alaohali A., **Salzlechner C.**, Chandrasekaran D., Gentleman E., Sharpe P.T.; *Delivering GSK-3 Antagonists via injectable hydrogels to promote natural dentinogenesis.;* manuscript in preparation

5.3 Supplementary movies

Movie 1: To demonstrate a sol-gel transition under aqueous conditions, the viscous solution (3 %, high MA, low Dopa, no 1 MDa HA) was pipetted into a cylindrical mould while fully submerged in water. The material settled to the base of the mould and was gelled with blue light. The hydrogel was removed from the mould after 4 minutes light exposure.

Movie 2: To demonstrate how Dopa-modified hydrogels adhere to tissue, a deep incision was made in the muscle of a mouse hindlimb. The muscle was then coated with sodium periodate to foster Dopa oxidation. The hydrogel precursor solution (3 %, High MA, low Dopa) was pipetted into the incision and exposed to blue light for 4 minutes and then left at RT for 30 minutes before recording the video. As the muscle tissue is pulled apart, the hydrogel remains adherent to the tissue surfaces.

Movie 3: To demonstrate the stability of the MA-HA-Dopa hydrogel-tissue interaction, the sample in Movie 2 was incubated for 5 days in PBS at 37 °C and the test repeated.

Movie 4: The movie demonstrates a 3D Raman image of a primary human mesenchymal stromal cell encapsulated in a MA-HA-Dopa hydrogel. The biochemical components of the cell identified using spectral unmixing data analysis are nucleus (red), proteins (blue and cyan) and lipids (yellow).

5.4 ^{1}NMR spectra

Figure 34 summarises the peaks to be expected according to ^{1}H-NMR for the single methacrylation as well as dopamination and methacrylation double-synthesis. ^{1}H-NMR spectra show a methyl peak (CH_3) for hyaluronic acid at ~ δ 2.1 ppm (**A**). Signals referring to methacrylation appeared at ~ δ 5.7 ppm and ~ δ 6.5 ppm (**C**), which refer to the methylene group of the coupled methacrylate ($C=CH_2$). Signals referring to dopamination refer to the hydrogens in the ring ($-CH_2$), appearing between ~ δ 6.5 ppm to ~ δ 7.3 ppm (**F**).

Peaks not used for quantifying the DOM are protons in N-terminus of Dopa ($-CH_2$) at ~ δ 2.8 (**E**), methyl group in the methacrylate (CH_3) at ~ δ 1.95 (**B**) as well as the proton of the secondary amine in N-acetylglucosamine at ~ δ 4.5 (**D**). Further peaks are generated by deuterium as solvent at ~ δ 4.8 (**D_2O**) and the hydrogens in the HA backbone at ~ δ 3.2-4.2 (HA hydrogens).

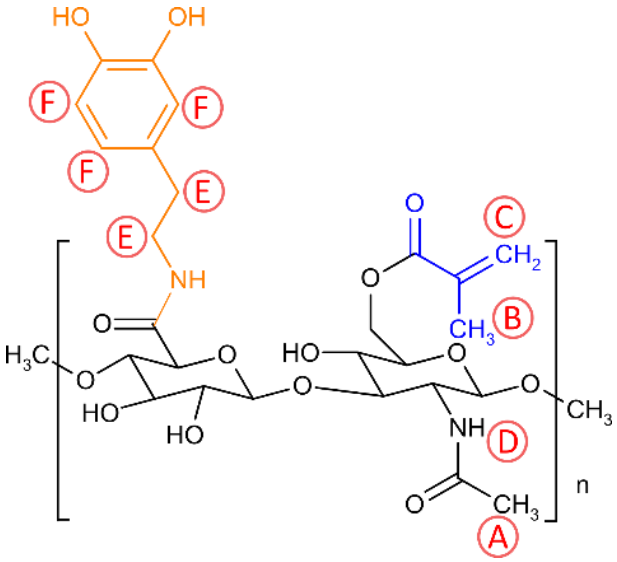

Figure 34: NMR peaks corresponding to protons.
*HA can be detected via methyl peak (CH_3) for at ~ δ 2.1 ppm (**A**) and the secondary amine in N-acetylglucosamine at ~ δ 4.5 (**D**), as well as aromatic groups at ~ δ 3.2-4.2. MA can be identified by methyl group ~ δ 1.95 (**B**) and methylene group at ~ δ 5.7 ppm and ~ δ 6.5 ppm (**C**). Dopa can be identified by N-terminus of Dopa (CH_2) at ~ δ 2.8 (**E**) and hydrogens in the ring (CH_2), ~ δ 6.5 ppm to ~ δ 7.3 ppm (**F**).*

5.4.1 ^{1}NMR plots for methacrylation reaction

Plots referring to manually adjusted pH protocol (Table 4).

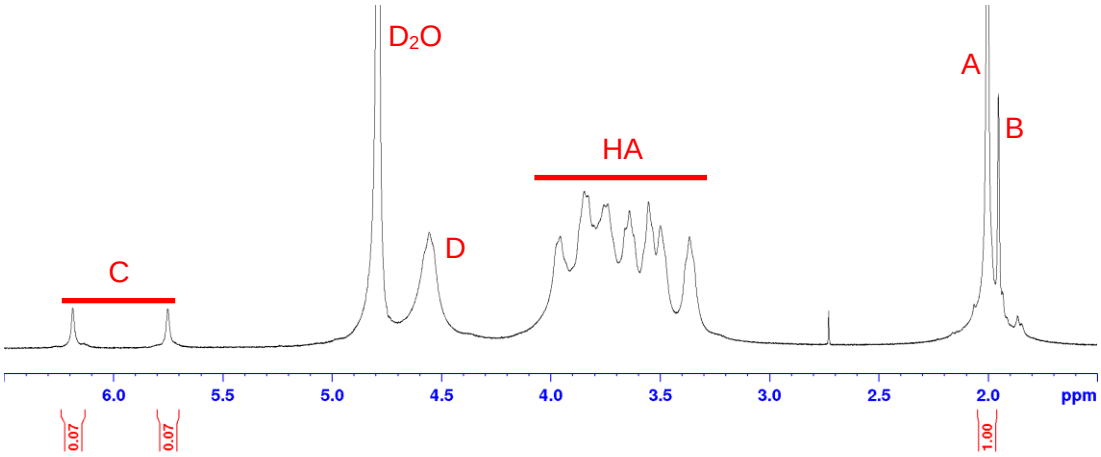

Figure 35: NMR plot for macromer MA21-Dopa0.
Spectra show presence of HA (A, HA and D) as well as MA groups (B, C) and the D_2O solvent.

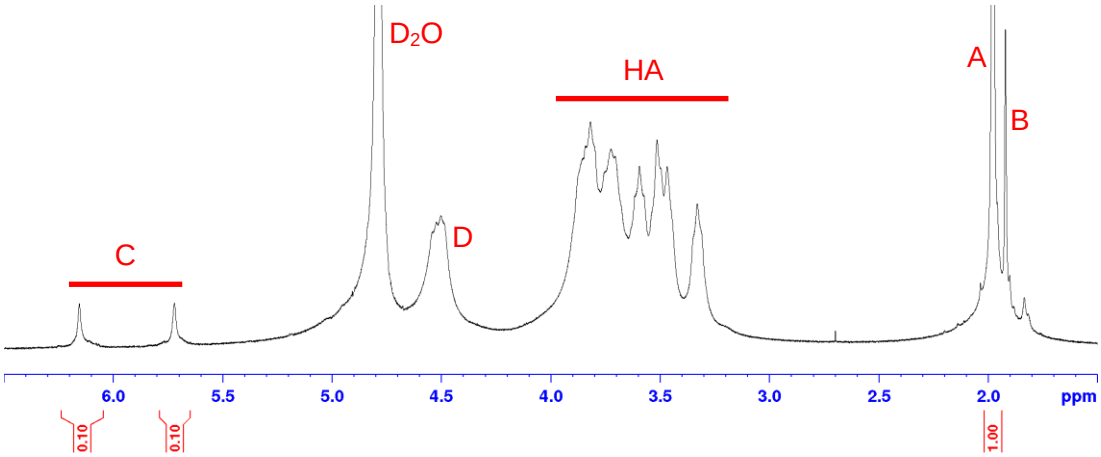

Figure 36: NMR plot for macromer MA30-Dopa0.
Spectra show presence of HA (A, HA and D) as well as MA groups (B, C) and the D_2O solvent.

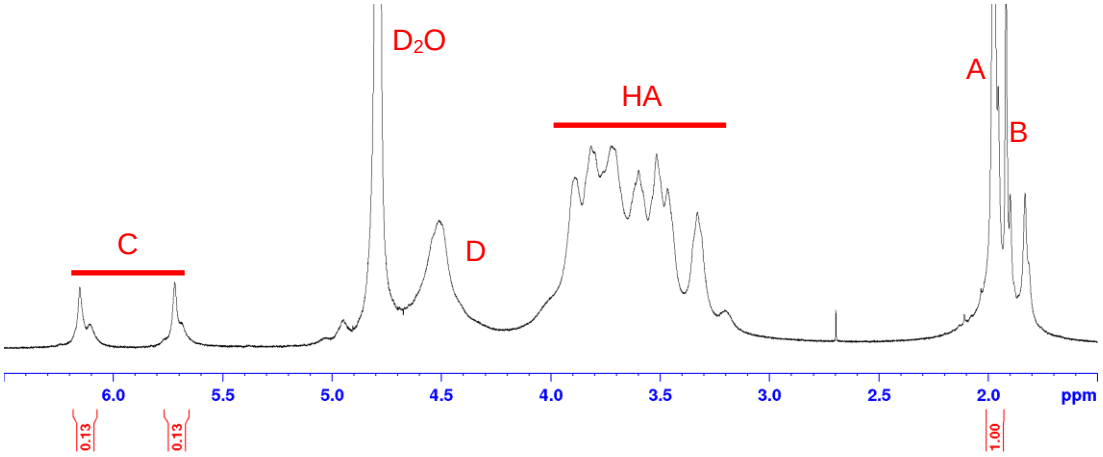

Figure 37: NMR plot for macromer MA40-Dopa0.

Spectra show presence of HA (A, HA and D) as well as MA groups (B, C) and the D_2O solvent.

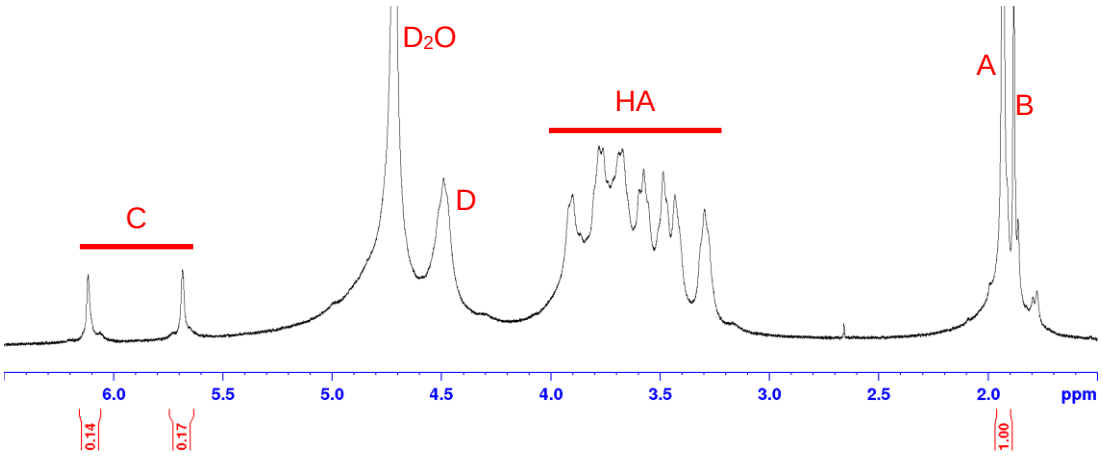

Figure 38: NMR plot for macromer MA47-Dopa0.

Spectra show presence of HA (A, HA and D) as well as MA groups (B, C) and the D_2O solvent.

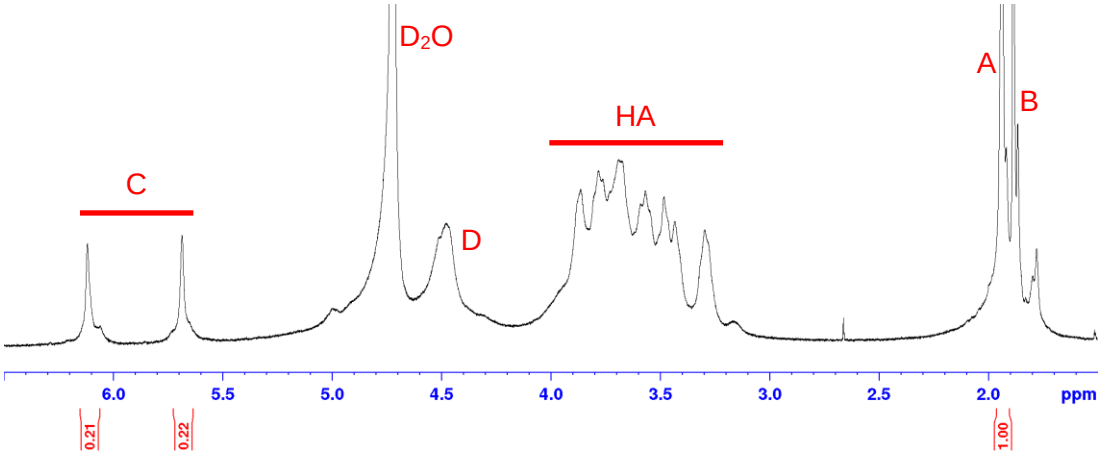

Figure 39: NMR plot for macromer MA65-Dopa0.

Spectra show presence of HA (A, HA and D) as well as MA groups (B, C) and the D_2O solvent.

5.4.2 ^{1}NMR plots for methacrylation (Tris)

Plots referring to Tis buffered methacrylation reaction (Table 5).

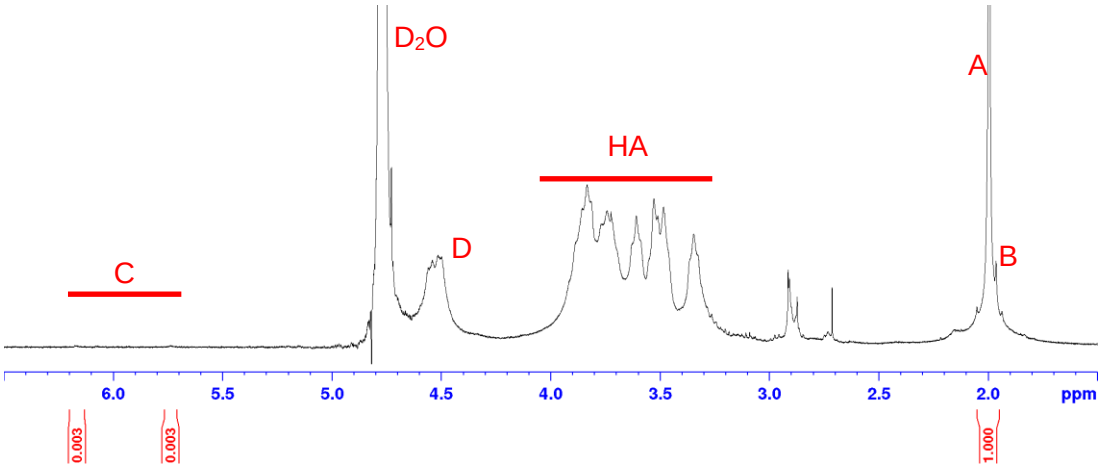

Figure 40: NMR plot for macromer MA1-Dopa0.
Spectra show presence of HA (A, HA and D) as well as MA groups (B, C) and the D_2O solvent.

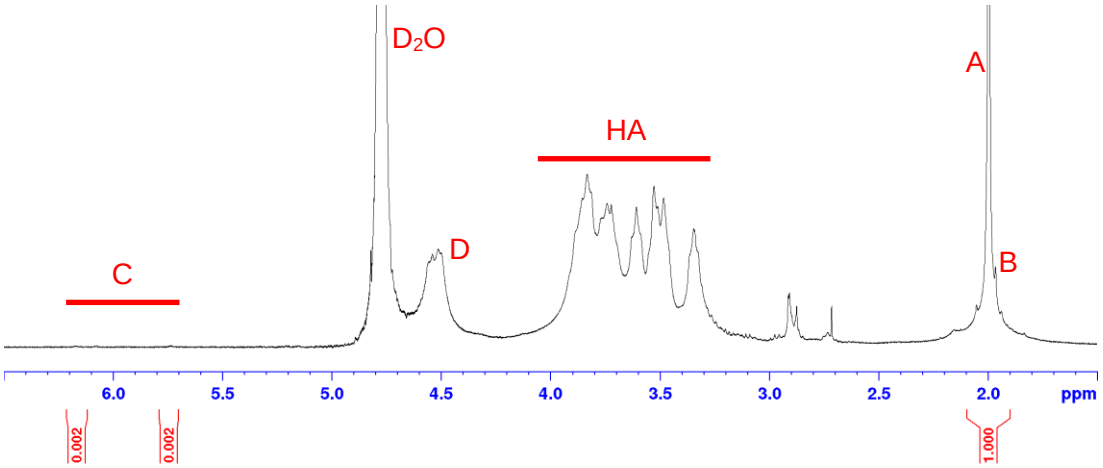

Figure 41: NMR plot for macromer MA1-Dopa0.
Spectra show presence of HA (A, HA and D) as well as MA groups (B, C) and the D_2O solvent.

5.4.3 ^{1}NMR plots for methacrylation reaction (MOPS)

Plots referring to MOPS buffered methacrylation reaction (Table 6).

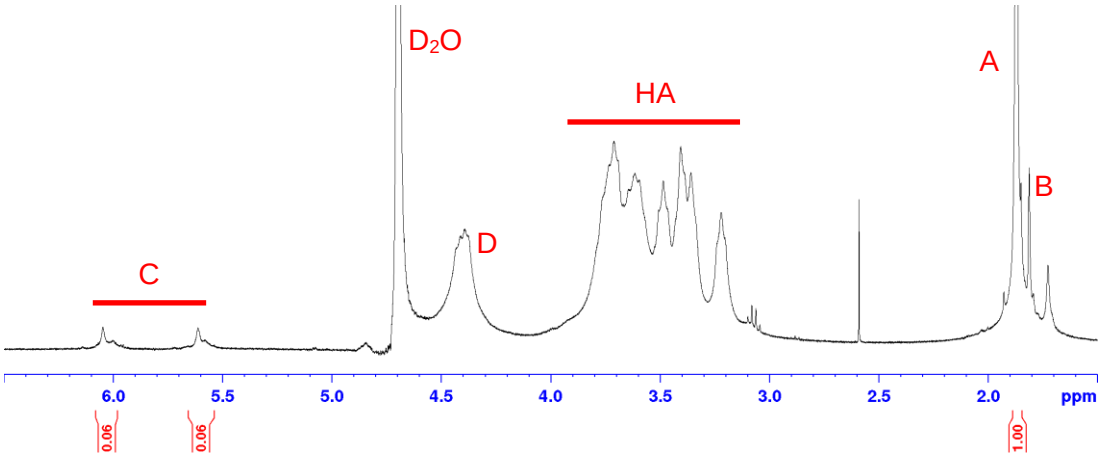

Figure 42: NMR plot for macromer MA18-Dopa0.

Spectra show presence of HA (A, HA and D) as well as MA groups (B, C) and the D_2O solvent.

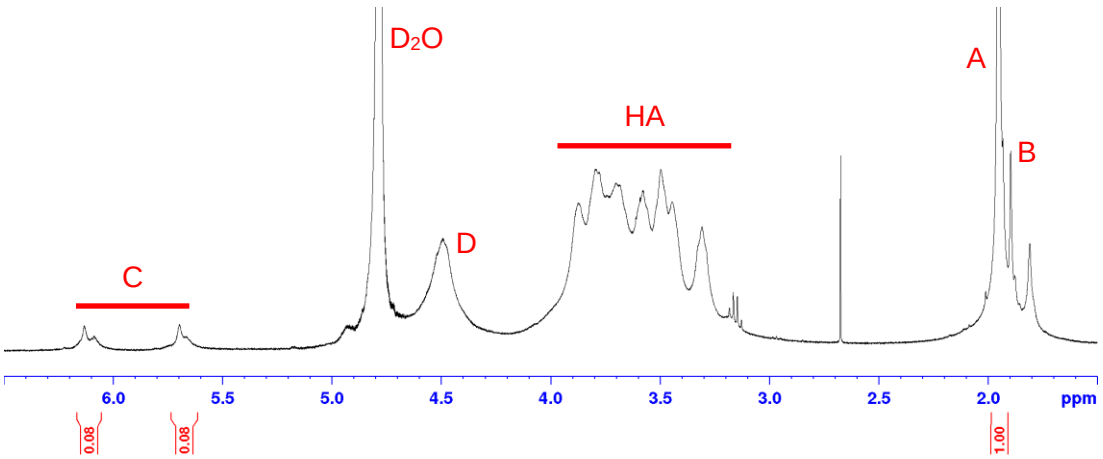

Figure 43: NMR plot for macromer MA24-Dopa0.

Spectra show presence of HA (A, HA and D) as well as MA groups (B, C) and the D_2O solvent.

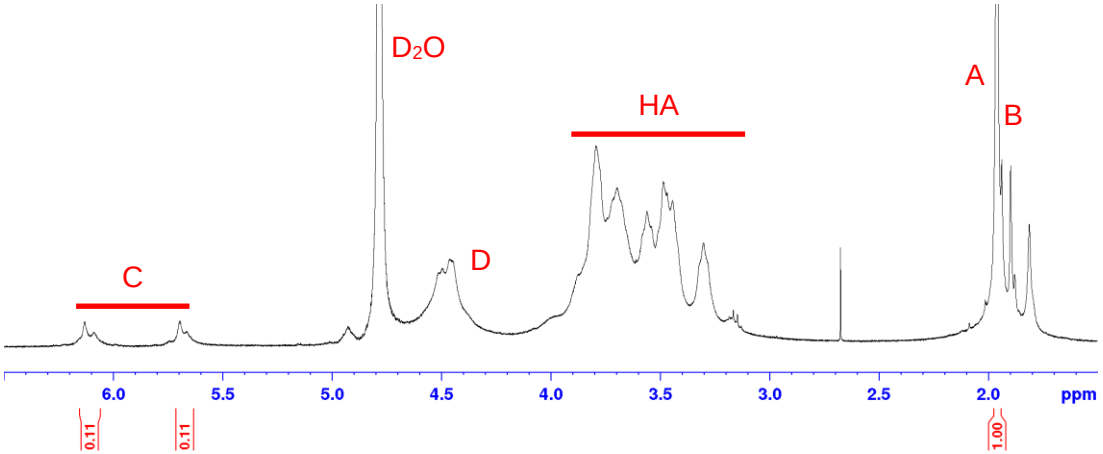

Figure 44: NMR plot for macromer MA33-Dopa0.

Spectra show presence of HA (A, HA and D) as well as MA groups (B, C) and the D_2O solvent.

5.4.4 ^{1}NMR plots for double-modified HA

Plots referring to HA modified with MA via manual pH adjustment and Dopa (Table 7).

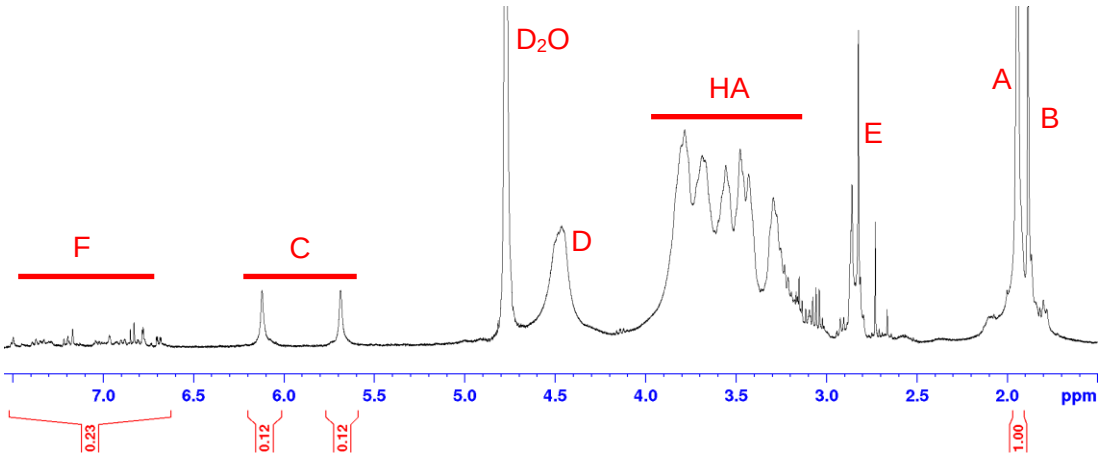

Figure 45: NMR plot for macromer MA36-Dopa23.
Spectra show presence of HA (A, HA and D) as well as MA groups (B, C), Dopa groups (E, F) and the D_2O solvent.

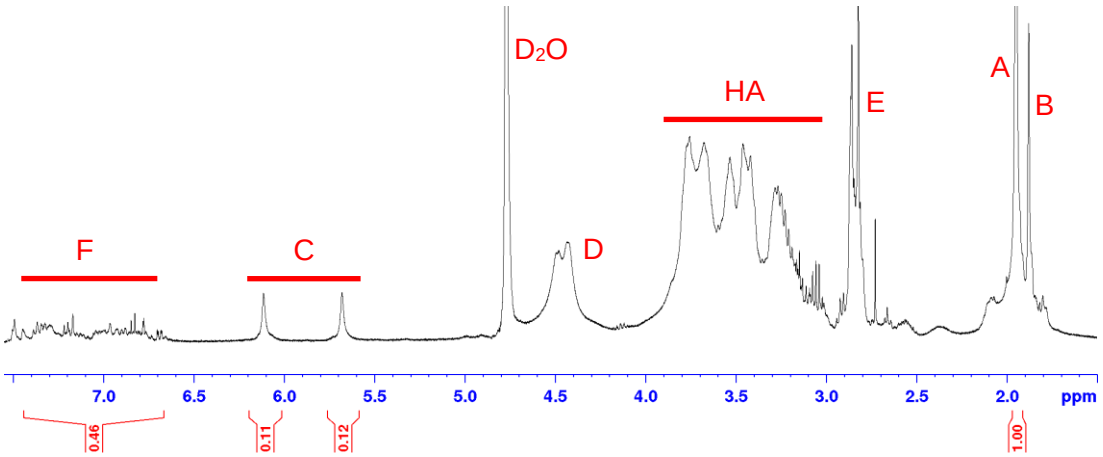

Figure 46: NMR plot for macromer MA36-Dopa46.
Spectra show presence of HA (A, HA and D) as well as MA groups (B, C), Dopa groups (E, F) and the D_2O solvent.

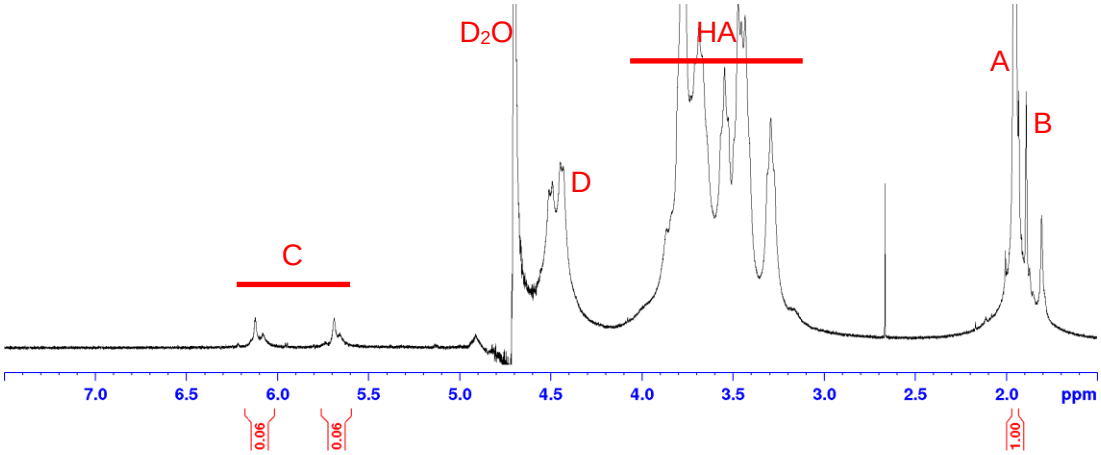

Figure 47: NMR plot for macromer MA18-Dopa0.
Spectra show presence of HA (A, HA and D) as well as MA groups (B, C) and the D_2O solvent.

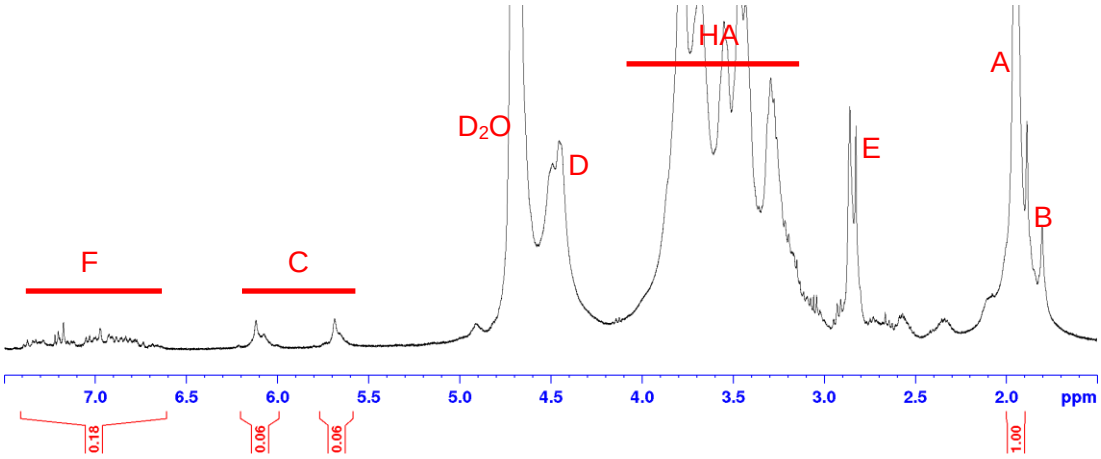

Figure 48: NMR plot for macromer MA18-Dopa18.
Spectra show presence of HA (A, HA and D) as well as MA groups (B, C), Dopa groups (E, F) and the D_2O solvent.

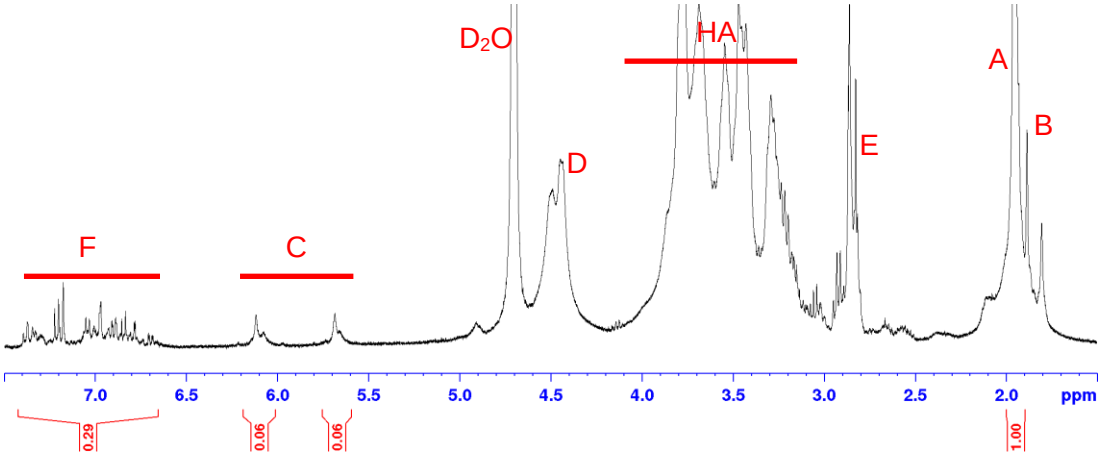

Figure 49: NMR plot for macromer MA18-Dopa29.

Spectra show presence of HA (A, HA and D) as well as MA groups (B, C), Dopa groups (E, F) and the D_2O solvent.

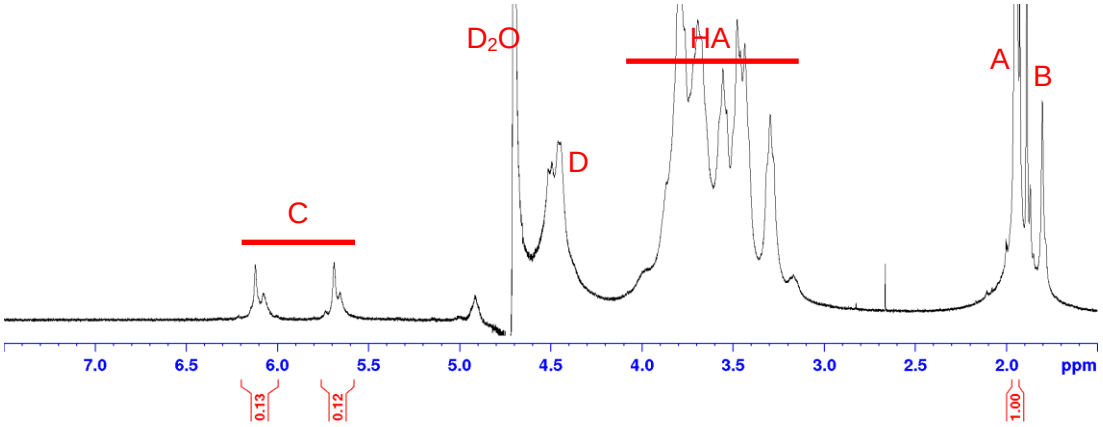

Figure 50: NMR plot for macromer MA38-Dopa0.

Spectra show presence of HA (A, HA and D) as well as MA groups (B, C) and the D_2O solvent.

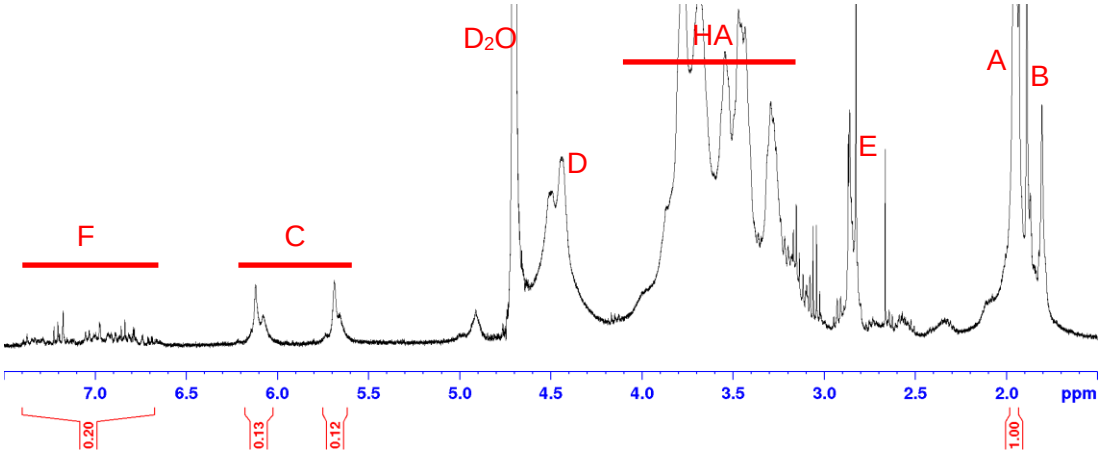

Figure 51: NMR plot for macromer MA38-Dopa20.

Spectra show presence of HA (A, HA and D) as well as MA groups (B, C), Dopa groups (E, F) and the D_2O solvent.

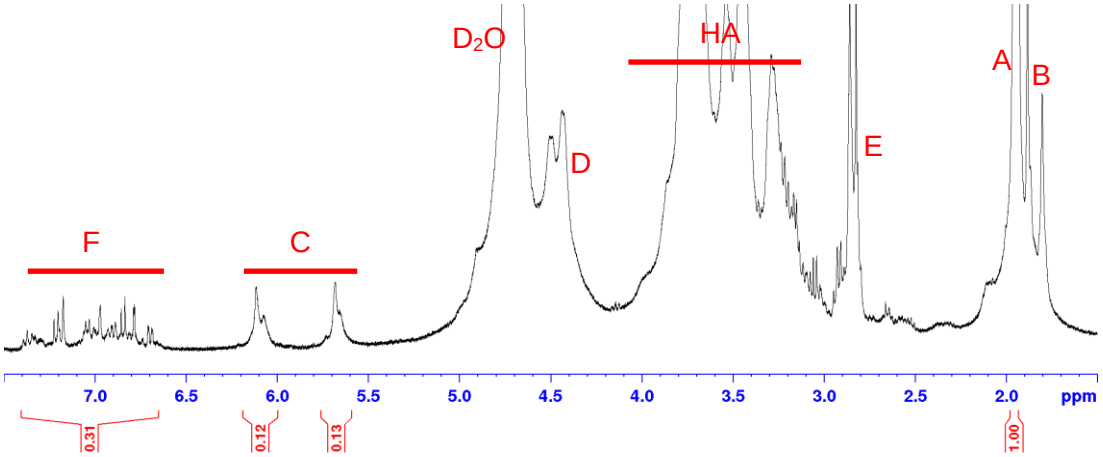

Figure 52: NMR plot for macromer MA38-Dopa31.

Spectra show presence of HA (A, HA and D) as well as MA groups (B, C), Dopa groups (E, F) and the D_2O solvent.

5.5 Gelation behaviour and bulk stiffness

Figure 17 represents the gelation behaviour of different hydrogel formulations after 4 minutes of light exposure, with Table 10 summarising the exact values.

Table 10: Summary of gelation times [37] after 4 minutes light exposure
Summary of gelation times [37], as determined by the cross-over of G' and G''. Formulations that did not achieve a sol-gel transition after 4 minutes light exposure are indicated with an X.

Gelation time [37]		No Dopa		Low Dopa		High Dopa	
	conc. HA ± 1MDa HA	1 %	3 %	1 %	3 %	1 %	3 %
Low MA	+ 0 %	X	5	X	114	X	X
	+ 2 %	11	3	10	143	X	X
High MA	+ 0 %	16	5	145	138	X	X
	+ 2 %	9	5	13	101	175	153

Table 11 summarises the bulk stiffness reached after 4 minutes light exposure. This time-point has been set as clinically relevant.

Table 11: Summary of stiffness of hydrogels after 4 minutes light exposure
Stiffness of hydrogels as determined by the elastic modulus G' (Pa) after 4 minutes light exposure. Data show means and standard deviations. Formulations that did not achieve a sol-gel transition after 4 minutes light exposure are indicated with an X.

Stiffness [Pa ±S.D.] 4 min light exposure		No Dopa		Low Dopa		High Dopa	
	conc. HA ± 1MDa HA	1 %	3 %	1 %	3 %	1 %	3 %
Low MA	+ 0 %	X	1,908 ±56	X	225 ±64	X	X
	+ 2 %	1,127 ±34	11,107 ±129	307 ±56	465 ±71	X	X
High MA	+ 0 %	343 ±29	6,965 ±120	173 ±37	491 ±29	X	37 ±4
	+ 2 %	2,791 ±74	10,054 ±57	449 ±75	600 ±39	277 ±29	335 ±45

Table 12 summarises the plateau stiffness reached after 9 minutes light exposure. As can be seen in Figure 53 - Figure 56, bulk stiffness reached its maximum value later than 4 minutes light exposure.

Table 12: Summary of stiffness of hydrogels after 9 minutes light exposure
Plateau stiffness of hydrogels as determined by the elastic modulus G' (Pa) after 9 minutes light exposure. Data show means and standard deviations. Formulations that did not achieve a sol-gel transition are indicated with an X.

Stiffness [Pa ±S.D.] 9 min light exposure		No Dopa		Low Dopa		High Dopa	
	conc. HA / ± 1MDa HA	1 %	3 %	1 %	3 %	1 %	3 %
Low MA	+ 0 %	X	2,366 ±65	X	519 ±11	X	X
	+ 2 %	1,057 ±18	14,264 ±48	336 ±39	657 ±42	X	X
High MA	+ 0 %	443 ±45	9,472 ±62	351 ±62	1,255 ±80	X	262 ±63
	+ 2 %	3,344 ±54	12,660 ±120	647 ±33	787 ±68	419 ±13	614 ±69

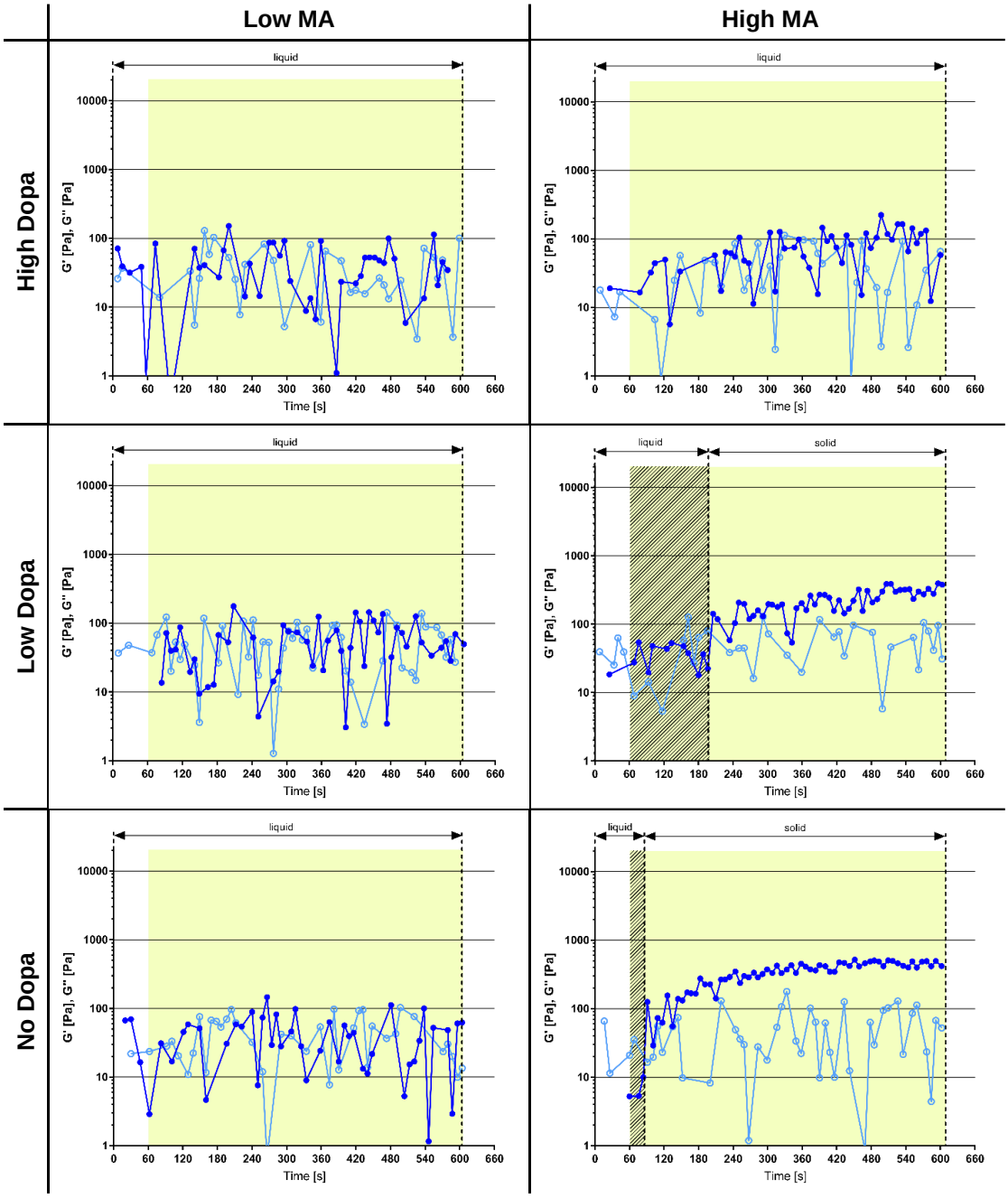

Figure 53: Gelation kinetics and hydrogel stiffness of 1 % hydrogels (without 2 % unmodified 1 MDa HA)

Gelation kinetics and hydrogel stiffness as measured by the storage (G'●) and loss (G''○) modulus by small amplitude oscillatory time-sweep rheology of 1 % hydrogels (without 2 % unmodified 1 MDa HA). Light exposure started after 60 seconds and lasted for a total of 9 minutes (yellow area□). Gelation was taken as the cross-over between G' and G'' as indicated by the striped area (▨). No sol-gel transition was achieved for the low MA formulations and the high MA formulation with high Dopa content.

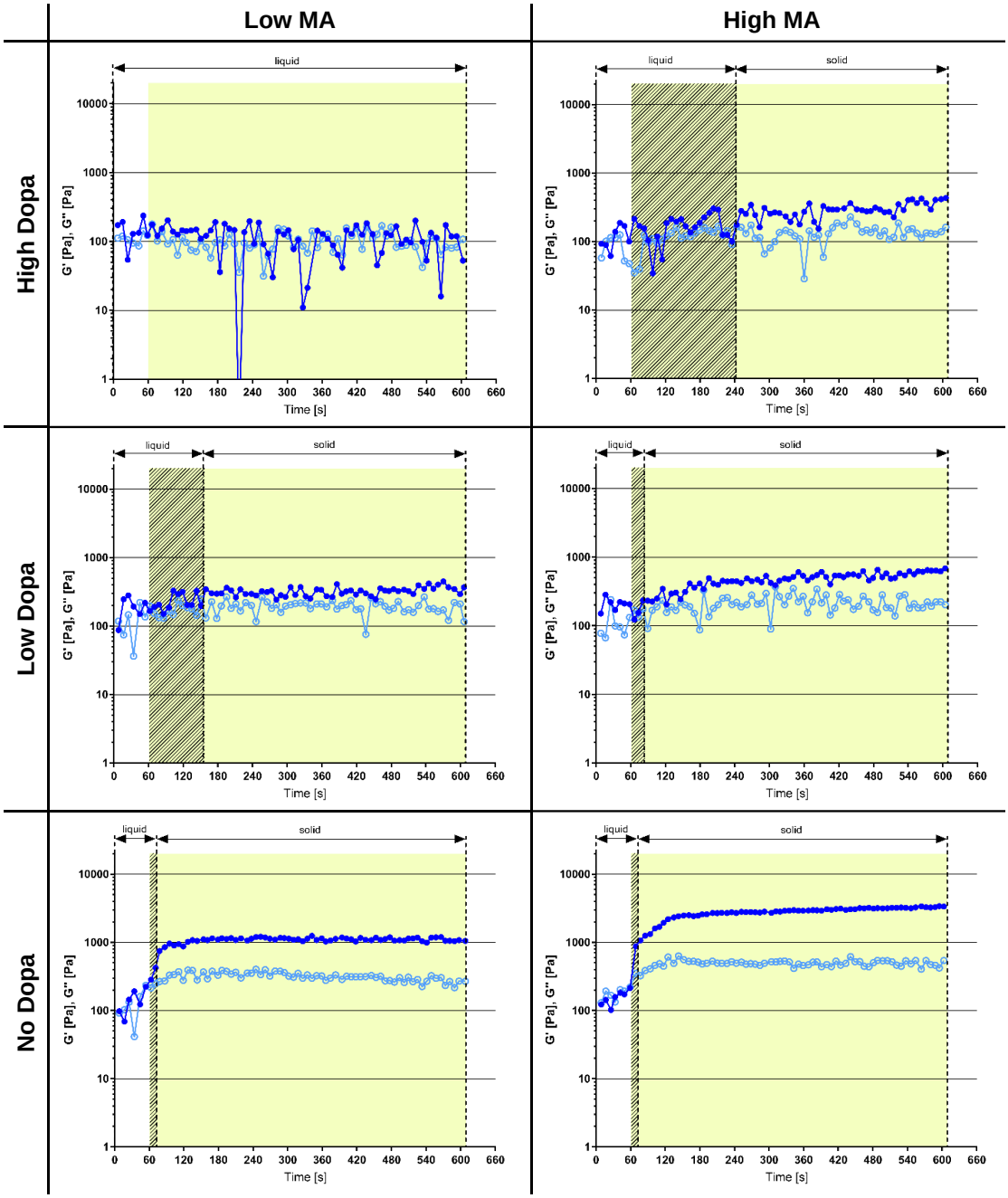

Figure 54: Gelation kinetics and hydrogel stiffness of 1 % hydrogels (with 2 % unmodified 1 MDa HA)

Gelation kinetics and hydrogel stiffness as measured by the storage (G'●) and loss (G''○) modulus by small amplitude oscillatory time-sweep rheology of 1 % hydrogels (with 2 % unmodified 1 MDa HA). Light exposure started after 60 seconds and lasted for a total of 9 minutes (yellow area□). Gelation was taken as the cross-over between G' and G'' as indicated by the striped area (▨). No sol-gel transition was achieved for the formulation with low MA and high Dopa.

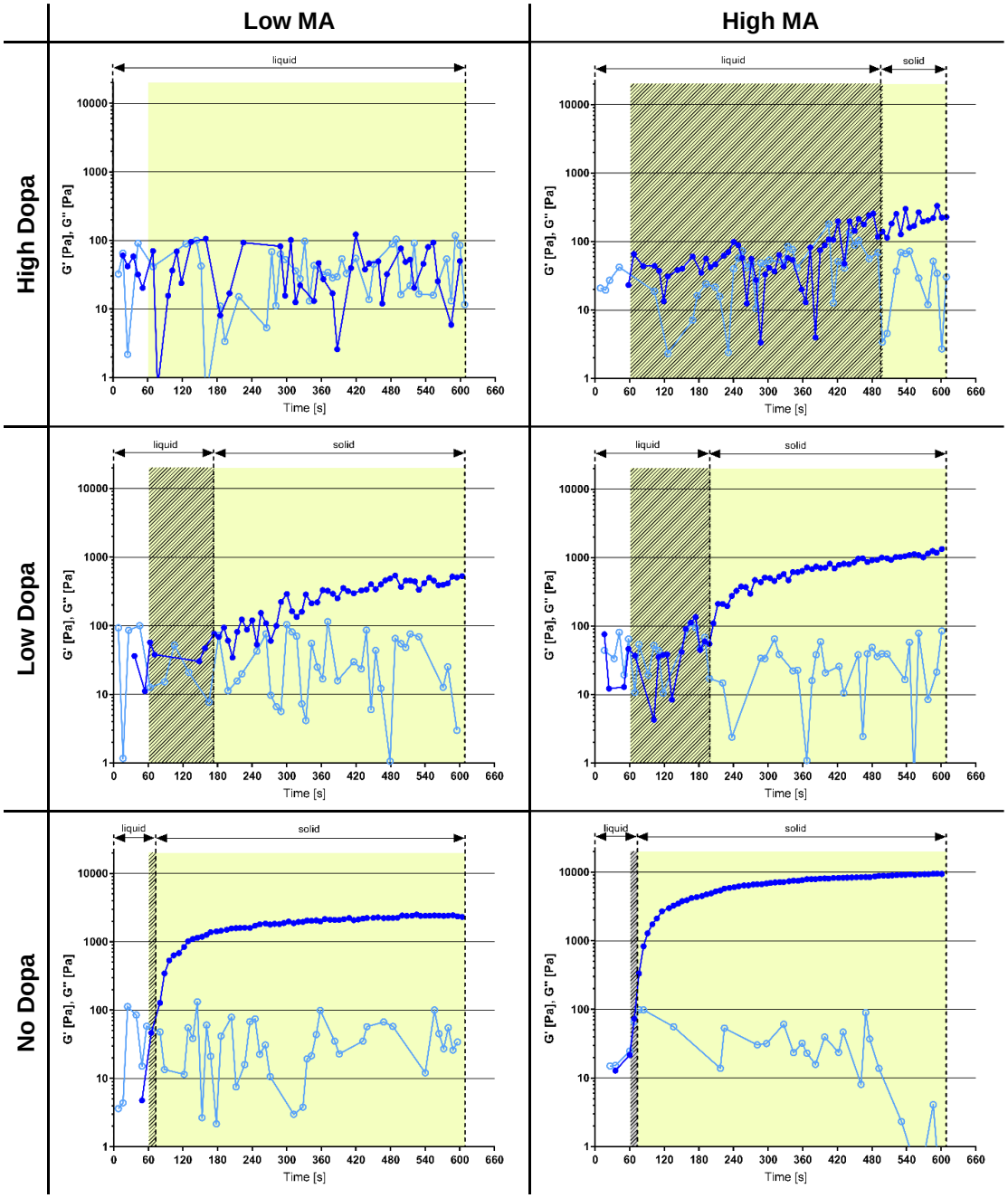

Figure 55: Gelation kinetics and hydrogel stiffness of 3 % hydrogels (without 2 % unmodified 1 MDa HA)

Gelation kinetics and hydrogel stiffness as measured by the storage (G'●) and loss (G''○) modulus by small amplitude oscillatory time-sweep rheology of 3 % hydrogels (without 2 % unmodified 1 MDa HA). Light exposure started after 60 seconds and lasted for a total of 9 minutes (yellow area□). Gelation was taken as the cross-over between G' and G'' as indicated by the striped area (▨). No sol-gel transition was achieved for the formulation with low MA and high Dopa.

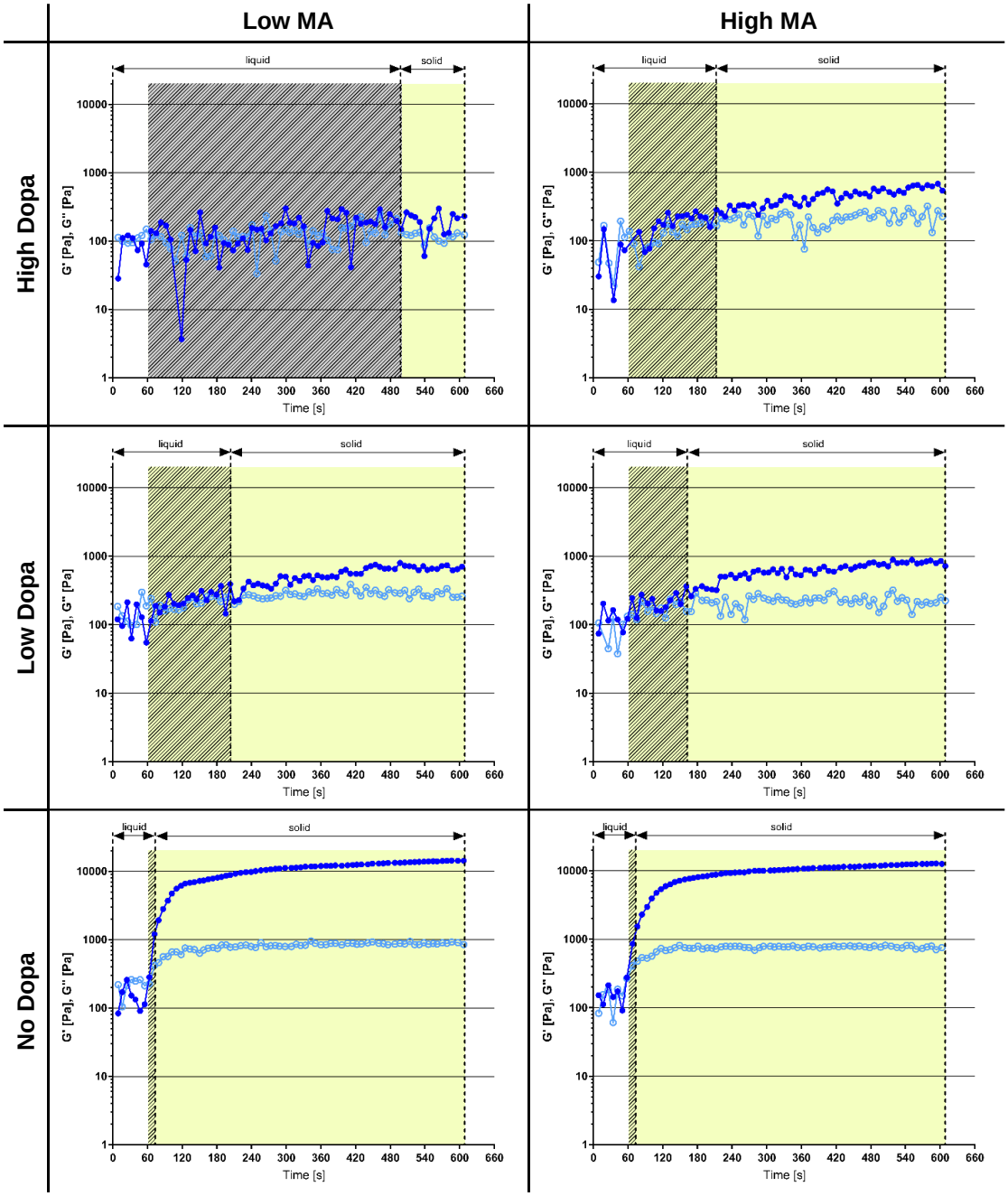

Figure 56: Gelation kinetics and hydrogel stiffness of 3 % hydrogels (with 2 % unmodified 1 MDa HA)

Gelation kinetics and stiffness as measured by the storage (G'●) and loss (G''○) modulus by small amplitude oscillatory time-sweep rheology of 3 % hydrogels (with 2 % unmodified 1 MDa HA). Light exposure started after 60 seconds and lasted for a total of 9 minutes (yellow area□). Gelation was taken as the cross-over between G' and G'' as indicated by the striped area (▨).

5.6 Shelf-life

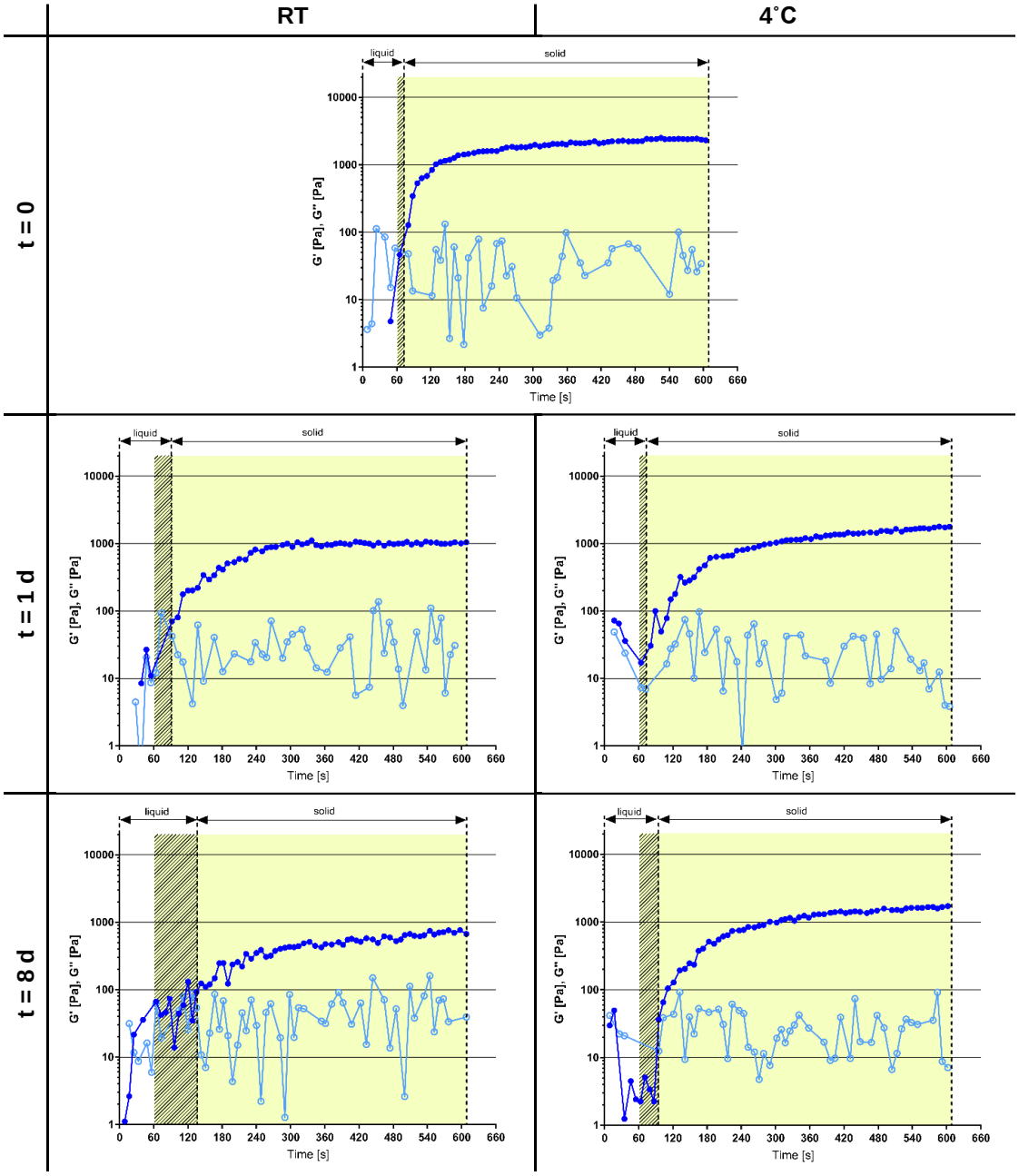

Figure 57: Stiffness of 3 % low MA and no Dopa hydrogels (without 2 % unmodified 1 MDa HA) before and after storage

Stiffness as measured by the storage (G'●) and loss (G''○) modulus by small amplitude oscillatory time-sweep rheology of 3 % low MA and no Dopa hydrogels (without 2 % unmodified 1 MDa HA) immediately after mixing components (t = 0) and after storage for 1 or 8 days at RT or 4 °C. Light exposure started after 60 seconds and lasted for a total of 9 minutes (yellow area□). Gelation was taken as the cross-over between G' and G'' as indicated by the striped area (▨).

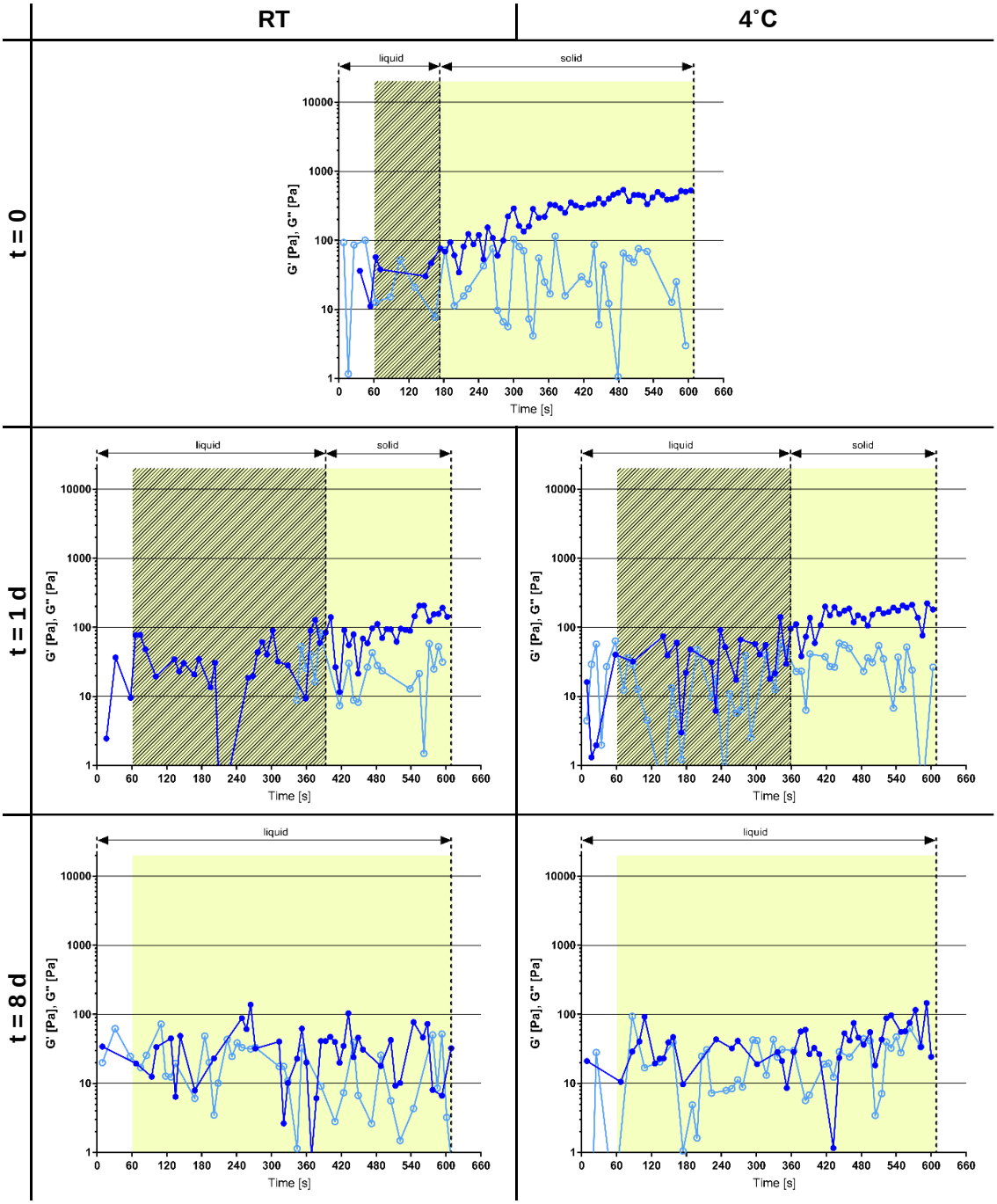

Figure 58: Stiffness of 3 % low MA and low Dopa hydrogels (without 2 % unmodified 1 MDa HA) before and after storage

Stiffness as measured by storage (G'●) and loss (G''○) modulus by small amplitude oscillatory time-sweep rheology of 3 % low MA and low Dopa hydrogels (without 2 % unmodified 1 MDa HA) after mixing components (t = 0) and after storage for 1 or 8 days at RT or 4 °C. Light exposure started after 60 seconds and lasted for a total of 9 minutes (yellow area□). Gelation was taken as the cross-over between G' and G'' as indicated by the striped area (▨). No sol-gel transition was achieved for the formulation after 8 days storage.

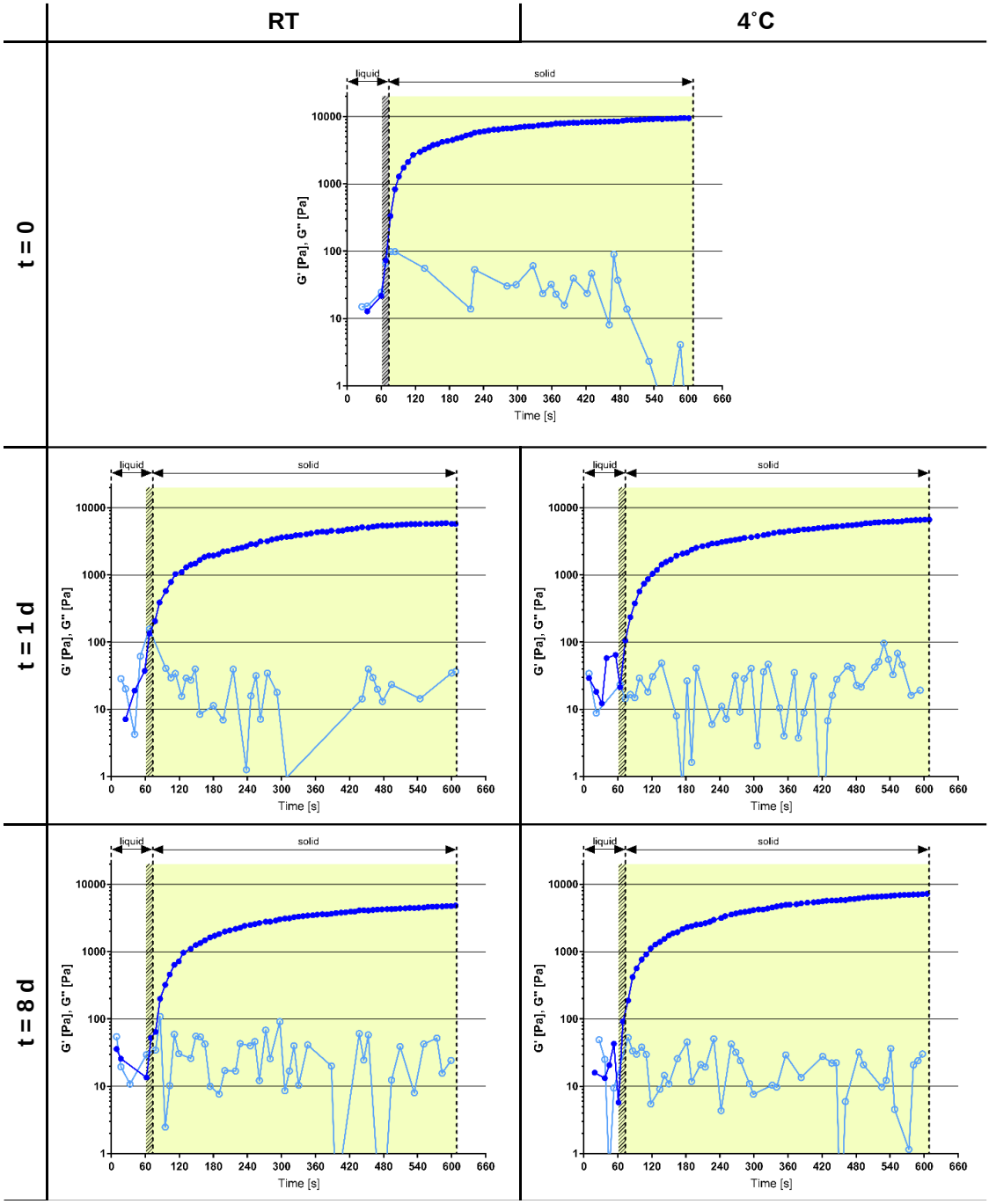

Figure 59: Stiffness of 3 % high MA and no Dopa hydrogels (without 2 % unmodified 1 MDa HA) before and after storage

Stiffness as measured by the storage (G'●) and loss (G''○) modulus by small amplitude oscillatory time-sweep rheology of 3 % high MA and no Dopa hydrogels (without 2 % unmodified 1 MDa HA) immediately after mixing components (t = 0) and after storage for 1 or 8 days at RT or 4 °C. Light exposure started after 60 seconds and lasted for a total of 9 minutes (yellow area□). Gelation was taken as the cross-over between G' and G'' as indicated by the striped area (▨).

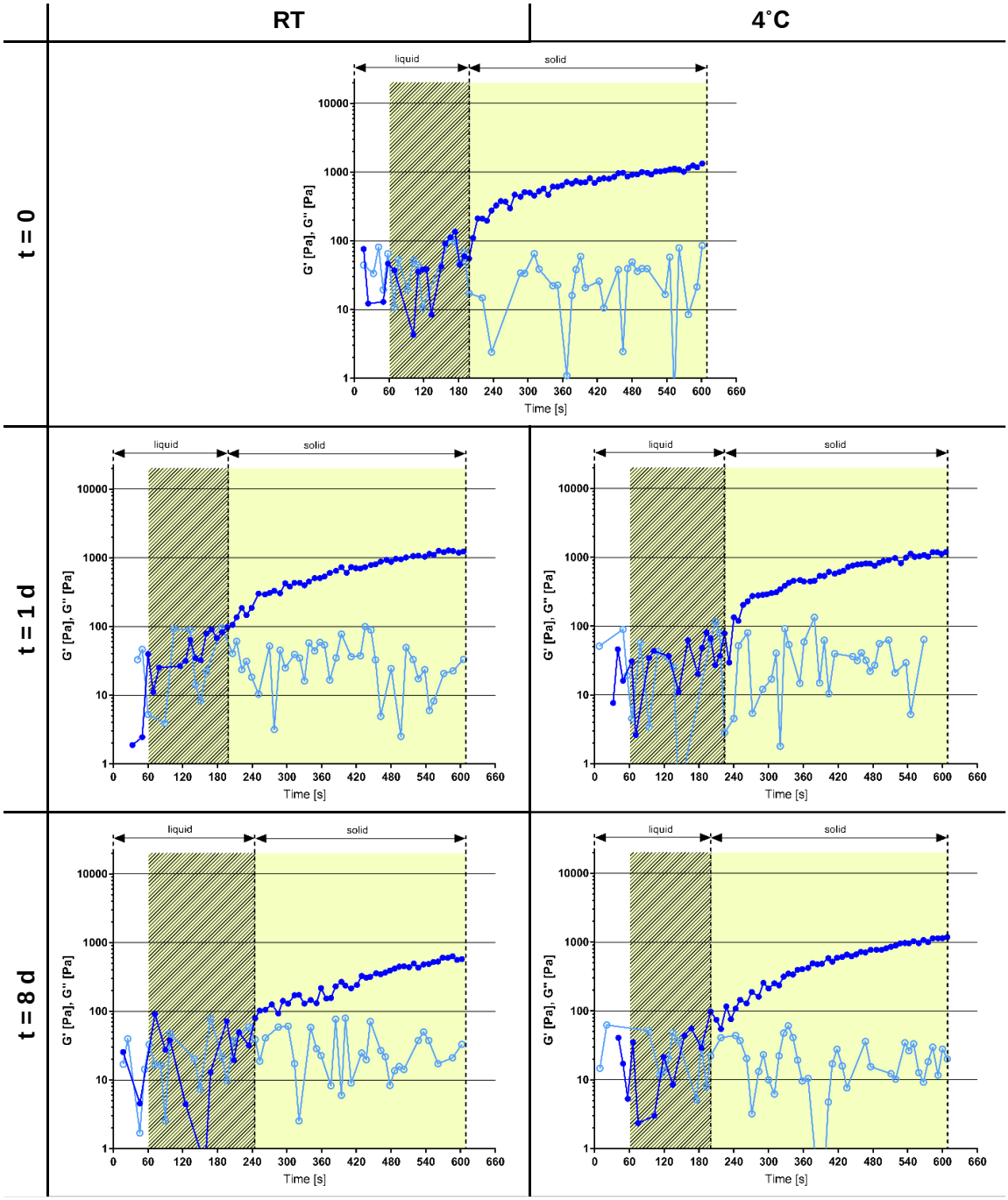

Figure 60: Stiffness of 3 % high MA and low Dopa hydrogels (without 2 % unmodified 1 MDa HA) before and after storage

Stiffness as measured by the storage (G'●) and loss (G''○) modulus by small amplitude oscillatory time-sweep rheology of 3 % high MA and low Dopa hydrogels (without 2 % unmodified 1 MDa HA) immediately after mixing components (t = 0) and after storage for 1 or 8 days at RT or 4 °C. Light exposure started after 60 seconds and lasted for a total of 9 minutes (yellow area□). Gelation was taken as the cross-over between G' and G'' as indicated by the striped area (▨).

5.7 Mass swelling ratio

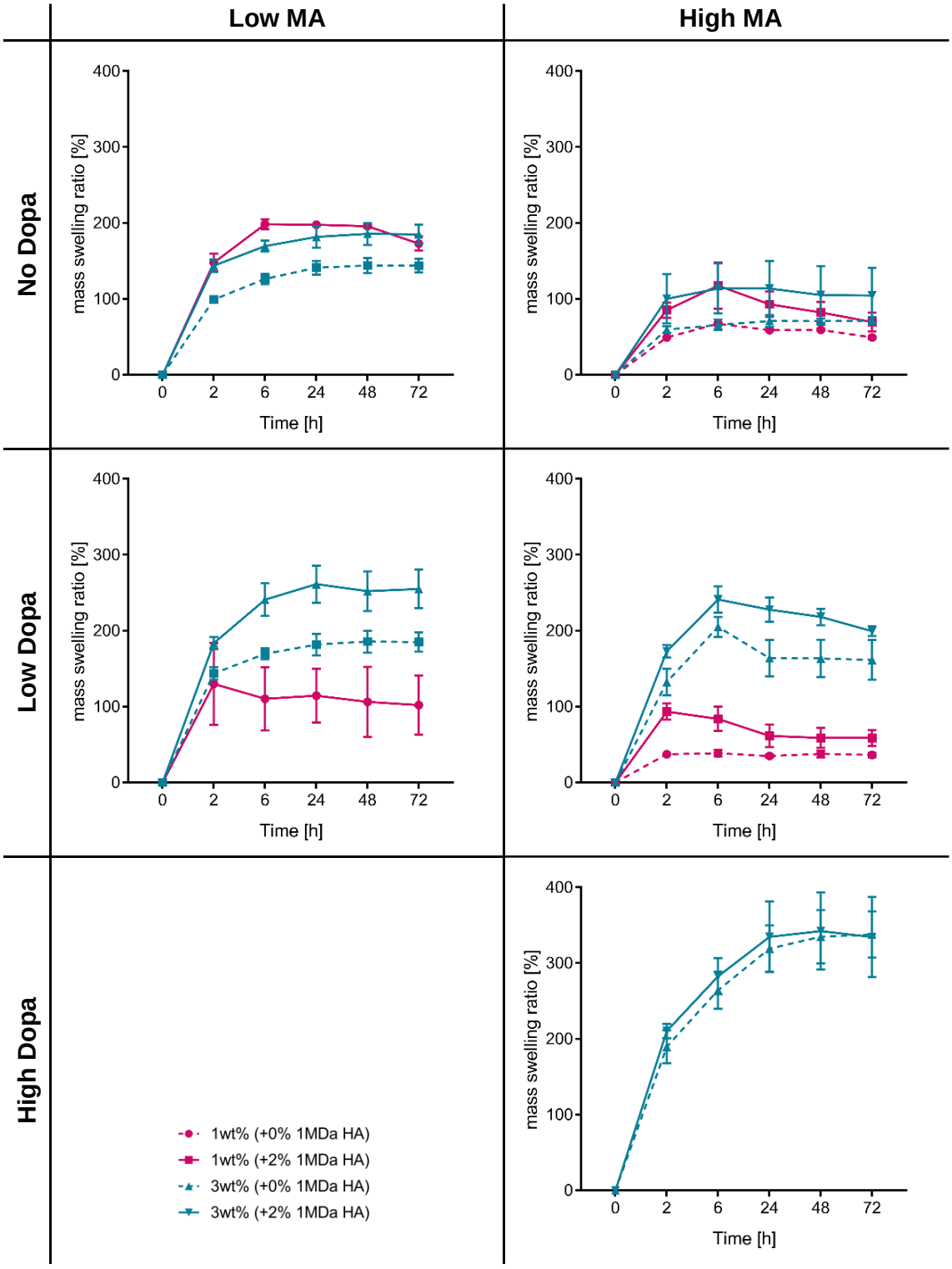

Figure 61: Mass swelling ratio

Mass swelling ratio as determined by gravimetric analysis. Hydrogels were incubated in PBS (+1 % ABAM) and weight changes were recorded over 72 h. Each data point represents an n = 3. Mean values with S.D.

Table 13: Summary of mass swelling ratio measurements from Figure 61

Mass swelling ratio [%]		No Dopa		Low Dopa		High Dopa	
	conc. HA / ± 1MDa HA	1 %	3 %	1 %	3 %	1 %	3 %
Low MA	+ 0 %	X	140 ±10	X	180 ±15	X	X
	+ 2 %	200 ±5	180 ±15	110 ±50	260 ±25	X	X
High MA	+ 0 %	60 ±5	70 ±10	40 ±5	160 ±25	X	320 ±30
	+ 2 %	80 ±15	110 ±40	60 ±10	220 ±10	X	340 ±50

5.8 Enzymatic degradation

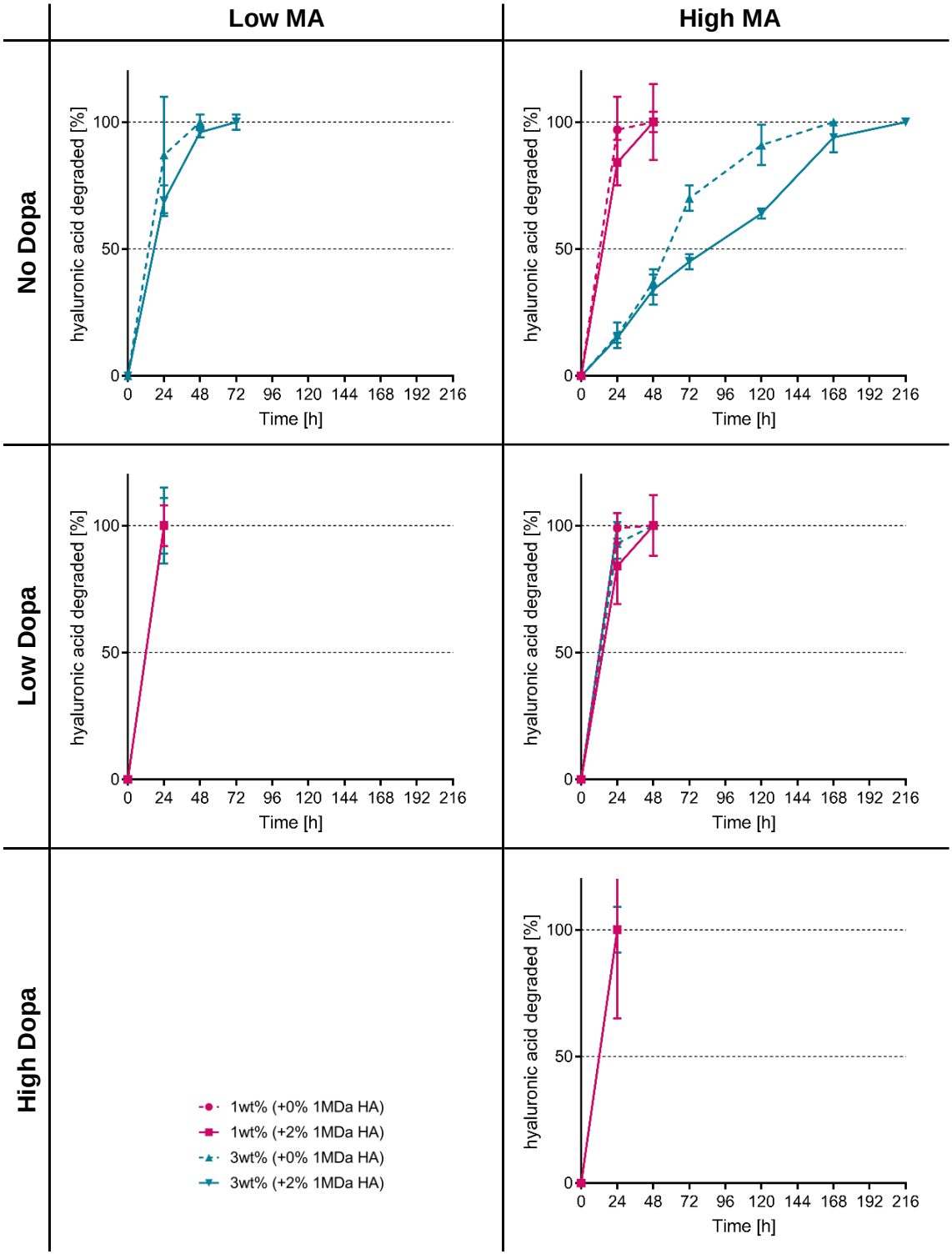

Figure 62: Enzymatic degradation

Enzymatic degradation kinetics of hydrogels treated with 10 U/mL hyaluronidase (Type I, from bovine testis). The percent of hyaluronic acid released (from gel total) was quantified by carbazole assay. Each data point represents an n = 3. Mean values with S.D.

5.9 3D cell survival

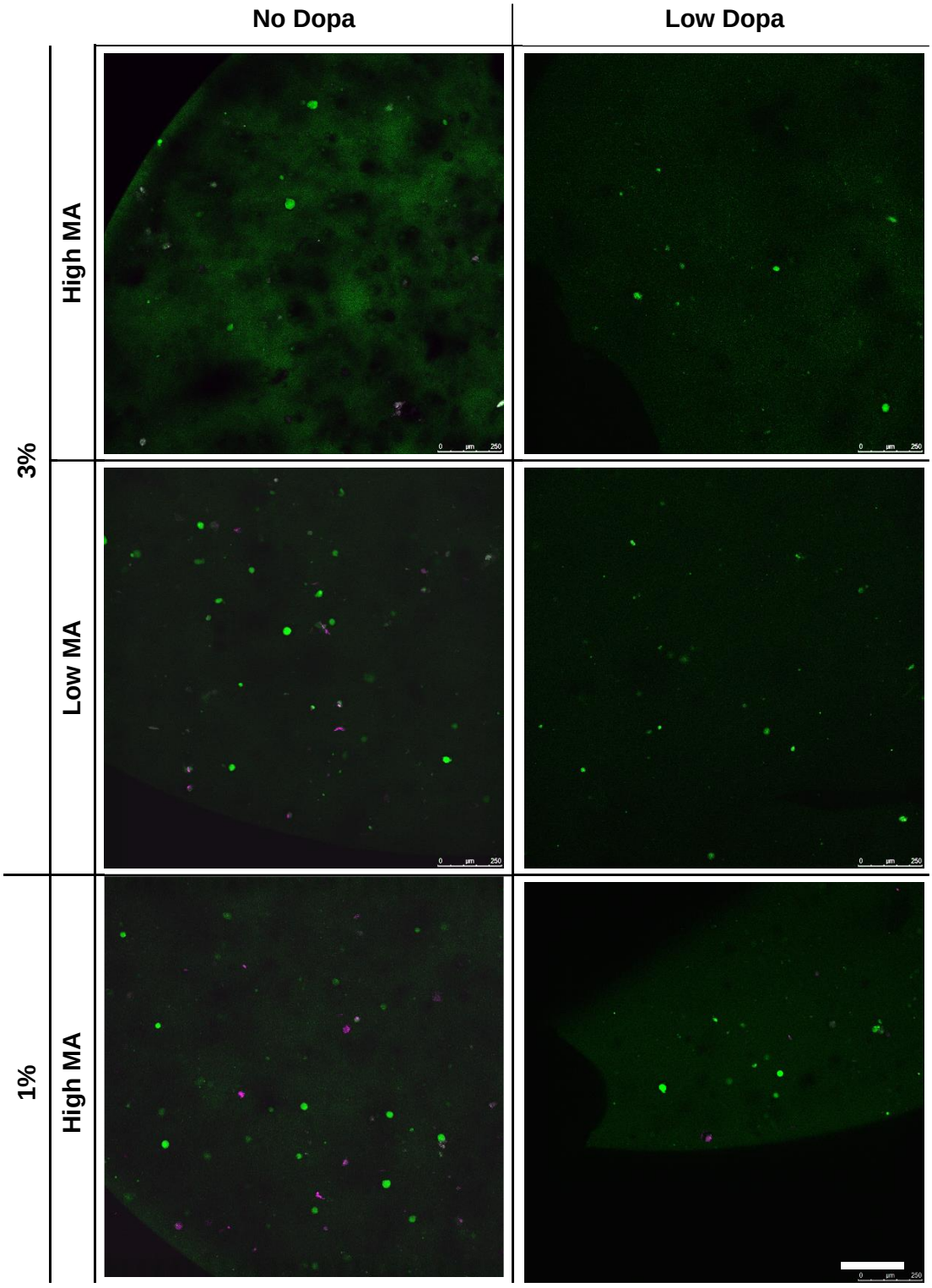

Figure 63: Live/dead analysis of 3D encapsulated BMMSCs

Representative images of BMMSC encapsulated within hydrogels and analysed using a live/dead viability/cytotoxicity kit. Live cells are labelled in green and dead cells appear magenta. Scale bar = 250 µm.